

BULGARIAN CHEMICAL COMMUNICATIONS

2010 Volume 42/ Number 1

*Journal of the Chemical Institutes
of the Bulgarian Academy of Sciences
and of the Union of Chemists in Bulgaria*

Hydrogen-bonded systems of water with dimethyl and diethyl sulfoxides. Theoretical study of structures, stability and vibrational spectra

Y. Dimitrova

*Institute of Organic Chemistry with Centre of Phytochemistry, Bulgarian Academy of Sciences,
Acad. G. Bonchev St., Block 9, 1113 Sofia, Bulgaria*

Received January 9, 2009; Revised June 11, 2009

The structural and vibrational characteristics (vibrational frequencies and infrared intensities) of the hydrogen-bonded systems dimethylsulfoxide (DMSO)–water (1:1, 1:2) and diethylsulfoxide (DESO)–water (1:1, 1:2) have been investigated employing *ab initio* and DFT calculations at different basis sets. The calculations show that the optimised structures of the studied systems 1:2 are cyclic while the optimised structures of the hydrogen-bonded systems 1:1 are linear. The corrected values of the dissociation energy for the hydrogen-bonded systems have been calculated by *ab initio* and DFT calculations at different basis sets in order to estimate their stability. It was established that the hydrogen-bonded systems DESO–water (1:1, 1:2) are more stable than the systems DMSO–water (1:1, 1:2). The influence of the hydrogen bonding on the properties of the monomers (H₂O, DMSO and DESO) has been investigated. The hydrogen bonding between H₂O and DMSO, and DESO leads to changes in the vibrational characteristics of the monomers. The predicted vibrational characteristics for the studied hydrogen-bonded systems are in very good agreement with the experimentally observed.

Key words: hydrogen-bonding; DMSO:H₂O and DESO:H₂O complexes; structures; vibrational spectra; *ab initio*; DFT.

INTRODUCTION

Hydrogen bonding is of fundamental importance in chemistry, physics and biology. Computational methods based on quantum theory and developed for the treatment of chemical bonding, intermolecular forces, reactivity and interactions with electromagnetic radiation can reproduce or predict the measurable characterizing the hydrogen bonds. A large number of theoretical studies on the structures, stability and vibrational spectra employing *ab initio* and DFT calculations have been undertaken in recent years for the hydrogen-bonded complexes [1–8].

In many industrial and biomedical fields dialkyl sulfoxides (DASO) have found applications because of their unusual physicochemical properties. DMSO and DESO are used as industrial solvents for polar and ionic substances in chemistry, biology and medicine. DESO exhibits strong self-associative effects, even stronger than in DMSO. To this purpose, vibrational spectroscopy (Raman and IR) has been widely used [9–14] for studying the vibrational features of DMSO and DESO both pure and in aqueous solutions. The biomedical significance of DESO has been reported also [15]. Thermodynamic measurements of DESO–water mixtures (heat of fusion and solidification, melting and freezing temperature) suggested very strong

deviations from ideality, like in DMSO–water solutions, but to a greater extent [16].

The objects of the present study are the hydrogen-bonded systems DMSO–H₂O (1:1, 1:2) and DESO–H₂O (1:1, 1:2). The aim of the study is first, to establish the most stable structures of the hydrogen-bonded systems, secondly, to study the nature of the hydrogen bonding and finally to estimate the changes in the vibrational characteristics upon hydrogen bonding.

METHODS

The structures, stability and vibrational characteristics of the hydrogen-bonded systems dimethylsulfoxide (DMSO)–water (1:1, 1:2) and diethylsulfoxide (DESO)–water (1:1, 1:2) are studied extensively in this work by *ab initio* and DFT calculations with various basis sets using the GAUSSIAN 98 series of programs [17]. Full geometry optimisation of the studied hydrogen-bonded complexes was performed. On Figs. 1 and 2 are presented the optimized structures with B3LYP/6-311++G (d,p) calculations for the DMSO–H₂O (1:1, 1:2) and DESO–H₂O (1:1, 1:2), complexes **1** and **2**. The optimized values of the hydrogen-bonded parameters (bond lengths and angles) obtained with B3LYP/6-311++G (d,p) calculations for the complexes studied are shown on Figs. 1 and 2.

* To whom all correspondence should be sent:
E-mail: dimj@orgchem.bas.bg

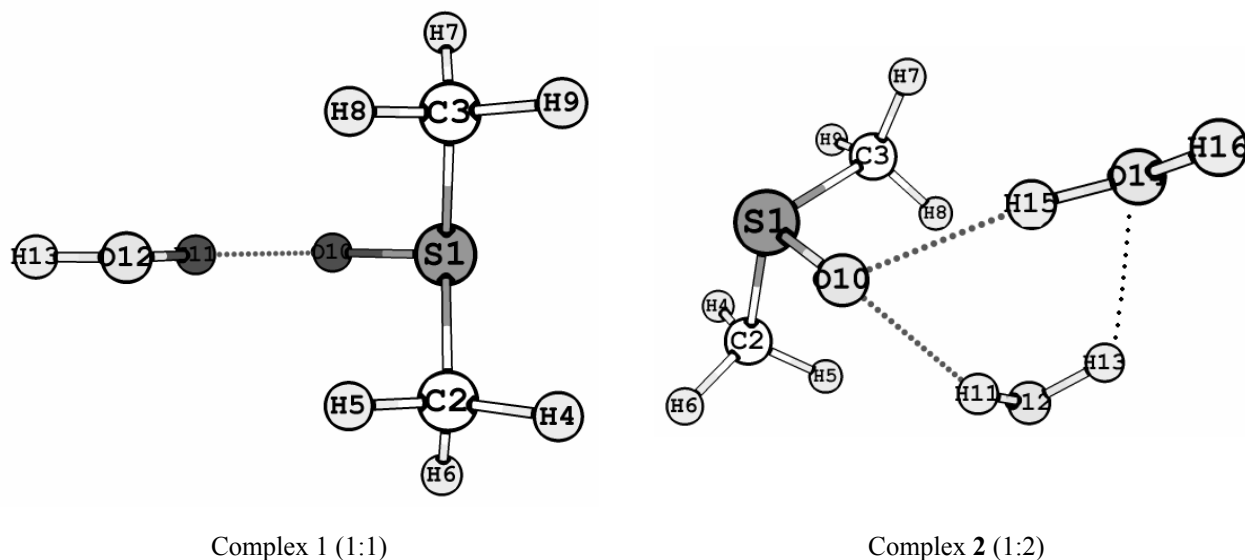


Fig. 1. Optimized structures with B3LYP/6-311++G(d,p) calculations for the hydrogen-bonded: DMSO and one molecule H₂O (Complex 1); DMSO and two molecules H₂O (Complex 2):

Complex 1: $R_{O_{10}\dots H_{11}}=1.822$ Å; Angles (°): $H_{11}\dots O_{10}S_1=41.3$; $O_{10}\dots H_{11}O_{12}=8.7$.

Complex 2: $R_{O_{10}\dots H_{15}}=1.851$ Å; $R_{O_{10}\dots H_{11}}=1.981$ Å; $R_{O_{14}\dots H_{13}}=2.436$ Å; Angles (°): $H_{15}\dots O_{10}\dots H_{11}=72.7$; $O_{10}\dots H_{15}O_{14}=161.2$; $O_{10}\dots H_{11}O_{12}=152.7$; $O_{14}\dots H_{13}O_{12}=122.1$; $H_{15}\dots O_{10}S_1=124.0$; $H_{11}\dots O_{10}S_1=40.1$.

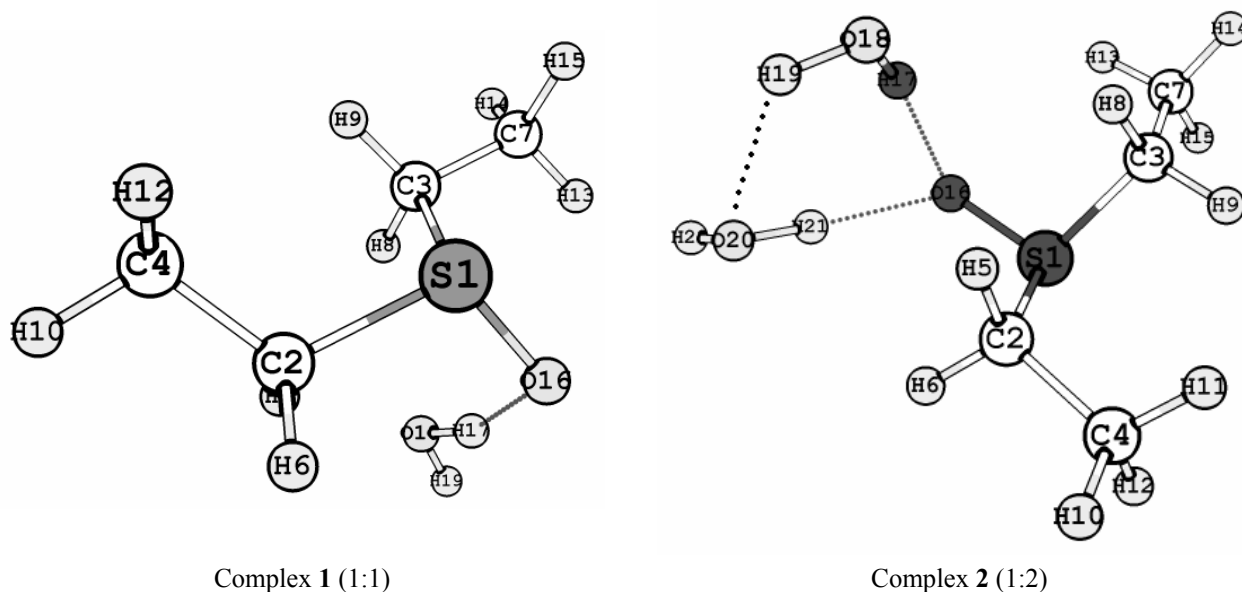


Fig. 2. Optimized structures with B3LYP/6-311++G(d,p) calculations for the hydrogen-bonded: DESO and one molecule H₂O (Complex 1); DESO and two molecules H₂O (Complex 2):

Complex 1: $R_{O_{16}\dots H_{17}}=1.811$ Å; Angles (°): $H_{17}\dots O_{16}S_1=31.1$; $O_{16}\dots H_{17}O_{18}=158.3$.

Complex 2: $R_{O_{16}\dots H_{17}}=1.961$ Å; $R_{O_{16}\dots H_{21}}=1.842$ Å; $R_{O_{20}\dots H_{19}}=2.460$ Å; Angles (°): $H_{19}\dots O_{20}H_{21}=83.7$; $H_{19}O_{18}\dots O_{20}=123.0$; $H_{17}\dots O_{16}\dots H_{21}=73.8$; $O_{18}H_{17}\dots O_{16}=156.3$; $O_{16}\dots H_{21}O_{20}=161.9$; $H_{17}\dots O_{16}S_1=29.9$; $H_{21}\dots O_{16}S_1=31.3$.

The density functional (DFT) calculations in this work were carried out in the framework of Kohn-Sham density-functional theory [18] (DFT) with the nonlocal three-parameter gradient-corrected exchange-correlation functional of Becke and Lee, Yang and Parr including partially exact HF-exchange (B3LYP) [19].

The dissociation energy is used for the estimation of the stability of the hydrogen-bonded systems between two and more partners. The supermolecular variation method determines dissociation energy (ΔE) as a difference between the energy of the complex and the energies of the isolated molecules:

$$\Delta E = E_{\text{com.}} - (E_1 + E_2 + E_3 \dots) \quad (1)$$

where $E_1, E_2, E_3 \dots$ are the energies of the isolated monomers in their own basis set and $E_{\text{com.}}$ is the energy of the complex.

The supermolecular approach is theoretically able to provide dissociation energy at any accuracy, however, only if a sufficiently large basis set and a sufficiently high level of correlation is used. For the exact determination of the interaction energy in the supermolecular approach the consideration of the zero-point energies is very important.

The zero-point vibrational energy correction for the studied complexes can be defined as a difference between the calculated zero-point vibrational energy of the complex and the zero-point energies of the monomers:

$$\Delta E_{\text{zp vib}} = E_{\text{zp vib.}}(\text{com.}) - (E_{\text{zp vib}}(1) + E_{\text{zp vib}}(2) + E_{\text{zp vib}}(3) \dots) \quad (2)$$

The dissociation energies, uncorrected and corrected with zero-point energy differences are calculated by *ab initio* and DFT calculations with different basis sets.

The MP2 method for different basis sets (6-31G(d,p); 6-311++G(d,p)) is used in this study in order to estimate the MP2 correlation contribution to the dissociation energy for the hydrogen-bonded systems dimethylsulfoxide (DMSO)–water (1:1, 1:2) and diethylsulfoxide (DESO)–water (1:1, 1:2) (See Figs. 1 and 2). The MP2 correlation contribution $\delta E(\text{MP2})$ to MP2 dissociation energy is:

$$\delta E(\text{MP2}) = \Delta E(\text{MP2}) - \Delta E(\text{SCF}) \quad (3)$$

where $\Delta E(\text{MP2})$ is the dissociation energy, calculated at the MP2 level, and $\Delta E(\text{SCF})$ is the dissociation energy, calculated at the SCF level.

RESULTS AND DISCUSSION

Structures and stability

In order to establish the most stable structures of the hydrogen-bonded hydrogen-bonded systems dimethylsulfoxide (DMSO)–water (1:1, 1:2) and diethylsulfoxide (DESO)–water (1:1, 1:2) full geometry optimization have been performed by *ab initio* and DFT (B3LYP) calculations with basis sets: 6-31G(d,p) and 6-311++G(d,p) using the GAUSSIAN 98 series of programs [17]. On Figs. 1 and 2 are shown the optimized structures of the complexes **1** and **2** with B3LYP/6-311++G(d,p) calculations. As can be seen the hydrogen bonding between two water molecules and DMSO, and DESO molecules leads to the formation of cyclic structures (Figs. 1 and 2, complexes **2**), while the

hydrogen-bonded systems of one water molecule with DMSO and DESO are open (Figs. 1 and 2, complexes **1**).

The dissociation energies, uncorrected and corrected with zero-point energy differences for the studied hydrogen-bonded systems of one and two water molecules with DMSO and DESO (complexes 1:1 and 1:2) are calculated by *ab initio* and DFT calculations with different basis sets. The results from the calculations are presented in Table 1. As can be seen from the data of ΔE (uncorrected and corrected with $\Delta E(\text{zp vib})$) the values of the dissociation energy calculated with *ab initio* SCF and MP2 level are different. The main cause for this effect is the MP2 correlation contribution to the dissociation energy ($\delta E(\text{MP2})$). The calculated values of the dissociation energy as well as of the MP2 correlation contribution to the dissociation energy for the hydrogen-bonded complexes of two water molecules with DMSO and DESO molecules (complexes 1:2) are approximately twice as much in comparison with the values calculated at the same basis set for the hydrogen-bonded complexes 1:1. In all cases, the complexes of water with DESO are more stable than the complexes of water with DMSO. On Figs. 1 and 2 is given the description of the full characteristics of hydrogen bonds with lengths and angles of all hydrogen-bonded bridges (distance between donor and acceptor of proton).

Vibrational spectra

It is known from previous studies [1–8] on the hydrogen-bonded complexes that the hydrogen bonding leads to the substantial changes in the vibrational characteristics of the stretching vibrations for the monomer bonds involved in the hydrogen bonding.

The changes in the vibrational frequencies and infrared intensities of the monomers characterizing their interactions have been evaluated by *ab initio* and DFT calculations employing the GAUSSIAN 98 series of programs [17].

The predicted values of the vibrational characteristics are presented in Tables 2 and 3 together with the detailed description of the normal modes based on the potential energy distribution (PED) obtained from MP2/6-311++G(d,p) calculations.

The changes in the vibrational characteristics arising from the hydrogen bonding of DMSO and DESO molecules with one and two water molecules have been estimated. The predicted frequency shift is:

$$\Delta v_i = v_i^{\text{complex}} - v_i^{\text{monomer}} \quad (4)$$

The changes in the infrared intensities (ΔA_i) upon hydrogen bond formation are also estimated using

ab initio and DFT calculations.

$$\Delta A_i = A_i^{\text{complex}} - A_i^{\text{monomer}} \quad (5)$$

The predicted changes in the vibrational frequencies and infrared intensities are shown in Tables 2 and 3. As it was noted the hydrogen bonding leads to the substantial changes in the vibrational characteristics of the stretching vibrations for the monomer

bonds involved in the hydrogen bonding. The data presented in Tables 2 and 3 show that for the complexes studied the hydrogen bonds are formed between O–H group from water molecule and S=O group from DMSO and DESO molecules. For the complexes of two water molecules with DMSO and DESO the weak hydrogen bonds are predicted between water molecules: O₁₄...H₁₃ and O₂₀...H₁₉.

Table 1. Dissociation energies ΔE (uncorrected and corrected), MP2 correlation contribution to the dissociation energy $\delta E(\text{MP2})$ and zero-point energy differences ΔE_{zpv} in kcal/mol for the hydrogen-bonded complexes DMSO–H₂O (1:1; 1:2) and DESO–H₂O (1:1; 1:2).

Basis set	ΔE_{uncorr}		ΔE_{zpv}		ΔE_{corr}		δE^{MP2}	
	DMSO–H ₂ O (1:1) ^a , (1:2) ^b	DESO–H ₂ O (1:1) ^a , (1:2) ^b	DMSO–H ₂ O (1:1) ^a , (1:2) ^b	DESO–H ₂ O (1:1) ^a , (1:2) ^b	DMSO–H ₂ O (1:1) ^a , (1:2) ^b	DESO–H ₂ O (1:1) ^a , (1:2) ^b	DMSO–H ₂ O (1:1) ^a , (1:2) ^b	DESO–H ₂ O (1:1) ^a , (1:2) ^b
SCF/	–10.20965 ^a	–10.37462 ^a	2.26955 ^a	2.21640 ^a	–7.94005 ^a	–8.15822 ^a	-	-
6-31G(d,p)	–19.15788 ^b	–19.33295 ^b	4.65554 ^b	4.50172 ^b	–14.50234 ^b	–14.83123 ^b	-	-
MP2/	–13.30635 ^a	–13.64866 ^a	2.22666 ^a	2.35560 ^a	–11.07969 ^a	–11.29306 ^a	–3.13960 ^a	–3.27404 ^a
6-31G(d,p)	–25.39533 ^b	–25.83961 ^b	5.17173 ^b	4.78348 ^b	–20.22360 ^b	–21.05613 ^b	–6.23745 ^b	–6.50665 ^b
B3LYP/	–12.89533 ^a	–12.94699 ^a	2.49229 ^a	2.10752 ^a	–10.40304 ^a	–10.83947 ^a	-	-
6-31G(d,p)	–24.40386 ^b	–24.71574 ^b	5.30508 ^b	5.19523 ^b	–19.09878 ^b	–19.52051 ^b	-	-
SCF/	–8.76556 ^a	–8.92809 ^a	2.2064 ^a	2.03070 ^a	–6.55916 ^a	–6.89739 ^a	-	-
6-311++G(d,p)	–15.92620 ^b	–16.25602 ^b	4.31929 ^b	4.13148 ^b	–11.60691 ^b	–12.12454 ^b	-	-
MP2/	–11.17922 ^a	–11.31106 ^a	2.27932 ^a	2.22151 ^a	–8.89990 ^a	–9.08955 ^a	–2.41366 ^a	–2.38297 ^a
6-311++G(d,p)	–20.21712 ^b	–20.54988 ^b	4.49494 ^b	4.35326 ^b	–15.72218 ^b	–16.19662 ^b	–4.29092 ^b	–4.29386 ^b
B3LYP/	–9.92093 ^a	–9.94363 ^a	2.30743 ^a	2.09343 ^a	–7.61350 ^a	–7.85020 ^a	-	-
6-311++G(d,p)	–17.36322 ^b	–17.52736 ^b	4.47088 ^b	4.41286 ^b	–12.89234 ^b	–13.11450 ^b	-	-

a - Complexes (1:1); b - Complexes (1:2).

Table 2. Calculated vibrational characteristics (ν in cm^{–1}, A in km·mol^{–1}) and changes in the vibrational characteristics ($\Delta\nu$ in cm^{–1}, ΔA in km·mol^{–1}) from monomers to a complex for the hydrogen-bonded systems DMSO–H₂O (1:1) and DMSO-2H₂O (1:2).

Mode	MP2/6-311++G(d,p)				B3LYP/6-311++G(d,p)			
	1:1		1:2		1:1		1:2	
	$\nu_i^{\text{compl.}}/\Delta\nu_i$	$A_i^{\text{compl.}}/\Delta A_i$						
$\nu(\text{O}_{12}\text{--H}_{11})$	3591/–282	443.9/430.8	3747/–126	221.3/208.2	3498/–319	483/473.9	3680/–137	243.8/234.6
$\nu(\text{O}_{12}\text{--H}_{13})$	3983/–12	72.6/23.6	3930/–65	103.8/42.9	3892/–31	60.4/3.4	3831/–95	110.6/53.5
$\nu(\text{O}_{14}\text{--H}_{15})$	-	-	3648/–225	446.1/432.9	-	-	3596/–221	432.9/423.7
$\nu(\text{O}_{14}\text{--H}_{16})$	-	-	3962/–33	98.8/37.9	-	-	3889/–34	87.9/30.8
59 $\nu(\text{C}_2\text{--H}_6)$ +41 $\nu(\text{C}_2\text{--H}_5)$	3213/22	1.1/–0.6	3216/25	1.0/–0.6	3150/15	0.9/0.8	3153/18	0.4/0.3
69 $\nu(\text{C}_3\text{--H}_8)$ +26 $\nu(\text{C}_3\text{--H}_7)$	3203/0	0.9/–0.7	3208/5	0.8/–0.8	3149/1	1.3/–0.2	3155/7	0.9/–0.5
49 $\nu(\text{C}_2\text{--H}_4)$ +29 $\nu(\text{C}_2\text{--H}_5)$ +19 $\nu(\text{C}_2\text{--H}_6)$	3191/112	1.3/–4.4	3190/111	1.2/–4.4	3142/104	4.4/–0.7	3145/107	2.4/–2.7
49 $\nu(\text{C}_3\text{--H}_9)$ +45 $\nu(\text{C}_3\text{--H}_7)$	3183/–12	1.5/–4.7	3188/–17	0.4/–5.8	3139/–9	0.6/–2.8	3141/–7	0.4/–2.9
48 $\nu(\text{C}_2\text{--H}_4)$ +28 $\nu(\text{C}_2\text{--H}_5)$ +21 $\nu(\text{C}_2\text{--H}_6)$	3078/–23	9.9/9.1	3078/–23	9.4/8.7	3041/–98	12.6/1.6	3044/–95	11.1/0.1
43 $\nu(\text{C}_3\text{--H}_9)$ +27 $\nu(\text{C}_3\text{--H}_7)$ +26 $\nu(\text{C}_3\text{--H}_8)$	3071/–14	6.7/0.4	3073/–12	4.2/–2.0	3038/–2	4.6/–4.8	3041/1	2.7/–6.5
$\nu(\text{S--O})$	1071/–24	112.1/6.7	1053/–41	133.6/35.2	1030/–21	112.1/3.8	1024/–27	92.8/43.2
$\nu(\text{S--C})$	701/–19	4.9/–12.8	704/–16	5.5/–12.3	631/8	4.9/–4.0	667/44	7.2/–1.7
$\tau(\text{O}_{12}\text{H}_{11}\dots\text{O}_{10}\text{S}_1)$	704	69.5	719	114.1	698	107.5	698	145.3
$\delta(\text{O}_{12}\text{H}_{11}\dots\text{O}_{10})$	442	134.3	462	70.1	478	158.8	452	56.6
$\tau(\text{O}_{14}\dots\text{H}_{13}\text{O}_{12}\text{H}_{11})$	-	-	356	61.1	-	-	341	61.3
$\delta(\text{H}_{15}\text{O}_{14}\dots\text{H}_{13})$	-	-	247	55.7	-	-	198	46.7
$\nu(\text{O}_{10}\dots\text{H}_{11})$	212	17.8	203	23.8	209	11.3	195	12.6
$\nu(\text{O}_{10}\dots\text{H}_{15})$	-	-	178	1.1	-	-	151	1.4
$\delta(\text{H}_{11}\dots\text{O}_{10}\text{S}_1)$	106	28.8	101	24.9	98	24.7	88	22.4
$\nu(\text{O}_{14}\dots\text{H}_{13})$	-	-	85	3.8	-	-	62	4.6

Table 3. Calculated vibrational characteristics (ν in cm^{-1} , A in $\text{km}\cdot\text{mol}^{-1}$) and changes in the vibrational characteristics ($\Delta\nu$ in cm^{-1} , ΔA in $\text{km}\cdot\text{mol}^{-1}$) from monomers to a complex for the hydrogen-bonded systems DESO–H₂O (1:1) and DESO–2H₂O (1:2).

Mode	MP2/6-311++G(d,p)				B3LYP/6-311++G(d,p)			
	1:1		1:2		1:1		1:2	
	$\nu_i^{\text{compl.}}/\Delta\nu_i$	$A_i^{\text{compl.}}/\Delta A_i$						
$\nu(\text{O}_{18}\text{--H}_{17})$	3583/–290	471.7/458.6	3753/–120	228.4/215.3	3479/–338	537.1/527.8	3669/–148	293.3/284.1
$\nu(\text{O}_{18}\text{--H}_{19})$	3933/–62	80.2/19.3	3890/–105	134.3/73.4	3890/–33	59.4/2.3	3832/–91	109.9/52.9
$\nu(\text{O}_{20}\text{--H}_{21})$	-	-	3670/–203	444.7/431.6	-	-	3579/–238	476.3/467.1
$\nu(\text{O}_{20}\text{--H}_{22})$	-	-	3951/–44	109.9/19.0	-	-	3887/–36	87.1/30.1
$56\nu(\text{C}_7\text{--H}_{13})+27\nu(\text{C}_1\text{--H}_{15})$	3181/–9	8.1/3.5	3183/–6	7.4/2.8	3122/3	12.3/–2.2	3124/5	8.9/–5.6
$48\nu(\text{C}_4\text{--H}_{11})+12\nu(\text{C}_4\text{--H}_{12})$	3174/–3	13.2/–1.2	3179/2	10.8/–3.6	3118/2	9.2/–11.3	3123/9	7.6/–12.8
$59\nu(\text{C}_4\text{--H}_{10})+38\nu(\text{C}_4\text{--H}_{12})$	3168/102	9.6/–3.2	3173/107	9.6/–3.2	3108/76	0.8/–15.3	3108/76	1.1/–15.0
$56\nu(\text{C}_7\text{--H}_{14})+31\nu(\text{C}_7\text{--H}_{15})$	3164/–3	10.2/–10.8	3161/–6	4.4/–16.6	3098/64	17.1/–8.1	3102/68	17.7/–7.5
$41\nu(\text{C}_3\text{--H}_9)+21\nu(\text{C}_3\text{--H}_8)$	3157/–19	2.9/–11.1	3157/–19	6.5/–7.4	3094/54	13.0/–4.7	3097/57	17.7/0.1
$31\nu(\text{C}_2\text{--H}_6)+18\nu(\text{C}_2\text{--H}_5)$	3153/51	2.5/–3.7	3155/53	1.8/–4.5	3092/39	10.4/–3.2	3096/43	2.3/–4.2
$+26\nu(\text{C}_4\text{--H}_{11})$								
$61\nu(\text{C}_2\text{--H}_5)+36\nu(\text{C}_2\text{--H}_6)$	3089/–80	2.8/–7.6	3091/–78	1.2/–9.2	3057/–44	1.9/–12.8	3062/–39	0.0/–14.6
$52\nu(\text{C}_3\text{--H}_8)+38\nu(\text{C}_3\text{--H}_9)$	3079/–66	19.3/18	3081/–64	17.2/16.0	3047/–43	14.6/12.8	3047/–43	10.8/8.9
$30\nu(\text{C}_4\text{--H}_{12})+28\nu(\text{C}_4\text{--H}_{11})$	3077/–73	5.3/–9.3	3079/–71	12.8/–1.7	3035/–57	23.7/5.0	3037/–55	20.8/6.1
$+26\nu(\text{C}_4\text{--H}_{10})$								
$40\nu(\text{C}_7\text{--H}_{14})+33\nu(\text{C}_7\text{--H}_{15})$	3075/–82	19.4/6.9	3077/–80	10.1/–2.4	3032/–62	17.8/2.4	3036/–58	17.6/2.23
$+26\nu(\text{C}_7\text{--H}_{13})$								
$\nu(\text{S--O})$	1032/–28	104.9/34.0	989/–71	133.1/62.3	984/–30	60.8/–10.1	955/–59	158.5/87.5
$\nu(\text{S--C})$	724/63	45.6/36.8	727/66	58.1/49.2	657/5	33.7/11.5	702/50	46.8/27.6
$\tau(\text{O}_{18}\text{H}_{17}\dots\text{O}_{16}\text{S}_1)$	692	61.3	459	55.7	697	102.7	442	63.0
$\delta(\text{H}_{21}\text{O}_{20}\dots\text{H}_{19})$	-	-	695	118.1	-	-	702	175.2
$\delta(\text{O}_{16}\dots\text{H}_{17}\text{O}_{18})$	458	110.6	616	204.1	458	153.5	649	194.7
$\tau(\text{O}_{20}\dots\text{H}_{19}\text{O}_{18}\text{H}_{17})$	-	-	398	95.9	-	-	367	112.1
$\tau(\text{O}_{16}\dots\text{H}_{21}\text{O}_{20}\text{H}_{22})$	-	-	356	61.1	-	-	341	61.3
$\nu(\text{O}_{16}\dots\text{H}_{21})$	-	-	304	28.1	-	-	335	24.8
$\tau(\text{H}_{19}\text{O}_{18}\text{H}_{17}\dots\text{O}_{16})$	272	114.4	150	91.1	253	111.1	156	125.3
$\nu(\text{O}_{16}\dots\text{H}_{17})$	240	31.5	202	30.1	243	20.2	257	24.1
$\delta(\text{S}_1\text{O}_{16}\dots\text{H}_{17})$	109	13.1	137	8.1	91	18.4	146	10.5
$\delta(\text{O}_{20}\dots\text{H}_{19}\text{O}_{18})$	-	-	133	3.4	-	-	138	10.5
$\nu(\text{O}_{20}\dots\text{H}_{19})$	-	-	73	3.4	-	-	146	0.5

Changes in the vibrational characteristics of the stretching O–H modes

As can be seen from the results in Tables 2 and 3, the predicted changes in the vibrational characteristics of the stretching O–H vibrations are the most considerable. For the complexes of DMSO with one and two water molecules (Table 2) the MP2/6-311++G(d,p) and B3LYP/6-311++G(d,p) calculations predict considerable changes in the vibrational frequencies and IR intensities for the stretching vibrations $\nu(\text{O}_{12}\text{--H}_{11})$ and $\nu(\text{O}_{14}\text{--H}_{15})$. The predicted frequency shifts for the stretching vibrations $\nu(\text{O}_{12}\text{--H}_{11})$ in the complex **1** (1:1) are in the range of -282 cm^{-1} to -319 cm^{-1} and for $\nu(\text{O}_{14}\text{--H}_{15})$ in the complex **2** (1:2) are from -225 to -221 cm^{-1} . The IR intensity of these vibrations increases dramatically upon hydrogen bonding. In the same time the changes in the vibrational characteristics for the vibrations $\nu(\text{O}_{12}\text{--H}_{13})$ and $\nu(\text{O}_{14}\text{--H}_{16})$ are negligibly. Bearing in mind these results it could be concluded that the stretching vibrations $\nu(\text{O}_{12}\text{--H}_{11})$

and $\nu(\text{O}_{14}\text{--H}_{15})$ (in the complex 1:2) taking part in the hydrogen bonding with DMSO, while the vibrations $\nu(\text{O}_{12}\text{--H}_{13})$ (in the complex 1:1) and $\nu(\text{O}_{14}\text{--H}_{16})$ (in the complex 1:2) are free from the hydrogen bonding.

For the hydrogen-bonded complexes of one and two water molecules with DESO the predicted changes in the vibrational characteristics for the stretching O–H vibrations show that the bonds $\text{O}_{18}\text{--H}_{17}$ and $\text{O}_{20}\text{--H}_{21}$ are taking part in the hydrogen bonding. Their frequencies are shifted to lower values more than -200 cm^{-1} . The IR intensities of these vibrations increase dramatically in the complexes. In the same time the vibrational characteristics of the modes $\nu(\text{O}_{18}\text{--H}_{19})$ (in the complex 1:1) and $\nu(\text{O}_{20}\text{--H}_{22})$ (in the complex 1:2) are changed negligibly. These vibrations are free from the hydrogen bonding.

Changes in the vibrational characteristics of the stretching S=O modes

As can be seen from the optimized structures of

the hydrogen-bonded systems between one and two water molecules with DMSO and DESO, shown on Figs. 1 and 2, the hydrogen bonds are formed between O–H group from water molecules and S=O group from DMSO and DESO. The experimental evidences based on the Raman and FT IR ATR studies of these hydrogen-bonded systems [16] also confirm that the S=O group is taking part in the hydrogen bonding: “The lower frequency peak near 1010 cm^{-1} both in the Raman and IR spectra, whose intensity of which increases with dilution with a simultaneous shift to lower frequency, is attributed to the $\nu(\text{SO})$ directly involved in H-bonds with water molecules only”. Bearing in mind this statement the changes in the S=O stretching vibrations upon hydrogen bonding are studied here by *ab initio* and DFT calculations with 6-311++G(d,p) basis set.

It was established for the hydrogen-bonded systems between one and two water molecules and DMSO (see Table 2) that the stretching vibration $\nu(\text{S=O})$ is shifted in the complexes (1:1; 1:2) to lower frequencies of about 24 cm^{-1} for the complex **1** (1:1) and of about 41 cm^{-1} for the complex **2** (1:2). The experimentally observed frequency shift [11] for this vibration is 8 cm^{-1} . The calculations show that the IR intensity of the stretching vibration $\nu(\text{S=O})$ increases in the complexes. As a consequence the double character of the S=O bond decreases, becoming more polar: $\text{S=O} \leftrightarrow \text{S}^+ - \text{O}^-$.

For the hydrogen-bonded systems of one and two water molecules with DESO (see Table 3) the observed appearances are the same as for the systems DMSO–H₂O (1:1; 1:2) only at higher extent. The predicted frequencies shifts by *ab initio* and DFT calculations at 6-311++G(d,p) basis set of the stretching vibration $\nu(\text{S=O})$ for the hydrogen-bonded systems DESO–H₂O (1:1; 1:2) are larger and the IR intensity increases in these complexes at higher extent. It can conclude that the water-sulfur dioxide interactions in the hydrogen-bonded systems DESO–H₂O (1:1; 1:2) are stronger than in the DMSO–H₂O (1:1; 1:2) systems.

Changes in the vibrational characteristics of the stretching C–H modes

The predicted values of the vibrational characteristics for the hydrogen-bonded systems of one and two water molecules with DMSO and DESO, presented in Tables 2 and 3 show that for the stretching C–H modes they are also sensitive to the complexations.

The potential energy distribution (PED), based on the MP2/6-311++G(d,p) calculations shows that for the hydrogen-bonded systems DMSO–H₂O (1:1; 1:2) the $\nu(\text{C}_2\text{–H})$ vibrations are more sensitive to the

complexation than the $\nu(\text{C}_3\text{–H})$ vibrations. In agreement with the experiment [16] the $\nu(\text{C}_2\text{–H})$ vibrations are shifted to higher frequency more than 100 cm^{-1} by water dilution and their IR intensities are changed negligibly.

The similar changes are observed for the stretching vibrations $\nu(\text{C}_2\text{–H})$ and $\nu(\text{C}_4\text{–H})$ of the hydrogen-bonded systems DESO–H₂O (1:1; 1:2) (see Table 3). Bearing in mind the experimental results from Raman and FT IR ATR spectra of these hydrogen-bonded systems the authors [16] supposed, “This effect could be due to the breaking of the hydrogen bonds CH...OS, the existence of which has been evidenced in both pure liquid DMSO and DESO”.

The $\nu(\text{C}_3\text{–H})$ vibrations for the hydrogen-bonded systems DMSO–H₂O (1:1; 1:2) and $\nu(\text{C}_3\text{–H})$, and $\nu(\text{C}_7\text{–H})$ for the hydrogen-bonded systems DESO–H₂O (1:1; 1:2) are shifted to lower frequency in the complexes. These bonds become weaker upon hydrogen bonding.

Intermolecular vibrations

The results from potential energy distribution (PED), obtained from MP2/6-311++G(d,p) calculations show that the hydrogen bonding of one and two water molecules with DMSO and DESO molecules leads to arising of the intermolecular vibrations (see Tables 2 and 3).

The stretching intermolecular vibrations for the hydrogen-bonded system water–DMSO (1:1; 1:2) are predicted with B3LYP/6-311++G(d,p) calculations in the range: from 62 cm^{-1} to 195 cm^{-1} (see Table 2). For the complexes water–DESO (1:1; 1:2) the predicted stretching $\nu(\text{O...H})$ vibrations are: from 146 cm^{-1} to 335 cm^{-1} (see Table 3). The calculated IR intensities of the stretching intermolecular vibrations for the complexes DMSO–H₂O (1:1; 1:2) and DESO–H₂O (1:1; 1:2) are low.

Having in mind the PED distribution, the torsional intermolecular vibrations for the studied hydrogen-bonded systems are in the range $156\text{--}698\text{ cm}^{-1}$ with medium IR intensities.

The predicted frequencies for the deformation vibrations are at lower wavenumbers in comparison with the frequencies of the torsional intermolecular vibrations. Their IR intensities are higher in comparison with the IR intensities of the torsional intermolecular vibrations for the studied hydrogen-bonded systems.

CONCLUSIONS

The structures, stability and vibrational spectra of the hydrogen-bonded complexes of one and two

water molecules with DMSO and DESO molecules have been studied using *ab initio* MP2 and DFT calculations. The main results of the study are:

- The hydrogen bonding of two water molecules with DMSO and DESO molecules leads to the formation of cyclic structures, while the hydrogen-bonded systems of one water molecule with DMSO and DESO are open.

- It was established that the hydrogen-bonded systems DESO–water (1:1, 1:2) are more stable than the systems DMSO–water (1:1, 1:2).

- The predicted changes in the vibrational characteristics for the stretching S=O and C–H vibrations in the complexes DMSO–H₂O (1:1; 1:2) and DESO–H₂O (1:1; 1:2) are in good agreement with the experiment. Having in mind this result, it could be concluded that the optimized structures are reliable.

Acknowledgements: *The financial support by the Bulgarian National Science Fund, contract X-1510 is gratefully acknowledged.*

REFERENCES

1. D. Hadzi, *Theoretical Treatment of Hydrogen Bonding*, John Wiley and Sons, New York, 1997.
2. J. E. Del Bene, I. Shavitt, *Intermolecular Interaction: From van der Waals to Strongly Bound Complexes*, S. Scheiner (ed.), Wiley, Chichester, West Sussex, 1997, p. 157–179.
3. Y. Dimitrova, *Rec. Res. Dev. Phys. Chem.*, **3**, 133 (1999).
4. Y. Dimitrova, *Rec. Res. Dev. Phys. Chem.*, **6**, 127 (2002).
5. J. Poater, X. Fradera, M. Sola, M. Duran, S. Simon, *Chem. Phys. Lett.*, **369**, 248 (2003).
6. Y. Dimitrova, *Trends Appl. Spectrosc.*, **6**, 43 (2007).
7. L. Pu, Q. Wang, Y. Zhang, Q. Miao, Y.-S. Kim, Z. Zhang, *Adv. Quant. Chem.*, **54**, 271 (2008).
8. B. Kojic-Prodic, K. Molcanov, *Acta Chim. Slovenia*, **55**, 692 (2008).
9. J. R. Scherer, M. K. Go, S. Kint, *J. Phys. Chem.*, **77**, 2108 (1973).
10. A. Beroluzza, S. Bonora, M. A. Mattaglia, P. Monti, *J. Raman Spectrosc.*, **8**, 231 (1979).
11. M. I. S. Sastry, S. Singh, *J. Raman Spectrosc.*, **15**, 80 (1984).
12. L. Rintoul, H. F. Shurvell, *J. Raman Spectrosc.*, **21**, 5 (1990).
13. W. N. Martens, R. L. Frost, J. Kristof, J. T. Klopogge, *J. Raman Spectrosc.*, **33**, 84 (2002).
14. S. A. Markarian, L. S. Gabrielian, S. Bonora, C. Fagnano, *Spectrochim. Acta, Part A*, **59**, 575 (2003).
15. S. A. Markarian, A. A. Poladyan, G. R. Kirakosyan, A. A. Trchounian, K. A. Bagramyan, *Lett. Appl. Microbiol.*, **34**, 417 (2002).
16. S.A. Markarian, A.L. Zatikyan, S. Bonora, C. Fagnano, *J.Mol.Struct.*, 655, 285 (2003).
17. M. J. Frisch, G. W. Trucks, H. B. Schlegel, G. E. Scuseria, M. A. Robb, J. R. Cheeseman, V. G. Zakrzewski, J. A. Montgomery, Jr., R. E. Stratmann, J. C. Burant, S. Dapprich, J. M. Millam, A. D. Daniels, K. N. Kudin, M. C. Strain, O. Farkas, J. Tomasi, V. Barone, M. Cossi, R. Cammi, B. Mennucci, C. Pomelli, C. Adamo, S. Clifford, J. Ochterski, G. A. Petersson, P. Y. Ayala, Q. Cui, K. Morokuma, D. K. Malick, A. D. Rabuck, K. Raghavachari, J. B. Foresman, J. Cioslowski, J. V. Ortiz, A. G. Baboul, B. B. Stefanov, G. Liu, A. Liashenko, P. Piskorz, I. Komaromi, R. Gomperts, R. L. Martin, D. J. Fox, T. Keith, M. A. Al-Laham, C. Y. Peng, A. Nanayakkara, C. Gonzalez, M. Challacombe, P. M. W. Gill, B. Johnson, W. Chen, M. W. Wong, J. L. Andres, C. Gonzalez, M. Head-Gordon, E. S. Replogle, J. A. Pople, Gaussian 98, Revision A.7, Gaussian Inc., Pittsburgh PA, 1998.
18. R.G. Parr, W. Yang, *Density-Functional Theory of Atoms and Molecules*, Oxford University Press, Oxford, 1989.
19. A. D. Becke, *J. Chem. Phys.*, **98**, 5648 (1993).

ВОДОРОДНО-СВЪРЗАНИ СИСТЕМИ НА ВОДА С ДИМЕТИЛ- И ДИЕТИЛСУЛФОКСИДИ. ТЕОРЕТИЧНО ИЗСЛЕДВАНЕ НА СТРУКТУРИ, СТАБИЛНОСТ И ВИБРАЦИОННИ СПЕКТРИ

Й. Димитрова

*Институт по органична химия с център по фитохимия, Българска академия на науките,
ул. „акад. Г. Бончев“ бл. 9, 1113 София*

Постъпила на 9 януари 2009 г.; Преработена на 11 юни 2009 г.

(Резюме)

Изследвани са структурните и вибрационните характеристики на водородно-свързаните системи диметилсулфоксид (ДМСО)–вода (1:1, 1:2) и диетилсулфоксид (ДЕСО)–вода (1:1, 1:2) посредством *ab initio* и ТФП пресмятания с различни базисни набори. Пресмятанията показват, че оптимизираните структури на изследваните системи 1:2 са циклични, докато оптимизираните структури на водородно-свързаните системи 1:1 са линейни. Коригираните стойности на енергията на свързване за водородно-свързаните системи са изчислени посредством *ab initio* и ТФП пресмятания с различни базисни набори с цел да се оцени тяхната стабилност. Установено е, че водородно-свързаните системи ДЕСО–вода (1:1, 1:2) са по-стабилни от системите ДМСО–вода (1:1, 1:2). Изследвано е влиянието на водородното свързване върху свойствата на мономерите (H_2O , ДМСО и ДЕСО). Установено е, че водородното свързване води до промени във вибрационните характеристики (вибрационни честоти и интензивности на ивиците) на мономерите. Предсказаните вибрационни характеристики за изследваните водородно-свързаните системи са в много добро съгласие с експериментално наблюдаваните.

Synthesis and antimicrobial activity of pyrazole derivatives via 1,3-dipolar cycloaddition of nitrile imines with ethyl acetoacetate

K. B. Umesha^{1*}, K. M. L. Rai²

¹Department of Chemistry, Yuvaraja's College, University of Mysore, Mysore - 570 005, India

²Department of Studies in Chemistry, University of Mysore, Manasagangothri, Mysore - 570 006, India

September 17, 2008; Revised June 18, 2009

The ethyl acetoacetate reacts with the nitrile imines generated *in situ* by the catalytic dehydrogenation of diphenyl hydrazones using chloramine-T (CAT) to afford regioselective cycloadducts in 80% yields respectively. The structures of these compounds have been characterized by FT-IR, ¹H NMR, ¹³C NMR and mass spectroscopic techniques and elemental analysis. All the pyrazole derivatives have been tested for their antibacterial and antifungal activities.

Key words: 1,3-dipolar cycloaddition, nitrile imines, pyrazoles.

INTRODUCTION

Heterocyclic compounds are considered as the most promising molecules for the design of new drugs. 1,3-Dipolar cycloaddition reactions are an efficient synthetic tool for constructing biologically potent five membered heterocyclic compounds [1, 2]. Pyrazoles, pyrazolines, pyrazolidines and pyrazolones are gaining importances as biologically active compounds possessing such as analgesic, antipyretic, antiinflammatory, germicidal and antifungal activities [3, 4], antiprotozoal [5], fungicidal [6], bactericidal [6], herbicidal and plant growth regulating properties.

Apart from the various dipolar reagent nitrile imines are used in numerous 1,3-dipolar cycloaddition reaction leading to pyrazoles, pyrazolines, pyrazolidines and other heterocyclic compounds [7]. Huisgen and co-workers first reported [8] the authentic *in situ* generation of nitrile imines by the thermolysis of 2,5-diphenyl tetrazole in the presence of ethyl phenyl propiolate and obtained 2,3,5-triphenyl carbethoxypyrazole. The usual synthesis of nitrile imines involves the thermolysis or photolysis of tetrazole [8], oxidation of aldehyde hydrazones with lead tetra acetate [9], CAT [10] and mercuric acetate [11].

In addition to this, nitrile imines are known to react with heterocyclic compounds to yield a variety of polyheterocycles [12]. Shawali and co-workers [13] prepared a numerous pyrazole derivatives by the reaction of *in situ* generated nitrile imines obtained from hydrazidoyl halides with sodium salt of active methylene compounds, such as β -keto-

sulphones, β -ketoanilides and β -cyanoketones. Baruah *et al.* [14] generated the *C*-acetyl and *C*-ethoxycarbonyl nitrile imines *in situ* from the corresponding hydrazoneyl halides in the presence of dry triethylamine in anhydrous chloroform, and have used these nitrile imines for the preparation of pyrazoles derivatives. The intramolecular cycloaddition of *in situ* generated nitrile imine with aldonitrone afforded triazoles [15]. Mogilaiah *et al.* [16] developed a solvent free method for the facile synthesis of 1,8-naphthyridinyl-pyrazoles using POCl₃-DMF (Vilsmeier-Haack reagent) over silica gel under microwave irradiation. Aly *et al.* [17] showed a new synthetic route for the synthesis of some pyrazole derivatives from 3-aryl-1-phenyl-1*H*-pyrazole-4-carbaldehydes.

Padmavathi and co-workers [18] prepared activated *bis* pyrazolines and *bis* isoxazolines by 1,3-dipolar cycloaddition of nitrile imines and nitrile oxides to activated *bis* olefinic systems in the presence of Chloramine-T. Bacchetti [19] prepared 1,4-dicarboethoxy pyrazoles by intermolecular cycloaddition of nitrile imines with ethyl acetoacetate. Though there are more references available in the literature on cycloaddition of nitrile imines with alkenes and alkyne, there is a less information about the use of keto-enol tautomers as dienophile for the cycloaddition. We have synthesized [20] the 1-(5-methyl-1,3-diphenyl-1*H*-pyrazol-4-yl)-ethanone in quantitative yield *via* 1,3-dipolar cycloaddition of enol form of acetyl acetone with the nitrile imines generated *in situ* by the catalytic dehydrogenation of diphenyl hydrazones using CAT. This prompted us to work in this area in detail to make it as a general method for the synthesis of pyrazoles derivatives.

* To whom all correspondence should be sent:
E-mail: kbu68umesha@rediffmail.com

RESULTS AND DISCUSSION

It is well known that acetyl acetone and ethyl acetoacetate exist in two dynamic equilibrium states *via*, keto and enol forms. It is also known that typical cycloaddition of nitrile imines with alkenes and alkynes afford pyrazolines and pyrazoles respectively. It is interesting to note that, though the expected products are pyrazolines as similar to that of addition of nitrile imines to alkenes, the reaction afforded pyrazoles with loss of water molecule (Scheme).

In typical reaction, a mixture of aldehyde hydrazone **1a** with excess of ethyl acetoacetate **3** and CAT in glacial acetic acid was stirred at room temperature for about 2–3 hours. After the usual work up, **5a** was isolated as light yellow oil in 80% yield. In similar manner, **1b–g** were converted into the corresponding pyrazole derivatives **5b–g** in good yields. IR, ¹H NMR, ¹³C NMR, MS studies and elemental analysis provide the structural proof for the products. In ¹H NMR spectra, the signals for the ethoxy protons appears as a quartet in the region δ 4.12–4.31 ppm, (2H, *J* = 7.2 Hz, –OCH₂–CH₃), while the protons for the methyl group at C-5 appear as a singlet in the region δ 2.68–2.75 ppm. The downward shift of the methyl group at the C-5 is probably due to deshielding by the –CO–OC₂H₅ group. These observations clearly indicate that the formation of the cycloadduct **5a** is obtained *via* pyrazolines **4** with the loss of water molecule. In ¹³C NMR spectra, the –C-3 and C-4 appear as singlet (decoupled) in the region δ 160.82–161.14 and δ 108.32–118.86 ppm respectively, C-5 appear as singlet in the region δ 176.14–176.26 ppm. All cycloadducts showed M+1 as a base peak in the mass spectra. Further, the elemental analysis supported the formation of the products.

ANTIMICROBIAL SCREENING

Synthesized pyrazoles (**5a–g**) were screened (dose of 100 µg) for their antibacterial activity against Gram-negative bacteria *Escherichia coli* (*E. coli*) and Gram-positive bacteria *Staphylococcus aureus* (*S. aureus*) using filter paper disc method [21]. Plates inoculated with *E. coli* were incubated for 48 h and plates inoculated with *S. aureus* for 24 h respectively at room temperature. *Streptomycin sulphate* was used as a standard. After the period of incubation the inhibition zones were measured in mm and results obtained are shown in Table 1. All the compounds were also screened (dose of 100 µg) for their antifungal activity against *Candida albicans* (*C. albicans*) and *Aspergillus niger* (*A. niger*) using *Griseofulvin* as a standard. The results are

shown in Table 1.

Compared with *Streptomycin sulphate* the compounds **5b** and **5e–g** showed moderate antibacterial activity against *E. coli* and **5b** and **5f** against *S. aureus*. Compared with the standard *Griseofulvin* the compounds **5b–c**, **5e** and **5f** showed promising antifungal activity against *C. albicans* and **5f** against *A. niger*.

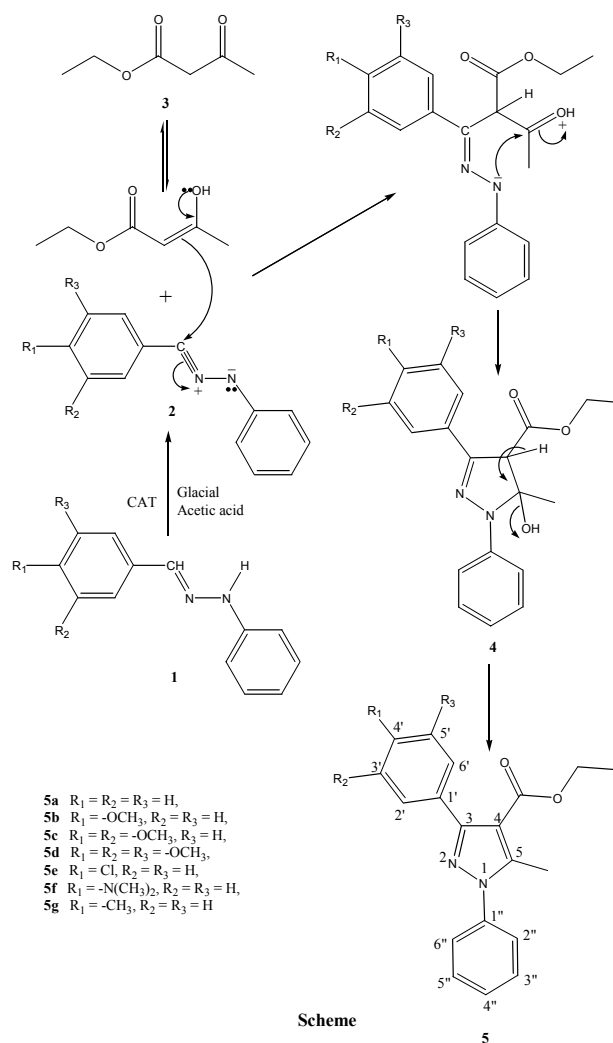


Table 1. Antibacterial and antifungal activity of synthesized pyrazole derivatives (**5a–g**). (Zone of inhibition in mm).

Compounds	Antibacterial activity		Antifungal activity	
	<i>E. coli</i>	<i>S. aureus</i>	<i>C. albicans</i>	<i>A. niger</i>
5a	08	10	06	06
5b	12	12	08	06
5c	10	08	08	04
5d	10	08	06	04
5e	12	10	08	06
5f	14	12	10	08
5g	12	10	06	04
<i>Streptomycin sulphate</i>	18	20	Not tested	Not tested
<i>Griseofulvin</i>	Not tested	Not tested	14	12

EXPERIMENTAL SECTION

The purity of all synthesized compounds was checked by thin layer chromatography using silica gel G. The final compounds were purified by column chromatography on silica gel (70–230 mesh, Merck) using mixture of chloroform:acetone (7:1) as eluent. ^1H NMR spectra were registered either on a Bruker 300 MHz or Jeol 60 MHz Hitachi Perkin Elmer spectrometer, and ^{13}C NMR spectra on a Jeol GSX 400 (75 MHz) instrument using 1% tetramethylsilane in CDCl_3 as an internal standard (chemical shifts are expressed in δ , ppm downfield from the tetramethylsilane). Mass spectra were obtained on an electron impact Maspec MSW 9629 spectrometer and important fragments are given with the relative intensities in brackets.

Typical procedure for the preparation of ethyl 5-methyl-1,3-diphenyl-1H-pyrazole-4-carboxylate (5a): A mixture of benzaldehyde hydrazone (**1a**, 2.35 g, 12.0 mmol), excess of freshly distilled ethyl acetoacetate **3** (2.6 g, 20.0 mmol) and CAT (3.94 g, 14.0 mmol) in glacial acetic acid (25 ml) were stirred at room temperature for 2–3 h. The progress of the reaction was monitored by TLC. After the completion of the reaction the residue was dissolved in ether (25 ml), washed successively with water (2 \times 20 ml), 1 N NaOH (1 \times 10 ml), brine solution (2 \times 15 ml) and dried over Na_2SO_4 . Evaporation of the solvent afforded crude oily substance. Purification was done by column chromatography using a mixture of dichloromethane:ethyl acetate (8:1) as eluent, which afforded **5a** as light yellow oil in 80% yield (2.93 g). The pyrazole **5a** showed IR bands (Nujol) ν : 1722 cm^{-1} (C=O), 1620 cm^{-1} (C=N), 1602 cm^{-1} (C=C); ^1H NMR (CDCl_3) δ : 1.24 (t, 3H, $J = 7.2$ Hz, $-\text{OCH}_2-\text{CH}_3$), 2.72 (s, 3H, $\text{H}_3\text{C}-\text{C}(5)$), 4.18 (q, 2H, $J = 7.2$ Hz, $-\text{OCH}_2-\text{CH}_3$), 7.05–7.26 (s, 5H, $\text{Ar}'-\text{H}$), 7.65–7.78 (m, 5H, $\text{Ar}''-\text{H}$); ^{13}C NMR (CDCl_3) δ : 0.92 (q, 1C, $\text{H}_3\text{C}-\text{C}(5)$), 13.56 (q, 1C, $-\text{CH}_2-\text{CH}_3$), 58.62 (t, 1C, $-\text{CH}_2-$), 108.32 (s, 1C), 118.08 (d, 2C), 124.42 (d, 1C), 124.56 (d, 2C), 126.22 (d, 2C), 128.74 (d, 2C), 130.28 (s, 1C), 131.08 (d, 1C), 132.42 (s, 1C), 161.12 (s, 1C), 176.22* (s, 1C, 5-C), 174.88* (s, 1C, CO). MS (relative intensity) m/e for $\text{C}_{19}\text{H}_{18}\text{N}_2\text{O}_2$: 307 (M+1, 100), 277(31), 233 (38), 218 (21), 194 (25), 112 (18), 103 (75), 91 (44), 88 (10), 29(22). Anal. Calcd: C, 74.49; H, 5.92; N, 9.14%. Found: C, 74.36; H, 5.72; N, 9.08%.

Ethyl 3-(4-methoxyphenyl)-5-methyl-1-phenyl-1H-pyrazole-4-carboxylate (5b): Obtained from 4-methoxybenzaldehyde hydrazone **1b** (2.71 g, 12 mmol), ethyl acetoacetate (2.6 g, 20.0 mmol) as an oily substance in 78% yield (3.14 g). IR bands (Nujol) ν : 1716 cm^{-1} (C=O), 1618 cm^{-1} (C=N), 1596 cm^{-1}

(C=C); ^1H NMR (CDCl_3): δ 1.18 (t, 3H, $J = 6.9$ Hz, $-\text{OCH}_2-\text{CH}_3$), 2.75 (s, 3H, $\text{H}_3\text{C}-\text{C}(5)$), 3.78 (s, 3H, $-\text{OCH}_3$), 4.12 (q, 2H, $J = 7.0$ Hz, $-\text{OCH}_2-\text{CH}_3$), 6.92 (d, 2H, $\text{Ar}'-\text{H}$), 7.22 (d, 2H, $\text{Ar}'-\text{H}$), 7.36–7.48 (m, 5H, $\text{Ar}''-\text{H}$); ^{13}C NMR (CDCl_3) δ : 0.86 (q, 1C, $\text{H}_3\text{C}-\text{C}(5)$), 13.54 (q, 1C, $-\text{CH}_2-\text{CH}_3$), 55.80 (q, 1C, $4'-\text{OCH}_3$), 58.62 (t, 1C, $-\text{CH}_2-$), 108.52 (s, 1C), 118.18 (d, 2C), 122.56 (d, 2C), 124.88 (d, 1C), 126.22 (d, 2C), 128.74 (d, 2C), 136.28 (s, 1C), 131.08 (d, 1C), 132.42 (s, 1C), 160.82 (s, 1C), 176.20* (s, 1C, 5-C), 171.68* (s, 1C, CO). MS (relative intensity) m/e for $\text{C}_{20}\text{H}_{20}\text{N}_2\text{O}_3$: 337 (M+1, 100), 307(32), 263 (40), 248 (20), 224 (24), 112 (16), 133 (78), 91 (46), 88 (10), 29(24). Anal. Calcd: C, 71.41; H, 5.99; N, 8.33%. Found: C, 71.38; H, 5.87; N, 8.25%.

Ethyl 3-(3,4-dimethoxyphenyl)-5-methyl-1-phenyl-1H-pyrazole-4-carboxylate (5c): Obtained from 3,4-dimethoxybenzaldehyde hydrazone **1c** (2.56 g, 10 mmol), ethyl acetoacetate (2.34 g, 18.0 mmol) as an oily substance in 82% yield (2.74 g). IR bands (Nujol) ν : 1720 cm^{-1} (C=O), 1622 cm^{-1} (C=N), 1596 cm^{-1} (C=C); ^1H NMR (CDCl_3) δ : 1.22 (t, 3H, $J = 7.0$ Hz, $-\text{OCH}_2-\text{CH}_3$), 2.68 (s, 3H, $\text{H}_3\text{C}-\text{C}(5)$), 3.75 (s, 6H, $-\text{OCH}_3$), 4.16 (q, 2H, $J = 7.1$ Hz, $-\text{OCH}_2-\text{CH}_3$), 6.98–7.12 (m, 3H, $\text{Ar}'-\text{H}$), 7.48–7.66 (m, 5H, $\text{Ar}''-\text{H}$); ^{13}C NMR (CDCl_3) δ : 1.02 (q, 1C, $\text{H}_3\text{C}-\text{C}(5)$), 13.66 (q, 1C, $-\text{CH}_2-\text{CH}_3$), 55.76* (q, 1C, $4'-\text{OCH}_3$), 55.84* (q, 1C, $3'-\text{OCH}_3$), 59.02 (t, 1C, $-\text{CH}_2-$), 108.86 (s, 1C), 118.28 (d, 2C), 122.52 (d, 2C), 124.86 (d, 1C), 126.34 (d, 2C), 128.78 (d, 2C), 136.36 (s, 1C), 131.12 (d, 1C), 132.44 (s, 1C), 161.14 (s, 1C), 176.24* (s, 1C, 5-C), 171.72* (s, 1C, CO). MS (relative intensity) m/e for $\text{C}_{21}\text{H}_{22}\text{N}_2\text{O}_4$: 367 (M+1, 100), 337(30), 293 (39), 278 (23), 254 (28), 163 (76), 112 (14), 91 (46), 88 (12), 29(26). Anal. Calcd: C, 68.84; H, 6.05; N, 7.65%. Found: C, 68.77; H, 5.96; N, 7.54%.

Ethyl 5-methyl-1-phenyl-3-(3,4,5-trimethoxyphenyl)-1H-pyrazole-4-carboxylate (5d): Obtained from 3,4,5-trimethoxybenzaldehyde hydrazone **1d** (2.86 g, 10 mmol), ethyl acetoacetate (2.34 g, 18.0 mmol) as an oily substance in 81% yield (3.20 g). IR bands (Nujol) ν : 1718 cm^{-1} (C=O), 1620 cm^{-1} (C=N), 1600 cm^{-1} (C=C); ^1H NMR (CDCl_3) δ : 1.26 (t, 3H, $J = 7.1$ Hz, $-\text{OCH}_2-\text{CH}_3$), 2.70 (s, 3H, $\text{H}_3\text{C}-\text{C}(5)$), 3.71 (s, 9H, $-\text{OCH}_3$), 4.22 (q, 2H, $J = 7.2$ Hz, $-\text{OCH}_2-\text{CH}_3$), 6.96 (m, 2H, $\text{Ar}'-\text{H}$), 7.52–7.68 (m, 5H, $\text{Ar}''-\text{H}$); ^{13}C NMR (CDCl_3) δ : 1.04 (q, 1C, $\text{H}_3\text{C}-\text{C}(5)$), 13.62 (q, 1C, $-\text{CH}_2-\text{CH}_3$), 56.6 (q, 2C, $3',5'-\text{OCH}_3$), 58.4 (q, 1C, $4'-\text{OCH}_3$), 59.22 (t, 1C, $-\text{CH}_2-$), 108.66 (s, 1C), 122.28 (d, 2C), 124.66 (d, 1C), 126.48 (d, 2C), 128.56 (d, 2C), 136.54 (s, 1C), 131.24 (d, 1C), 132.46 (s, 1C), 136.12 (d, 2C), 161.04 (s, 1C), 176.22* (s, 1C, 5-C), 169.88* (s, 1C, CO). MS

(relative intensity) m/e for $C_{22}H_{24}N_2O_5$: 397 (M+1, 100), 367(29), 323 (42), 308 (24), 284 (22), 193 (76), 112 (21), 91 (46), 88 (14), 29(30). Anal. Calcd: C, 66.65; H, 6.10; N, 7.07%. Found: C, 66.56; H, 5.98; N, 7.04%.

Ethyl 3-(4-chlorophenyl)-5-methyl-1-phenyl-1H-pyrazole-4-carboxylate (5e). Obtained from 4-chlorobenzaldehyde hydrazone **1e** (2.76 g, 12 mmol), ethyl acetoacetate (2.6 g, 20.0 mmol) as an oily substance in 79% yield (3.21g). IR bands (Nujol) ν : 1724 cm^{-1} (C=O), 1616 cm^{-1} (C=N), 1598 cm^{-1} (C=C); 1H NMR ($CDCl_3$) δ : 1.25 (t, 3H, $J = 7.2$ Hz, $-OCH_2-CH_3$), 2.74 (s, 3H, $H_3C-C(5)$), 4.22 (q, 2H, $J = 7.1$ Hz, $-OCH_2-CH_3$), 6.98 (d, 2H, $Ar'-H$), 7.18 (d, 2H, $Ar'-H$), 7.44–7.60 (m, 5H, $Ar''-H$); ^{13}C NMR ($CDCl_3$) δ : 1.02 (q, 1C, $H_3C-C(5)$), 13.58 (q, 1C, $-CH_2-CH_3$), 59.22 (t, 1C, $-CH_2-$), 108.48 (s, 1C), 123.36 (d, 2C), 124.36 (d, 1C), 127.22 (d, 2C), 128.62 (d, 2C), 134.62 (d, 1C), 132.46 (s, 1C), 136.12 (d, 2C), 138.14 (s, 1C), 161.84 (s, 1C), 176.14* (s, 1C, 5-C), 169.88* (s, 1C, CO). MS (relative intensity) m/e for $C_{19}H_{17}N_2O_2Cl$: 341 (M+1, 100), 311 (30), 267 (41), 252 (18), 228 (34), 137 (76), 112 (16), 91 (42), 88 (12), 29(26). Anal. Calcd: C, 66.96; H, 5.03; N, 8.22%. Found: C, 66.91; H, 4.90; N, 8.16%.

Ethyl 3-(4-N,N-dimethylaminophenyl)-5-methyl-1-phenyl-1H-pyrazole-4-carboxylate (5f). Obtained from 4-N,N-dimethylbenzaldehyde hydrazone **1f** (2.86 g, 12 mmol), ethyl acetoacetate (2.6 g, 20.0 mmol) as an oily substance in 78% yield (3.25 g). IR bands (Nujol) ν : 1728 cm^{-1} (C=O), 1624 cm^{-1} (C=N), 1602 cm^{-1} (C=C); 1H NMR ($CDCl_3$) δ : 1.28 (t, 3H, $J = 6.9$ Hz, $-OCH_2-CH_3$), 2.68 (s, 3H, $H_3C-C(5)$), 2.98 (s, 6H, $-N(CH_3)_2$), 4.31 (q, 2H, $J = 6.8$ Hz, $-OCH_2-CH_3$), 7.08 (d, 2H, $Ar'-H$), 7.24 (d, 2H, $Ar'-H$), 7.48–7.66 (m, 5H, $Ar''-H$); ^{13}C NMR ($CDCl_3$) δ : 1.04 (q, 1C, $H_3C-C(5)$), 13.62 (q, 1C, $-CH_2-CH_3$), 44.36 (q, 2C, $-N(CH_3)_2$), 59.28 (t, 1C, $-CH_2-$), 108.38 (s, 1C), 123.16 (d, 2C), 124.30 (d, 1C), 127.44 (d, 2C), 128.56 (d, 2C), 130.04 (d, 2C), 132.46 (s, 1C), 134.78 (d, 1C), 138.24 (s, 1C), 161.12 (s, 1C), 176.26* (s, 1C, 5-C), 169.36* (s, 1C, CO). MS (relative intensity) m/e for $C_{21}H_{23}N_3O_2$: 350 (M+1, 100), 320 (28), 276 (42), 261 (22), 237 (26), 146 (74), 112 (22), 91 (40), 88 (14), 29(30). Anal. Calcd: C, 72.18; H, 6.63; N, 12.03%. Found: C, 72.12; H, 6.51; N, 11.96%.

Ethyl 5-methyl-1-phenyl-3-p-tolyl-1H-pyrazole-4-carboxylate (5g). Obtained from 4-methylbenzaldehyde hydrazone **1g** (2.10 g, 10 mmol), ethyl acetoacetate (2.08 g, 16.0 mmol) as an oily substance in 80% yield (2.56 g). IR bands (Nujol) ν : 1726 cm^{-1} (C=O), 1626 cm^{-1} (C=N), 1598 cm^{-1} (C=C); 1H NMR ($CDCl_3$) δ : 1.30 (t, 3H, $J = 6.7$ Hz,

$-OCH_2-CH_3$), 2.16 (s, 3H, $H_3C-C(5)$), 2.72 (s, 3H, $-CH_3$), 4.26 (q, 2H, $J = 6.8$ Hz, $-OCH_2-CH_3$), 7.06 (d, 2H, $Ar'-H$), 7.28 (d, 2H, $Ar'-H$), 7.42–7.64 (m, 5H, $Ar''-H$); ^{13}C NMR ($CDCl_3$) δ : 0.96 (q, 1C, $H_3C-C(5)$), 13.58 (q, 1C, $-CH_2-CH_3$), 21.06 (q, 3H, $H_3C-C(4')$), 59.08 (t, 1C, $-CH_2-$), 108.44 (s, 1C), 124.04 (d, 2C), 124.44 (d, 1C), 127.66 (d, 2C), 128.58 (d, 2C), 130.18 (d, 2C), 132.52 (s, 1C), 134.86 (d, 1C), 138.32 (s, 1C), 161.02 (s, 1C), 176.16* (s, 1C, 5-C), 169.22* (s, 1C, CO). MS (relative intensity) m/e for $C_{20}H_{20}N_2O_2$: 321 (M+1, 100), 291(30), 247 (40), 232 (22), 208 (26), 164 (78), 112 (18), 91 (42), 88 (12), 29(26). Anal. Calcd: C, 74.98; H, 6.29; N, 8.74%. Found: C, 74.92; H, 6.17; N, 8.66%.

Acknowledgements: The authors are thankful to the Principal, Yuvaraja's College, University of Mysore, Mysore for providing necessary facilities and constant encouragement and sincere thanks to Dr. Satheesha, Department of Studies in Microbiology, University of Mysore for their help in recording the antimicrobial activity of synthesized compounds. One of the authors (Dr. K. B. Umesha) thanks to the University Grant Commission for sanctioned Minor Research Project (Science).

REFERENCE

1. R. Huisgen, in: 1,3-Dipolar Cycloaddition Chemistry, A. Padwa (ed.), Wiley Interscience, New York, 1984, and references therein.
2. P. Caramella, P. Grunanger in: 1,3-Dipolar Cycloaddition Chemistry, A. Padwa (ed.), Wiley Interscience, New York, 1984, pp. 337.
3. a) The Pharmacological Basis of Therapeutics, 6th ed., A. G. Gilman, L. S. Goodman, A. Gilman, (eds.) Macmillan, New York, 1980, p. 337; b) M. Wachter, M. Ferro, *US Patent*, 4,826,868, (1989), *Chem. Abstr.*, **108**, 186735 (1988); c) D. Argentieri, D. Ritchie, E. Tolman, M. Ferro, M. Wachter, J. Mczick, R. Capetola, *The FASEB J. Antiinflammatory Agents*, **4**, A369 (1988).
4. a) H. V. Sector, J. F. De Bardelaben, *J. Med. Chem.*, **14**, 997 (1971); b) V. J. Bauer, W. J. Fanshawe, H. P. Dalalian, S. R. Safir, E. C. Tocus, C. R. Boshart, *J. Med. Chem.*, **11**, 981 (1968); c) G. Corsi, C. Germani, G. Palazzo, B. Rani Silvest, P. S. Barcellone, *J. Med. Chem.*, **19**, 778 (1976); d) N. N. Dueham, R. W. Chesnut, M. M. Hashen, K. D. Berlin, *J. Med. Chem.*, **19**, 229 (1976).
5. R. J. Bochis, R. A. Dybas, E. F. Rogers, *US Patent*, 4,622,330 (1986); *Chem. Abstr.*, **106**, 102279 (1987).
6. P. N. Dhol, T. E. Achary, A. Nayak, *J. Indian Chem. Soc.*, **52**, 1196 (1975).
7. R. Huisgen, M. Seidel, J. Sauer, J. M. McFarland, G. Wallibillich, *J. Org. Chem.*, **24**, 892 (1959).
8. R. Huisgen, M. Seidel, G. Wallibillich, H. Knupfer, *Tetrahedron*, **17**, 3 (1962).

9. W. A. Gladstone, J. B. Aylward, R. O. C. Norman, *J. Chem. Soc.*, 2587 (1969).
10. K. M. L. Rai, A. Hassner, *Synth. Commun.*, **19**, 2799 (1989).
11. K. M. L. Rai, N. Linganna, *Synth. Commun.*, **27**, 3737 (1997).
12. M. Marky, H. Meier, A. Wunderli, H. Hemigartner, H. Schmidt, H. J. Hansen, *Helv. Chim. Acta*, **61**, 1477 (1978).
13. a) A. S. Shawali, H. M. Hassaneen, *Tetrahedron*, **29**, 121 (1973); b) A. S. Shawali, H. M. Hassaneen, M. Sami, H. M. Fahham, *J. Heterocyclic Chem.*, **13**, 1137 (1976); c) A. S. Shawali, C. Parkanyi, *J. Heterocyclic Chem.*, **17**, 833 (1980).
14. A. K. Baruah, D. Prajapati, J. S. Sandhu, *J. Chem. Soc., Perkin Trans. I*, 1995 (1987); A. K. Baruah, D. Prajapati, J. S. Sandhu, *Tetrahedron*, **44**, 6137 (1988).
15. D. Prajapati, J. S. Sandhu, T. Kametani, H. Nagase, K. Kawai, T. Honda, *Heterocycles*, **23**, 1123 (1985).
16. K. Mogilaiah, C. S. Reddy, *Indian J. Chem., Sec. B*, **41B**, 1450 (2002).
17. E. A. Aly, M. A. El-Borai, M. A. Barren, *Indian J. Chem., Sec. B*, **43B**, 1355 (2004).
18. a) V. Padmavathi, K. Venugopal Reddy, A. Balaiah, A. Padmaja, D. Bhaskar Reddy, *Synth. Commun*, **32**, 1227 (2002); b) V. Padmavathi, K. Venugopal Reddy, A. Balaiah, T. V. Ramana Reddy, D. Bhaskar Reddy, *Heteroatom Chem.*, **13**, 677 (2002); c) V. Padmavathi, K. Venugopal Reddy, A. Padmaja, D. Bhaskar Reddy, *Phosphorus, Sulfur and Silicon*, **178**, 171 (2003).
19. T. Bacchetti, *Gazz. Chem. Ital.*, **91**, 866 (1961).
20. K. B. Umesha, K. M. L. Rai, K. Ajaykumar, *Indian J. Chem., Sec. B*, **41B**, 1450 (2002).
21. Anon., in: Textbook of Pharmacopoeia of India (The Indian Pharmacopoeia), 3rd ed., Ministry of Health and Family Welfare, Government of India, New Delhi, 1996.

СИНТЕЗ И АНТИМИКРОБНА АКТИВНОСТ НА ПИРАЗОЛОВИ ПРОИЗВОДНИ ПОЛУЧЕНИ ЧРЕЗ 1,3-ДИПОЛЯРНО ЦИКЛОПРИСЪЕДИНЯВАНЕ НА НИТРИЛИМИНИ И ЕТИЛАЦЕТОАЦЕТАТ

К. Б. Умеша^{1*}, К. М. Л. Рай²

¹ Департамент по химия, Колеж на Ювараджа, Университет на Майсур, Майсур 570005, Индия

² Департамент за химически изследвания, Университет на Майсур, Манасаганготри, Майсур 570006, Индия

Постъпила на 17 септември 2008 г.; Преработена на 18 юни 2009 г.

(Резюме)

Етилацетоацетат реагира с нитрилимини получени *in situ* чрез каталитично дехидрогениране на дифенилхидразон в присъствие на хлорамин-Т (САТ) до получаване на съответни региоселективни циклоадукти с добив 80%. Структурата на тези съединения е охарактеризирана с ИЧС, ¹H ЯМР, ¹³C ЯМР, масспектрометрия и елементарен анализ. Всички пиразолови производни са изпитани за техните антибактериална и антигъбична активности.

Synthesis of nanoporous carbon from plant wastes and coal treatment products

N. Petrov¹, T. Budinova^{1*}, B. Tsyntsarski¹, B. Petrova¹, D. Teodosiev², N. Boncheva³

¹ Institute of Organic Chemistry, Bulgarian Academy of Sciences, Acad. G. Bonchev St., Block 9, Sofia 1113, Bulgaria

² Space Research Institute, Bulgarian Academy of Sciences, 6 Moskovska St., Sofia 1000, Bulgaria

³ Prof. Asen Zlatarov University, 1 Prof. Yakimov Blvd., Burgas 8010, Bulgaria

Received April 8, 2009; Revised June 25, 2009

Synthetic nanoporous carbons are produced from mixtures containing coal tar pitch and furfural in different proportions. It was determined that the surface area and amount of oxygen containing groups on the surface significantly depend on the composition of the initial mixture. Best quality carbon with developed pore structure with prevailing content of micropores was obtained from the precursor containing 50% furfural. Various oxygen containing structures are established on the synthetic nanoporous carbon surface.

Key words: nanoporous carbon, synthesis, treatment products, plant, coal.

INTRODUCTION

Considerable amount of liquid products is separated during the different thermal treatments (pyrolysis, gasification, etc.) of plant wastes and coals, but efficient exploitation of these liquid products has not been found yet. Therefore there is a need to promote the development of successful solution for their effective utilization. Thus liquid products from pyrolysis of agricultural wastes and low rank coals can be used for the fabrication of monolithic carbon as a precursor for the production of porous carbon. When produced on the base of pyrolysis liquid products, microporous carbons are practically ash free carbons. By using a combination of sources and appropriate methods of treatment, porous carbons with different chemical surface properties could be obtained. Synthetic carbons with various surface chemistry can be obtained by pyrolysis of raw materials containing heteroatoms in different forms or pyrolysis of raw material in the presence of heteroatom-containing substances [1–3]. Other possibility is modification of the carbon surface with heteroatom-containing reagents [4–6].

Investigations are intended to obtain nanoporous carbons with different chemical character of the surface from mixtures of coal tar pitch and biomass treatment products – this could reveal the possibility for effective utilization of pyrolysis liquid products by production of synthetic carbons with wide application area.

The aim of our investigations is the invention and development of process for production of nanoporous carbons with different chemical character of

the surface on the base of coal and plant treatment products. Present work deals with the investigation of the influence of the proportion of the initial mixture from coal tar pitch and furfural on the properties of produced nanoporous carbons.

EXPERIMENTAL

Synthesis procedure

Coal tar pitch with softening point 72°C was heated up to 140°C until melting and furfural was added. The obtained mixtures was treated with conc. H₂SO₄ with continuously stirring until solidification. The solid product obtained was heated up to 600°C in a covered silica crucible with a heating rate of 10°C/min under nitrogen atmosphere (carbonization process). Steam activation with water vapour at 800°C for 1 h of obtained carbonizates was used for nanoporous carbon producing.

Porous carbon characterization

The porous structure of carbon adsorbents was studied by N₂ adsorption at 77 K. The total pore volume (V_{total}) is derived from the amount of N₂ adsorbed at a relative pressure of 0.95, assuming that the pores are then filled with liquid adsorbate. The Dubinin-Radushkevich equation was used to calculate the micropore volume (V_{micro}) [7]. The mesopore volume was calculated by subtracting the amount adsorbed at a relative pressure of 0.1 from that at a relative pressure of 0.95.

Oxygen-containing functional groups.

The amount of oxygen-containing functional groups with increasing acidity was determined by Boehm's method of titration with basic solutions of

* To whom all correspondence should be sent:
E-mail: goriva@orgchm.bas.bg

different base strength (NaHCO₃, Na₂CO₃, NaOH, C₂H₅ONa). For this purpose the samples were agitated for at least 16 h with 0.05 N solutions of the four bases. The amount of Na⁺ ions remaining in the solution is determined by adding an excess of standard HCl and backtitrating [8]. The basic groups content of the oxidized samples is determined with 0.05 N HCl [9].

pH determination

The procedure is as follows: 4.0 g of carbon (ground, undried) is weighed into a 250 ml beaker and 100 ml of water is added. The beaker is covered with a watch glass and heated to boiling temperature for 5 minutes. The mixture is set aside and the supernatant liquid is poured off at 60°C. The decanted portion is cooled down to room temperature and is measured to nearest 0.01 pH.

RESULTS AND DISCUSSION

For the production of synthetic nanoporous carbon, 100 g of the mixture of pitch obtained from apricot stones steam pyrolysis tar and furfural in the proportion 70:30, 60:40, 50:50 and 40:60.

The characterization of initial pitch (Table 1) is valuable for understanding the processes taking place during the preparation and modification of the precursor mixture with H₂SO₄.

Table 1. Elemental analysis of coal tar pitch.

Sample	Softening point, °C	Elemental analysis (daf), %					
		C	H	N	S	O (diff.)	C/H
Pitch initial	72	90.90	4.95	0.90	0.50	2.75	1.53

daf – dry and ash free basis.

Data show, that pitch precursor possess middle value of softening point temperature. The amount of oxygen containing structures is not high. C/H ratio indicates mainly presence of aromatic structures in the pitch.

Content of neutral parts, bases, acids and phenols in the pitch precursor was determined by the following scheme (Fig. 1).

Obtained results are presented in Table 2. Data in Table 2 show, that precursor pitch contains predominantly neutral compounds. The presence of small amounts of phenols, acids and relatively higher amount of organic basis is determined. The results indicate that small quantity of structures can be involved in condensed reaction with formation of higher molecular products to produce solid product. This fact determines the necessity for adding reactive structures to the pitch what will allow easier

solidification of the precursor. We used furfural as reactive structure.

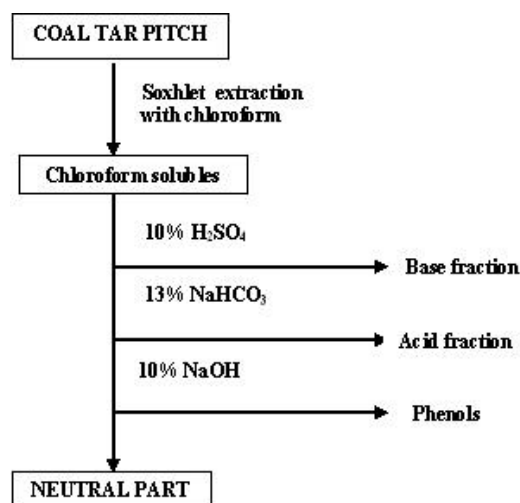


Fig. 1. Scheme for the separation of pitch.

Table 2. Content of neutral parts, bases, acids and phenols in the pitch precursor.

Samples	Solubility class separation of CHS* part of pitches, %			
	Neutral part	Phenols	Bases	Acids
Pitch initial	86.68	2.57	9.16	1.59

* - CHS - chloroform soluble.

We decided to use as a precursor mixture of coal tar pitch and furfural, because the last is inclined to polymerization reactions and will promote solidification of the mixture. The mixtures containing different amounts of furfural were used. The proximate and elemental analysis of obtained carbons is presented in Table 3. Data show, that with decreasing the content of furfural in the initial mixture increase the content of carbon in the final product due to the prevailing content of aromatic structures in the pitch. As the furfural inserts oxygen in the precursor, higher amount of furfural increases the content of oxygen in the synthesized carbon and make it more alkaline. Pitch contains mineral compounds and introduces them in the precursor and respectively in the final product.

Table 3. Chemical composition of the carbon adsorbents obtained from mixtures of biomass products.

Sample	Proximate analysis, %			Elemental analysis (daf), %				
	W	Ash ^d	pH	C	H	N	S	O _{diff.}
S ₆₀	5.8	0.61	8.4	80.27	2.31	0.31	0.29	16.82
S ₅₀	5.1	0.72	7.5	81.14	2.56	0.28	0.54	15.48
S ₄₀	5.5	0.82	7.5	82.16	2.66	0.30	0.66	14.22
S ₃₀	5.2	0.93	7.3	82.87	2.71	0.32	0.71	13.39

daf – dry and ash free basis; d – dry basis; W – water content.

It is known that the value of iodine number is close to surface area of sample determined by N₂ adsorption [10]. That is why the iodine number was used as preliminary test for surface area of S₆₀, S₅₀, S₄₀, S₃₀ – carbons obtained from mixtures containing 60, 50, 40, 30% furfural obtained synthetic carbons.

Table 4 present the iodine numbers of the carbons obtained from mixtures of coal tar pitch with furfural in different proportions using the same conditions (activation temperature 800°C, duration of activation 1 h). The results confirm that there are significant differences in the surface areas of the obtained carbons. With the increase of the amount of furfural in the mixture the surface area of obtained carbon also increases. Data indicate that texture of this carbon is not too firm, but it is more reactive and this allows the formation of higher surface area in the result of interaction with activation reagent. This is confirmed from the decrease of the yield of the final product with the rising the content of furfural in initial mixture.

Table 4. Data for the adsorption of iodine on the surface of synthetic carbons, obtained from mixtures containing coal tar pitch and furfural in different proportion.

Parameter	Synthetic carbons			
	S ₆₀	S ₅₀	S ₄₀	S ₃₀
Iodine number, mg/g	1210	1100	900	750
Yield of nanoporous carbon, %	40	49	55	62

In addition to pore structure and surface area, other important characteristic of obtained carbon is the surface chemistry. Table 5 show the determined content of oxygen containing groups with acidic and basic character on the surface of obtained carbons.

The increased content of acidic oxygen groups in the sample with higher content of furfural unambiguously indicates that inserting of oxygen in the precursor by furfural increases the formation of oxygen containing structures in the final product, particularly the acidic surface oxides. The amount of basic oxides does not depend significantly on the content of furfural in initial mixture.

Table 5. Acid-base neutralization capacities of the obtained carbons.

Sample	Base uptake, meq·g ⁻¹				Acid uptake
	NaHCO ₃	Na ₂ CO ₃	NaOH	EtONa	
S ₆₀	0.043	0.092	0.293	1.386	0.592
S ₅₀	0.024	0.053	0.138	0.977	0.585
S ₄₀	0.019	0.034	0.081	0.739	0.575
S ₃₀	0.012	0.023	0.049	0.599	0.555

More detailed characterization was performed with the sample obtained from mixture containing

50% furfural. The N₂ (77 K) adsorption isotherm of carbon obtained from mixture furfural: pitch – 50:50 is presented in Figure 2.

The adsorption investigations (steep increase in the beginning of the isotherm) reveal that the activation with water vapour leads to the formation of microporous carbon.

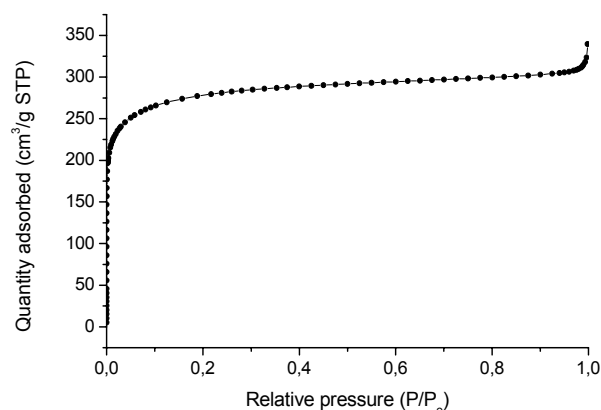


Fig. 2. N₂ (77 K) adsorption isotherm of synthetic carbon obtained from mixture containing 50% furfural.

The surface area and volumes of micro-, meso- and macropores of the carbons are presented in Table 6. Data show prevailing content of micropores in the obtained carbon and high surface area.

Table 6. Porosity characteristic of activated carbon obtained from mixture of biomass products.

Sample	N ₂ BET surface area (m ² ·g ⁻¹)	Pore volume, (cm ³ ·g ⁻¹)			
		Total	Micro	Meso	Macro
S ₅₀	1100	0.492	0.236	0.138	0.118

The Pore size distribution of S₅₀ sample is presented in Figure 3.

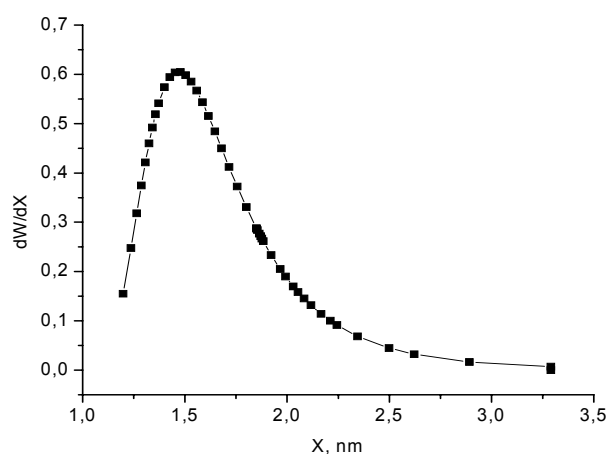


Fig. 3. Micropore size distribution of synthetic carbon obtained from mixture containing 50% furfural and 50% coal tar pitch.

Figure 3 show that carbon obtained from initial mixture containing 50% furfural possesses predominantly micropores with size from 1.2 to 2.0 nm. The

prevailing amount of pores is with size around 1.6 nm. This pore size distribution is appropriate for application of obtained carbon in many fields of industry because prevailing amount of pores are accessible for great number of organic and inorganic molecules.

CONCLUSIONS

It was determined that mixtures of furfural and coal tar pitch are appropriate raw material for synthesis of nanoporous carbon with insignificant ash content. The surface value and amount of oxygen containing groups on the surface significantly depend on the composition of the mixture. The activation is faster when carried out with carbon obtained from mixture with higher content of furfural. Considerably amount of oxygen structures is established on synthetic carbon surface. Best result was achieved using precursor containing 50% furfural. The obtained carbon possesses developed pore structure with prevailing content of micro-pores.

Acknowledgements: *The authors acknowledge financial support for this work by MEYS-NFSI, Bulgaria (Contract 02-222/17.12.2008).*

REFERENCES

1. D. Mang, H. P. Boehm, K. Stanczyk, H. Marsh, *Carbon*, **30**, 391 (1992).
2. L. Singoredjo, F. Kapteijn, J. A. Moulijn, J. M. Martin-Martinez, H. P. Boehm, *Carbon*, **31**, 213 (1993).
3. S. J. Ootani, *Jpn. Chem. Soc., Ind. Chem. Sect.*, **61**, 447 (1958).
4. T. Badosz, J. Jagiello, C. Contescu, J. A. Schwarz, *Carbon*, **31**, 1193 (1993).
5. A. Mueden, F. Carrasco-Marin, C. Moreno-Castilla, in: "Carbon 96", (Proc. European Carbon Conf., July 7–12, 1996, Newcastle-upon-Tyne, UK), vol. 2, British Carbon Group, London, 1996, p. 610.
6. H. P. Boehm, G. Mair, T. Stohr, A. R. de Rincon, B. Tereczki, *Fuel*, **63**, 1061 (1984).
7. S. J. Gregg, K. S. W. Siny, Adsorption, Surface Area and Porosity, Academic Press, London, 1982, p. 218.
8. H. P. Boehm, in: Advances in Catalysis, vol. 16, D. D. Eley, H. Pines, P. B. Weisz, (eds.), Academic Press, New York, 1966, p. 179.
9. E. Papirer, S. Li, J.-B. Donnet, *Carbon*, **25**, 243 (1987).
10. M. Molina-Sabio, C. Salinas-Martinez de Lecea, F. Rodriguez-Reinoso, C. Puente-Ruiz, A. Linares Solano, *Carbon*, **23**, 91 (1985).

СИНТЕЗ НА НАПОРОРЕСТ ВЪГЛЕН ОТ ПРОДУКТИ НА ПРЕРАБОТКА НА РАСТИТЕЛНИ ОТПАДЪЦИ И ВЪГЛИЩА

Н. Петров¹, Т. Будинова^{1*}, Б. Цинцарски¹, Б. Петрова¹, Д. Теодосиев², Н. Бончева³

¹ *Институт по органична химия с център по фитохимия, Българска академия на науките,
ул. „Акад.Г.Бончев“, бл. 9, 1113, София*

² *Институт за космически изследвания, Българска академия на науките,
ул. „Московска“ № 6, 1000, София*

³ *Университет „Проф. Асен Златаров“, бул. „Проф. Якимов“ № 1, 8010, Бургас*

Постъпила на 8 април 2009 г.; Преработена на 25 юни 2009 г.

(Резюме)

Синтетични нанопорести въглени са получени на основата на смеси, съдържащи каменовъглен пек и фурфурол в различно съотношение. Определено е, че специфичната повърхност и съдържанието на кислородни групи върху нея в значителна степен зависи от състава на изходната смес. Най-висококачествен въглен, с развита порьозна структура и преобладаващо съдържание на микропори, е получен от суровина, съдържаща 50% фурфурол. Кислородсъдържащи структури с различен характер са определени върху повърността на получените синтетични нанопорести въглени.

Novel synthesis of new symmetrical bis-heterocyclic compounds: synthesis of bis-thiazolo, bis-pyrazolo-, bis-benzotriazolo, bis-indolo- and bis-pyrazolyl thiazolo-2,6-diamino pyridine derivatives

N. I. Abdel-Sayed

Chemistry Department, Faculty of Women for Arts, Science and Education, Ain Shams University, Heliopolis, P.O. Box 11757, Cairo, A. R. Egypt

Received December 25, 2008; Revised June 8, 2009

The reaction of 2,6-diaminopyridine with chloroacetyl chloride yielded 2,6-bis-(2-chloroacetamido-N-yl) pyridine. The later reacted with KCN, KSCN, indole and benzotriazole separately to give 2,6-bis-(cyanoacetamido-N-yl)pyridine [which on coupling with benzenediazonium chloride yielded the bis-cyanophenyl hydrazone derivative and by refluxing the later compound with chloroacetonitrile afforded 2,6-diamido-bis-(4-amino-5-cyano-1-phenylpyrazol-3-yl)pyridine], 2,6-bis-(thiocyanate acetamido-N-yl)pyridine, 2,6-bis-[2-(1[H]-indol-3-yl)acetamido-N-yl] pyridine and 2,6-bis-[2-(1,2,3-benzotriazol-1-yl)acetamido-N-yl]pyridine, respectively. Acetylation of 2,6-diaminopyridine with acetic anhydride afforded 2,6-bis-(acetamido-N-yl) pyridine which on coupling with benzenediazonium chloride yielded the bis-phenylhydrazone derivative. By reacting the later with chloroacetonitrile afforded 2,6-diamino-bis-(5-cyano-1-phenylpyrazol-4-yl)pyridine. Under basic conditions the reaction of 2,6-diaminopyridine with CS₂ followed by ethyl- α -bromocanoacetate and phenacyl bromide separately afforded 2,6-bis-(5-cyano-4-hydroxythiazol-3-yl-2-thione)pyridine and 2,6-bis-(4-phenyl thiazol-3-yl-2-thione)pyridine respectively. Condensation of the later compounds separately with malononitrile yielded the dicyanomethinothiazole derivatives. The reaction of either hydrazine hydrate or phenyl hydrazine with the thiazolyl thione derivatives or with the dicyanomethinothiazole derivatives afforded the hydrazone-thiazole and the pyrazole derivatives respectively.

Key words: 2,6-diaminopyridine; bis-(thiazolo)pyridine; bis-(pyrazolo)pyridine; bis-(hydrazonopyrazolo)pyridine.

INTRODUCTION

The incorporation of two moieties increases biological activity of both and thus it was of value to synthesize some new heterocyclic derivatives having two moieties in the same molecules. In continuation to our programme [1–10], this research has been devoted to the development of new classes of bis-heterocycle systems which incorporate the bis-thiazolo-, bis-pyrazolo-, bis-benzotriazolo-, bis-indolo-, bis-triazolo- and bis-pyrazolyl thiazolo- pyridine derivatives moiety. The importance of such compounds lies in their diverse pharmaceutical activities namely antibacterial [11, 12], antidiabetic [13], anti HIV [14], antiviral [15, 16] and analgesic activities.

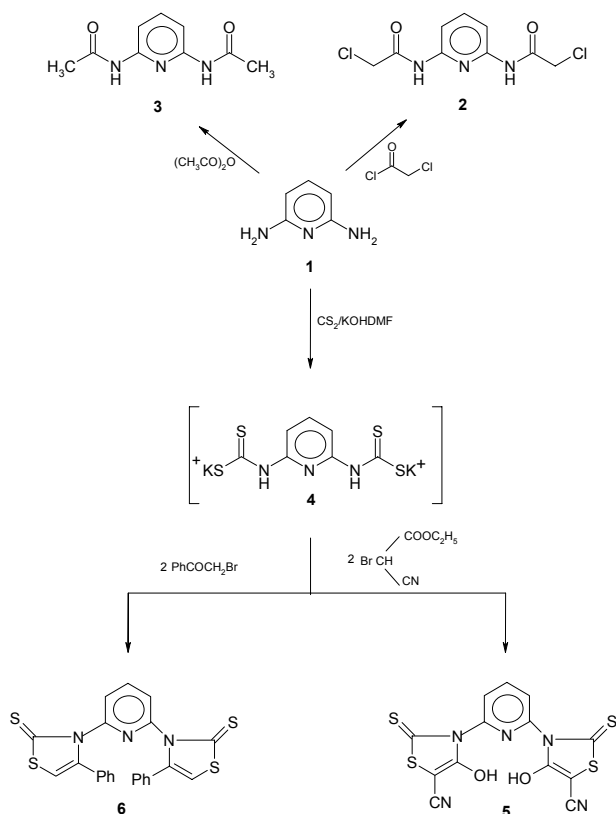
RESULTS AND DISCUSSION

Mixing 2,6-diaminopyridine with chloroacetylchloride in dioxane afforded the 2,6-bis-(2-chloroacetamido)pyridine **2** (Scheme 1). Compound **2** could be converted into **7** on treatment with potassium cyanide and into **8** on treatment with potassium thio-

cyanate. Treatment of **2** with indole and with benzotriazole separately in toluene/triethylamine afforded **9** and **10**, respectively. The ¹H NMR of **10** revealed non identity of all four benzotriazolyl protons.

Compound **11** is symmetrical and should have shown only two signals for these protons (Scheme 2). Compound **7** coupled readily with benzene diazonium chloride to yield the bis-aryl hydrazone derivative **12** which on refluxing in DMF with chloroacetonitrile afforded the bis-pyrazolyl diamidopyridine derivative **14** (Scheme 2). On the other hand acetylation of compound **1** yielded the 2,6-bis-(acetamido)pyridine **3** (Scheme 1). Coupling of **3** with benzene diazonium chloride afforded the bis-hydrazone derivative **15**. Thus, reacting **15** with chloroacetonitrile in a mixture of DMF and triethylamine has afforded **17** in excellent yield. Intermediacy of **16** is most likely (Scheme 2). Further, the reaction of **1** with carbon disulphide under basic conditions in KOH/DMF solution affords the non isolable intermediate, the N-potassium thiocarbamate salt **4** [17]. Thus, the reaction of **4** with ethyl- α -bromocanoacetate and with phenacyl bromide separately afforded the thiazole derivatives **5** and **6** respectively (Scheme 1).

* To whom all correspondence should be sent:
E-mail: nadia_iskandar@yahoo.com



Scheme 1.

Confirmation of the structures of **5** and **6** were obtained through studying their reactivity towards chemical reagents. The reaction of compounds **5** or **6** with either hydrazine hydrate or phenyl hydrazine afforded the corresponding hydrazone derivatives **18a,b** and **22a,b** respectively (Scheme 3). Formation of the latter compounds took place through elimination of hydrogen sulphide. Their structures were confirmed by analytical and spectral data. The reaction of **5** and **6** with malononitrile gave the condensed products the dicyanomethino derivatives **19** and **23** respectively (Scheme 3); their formation took place *via* elimination of hydrogen sulphide. The reaction of **19** and **23** with either hydrazine hydrate or phenylhydrazine afforded the pyrazole derivatives **20**, **21**, **24** and **25** (Scheme 3). The structures of the latter compounds were confirmed by analytical and spectral data.

EXPERIMENTAL

All melting points are uncorrected. IR spectra (KBr) were recorded on a Pye Unicam SP-100 spectrophotometer. ^1H and ^{13}C NMR spectra (DMSO- d_6 as a solvent) were obtained on a Varian Gemini 200 and on a Bruker AC200 and AC600 MHz spectrometers respectively, TMS as internal standard, chemical shifts in δ (ppm); mass spectra: AEI MS 30 mass spectrometer operating at 70 eV; elemental analysis were obtained from Microanalytical Data

Unit at Cairo University, Egypt.

2,6-Bis-(2-chloroacetamido-N-yl) pyridine (2): A mixture of **1** (1.09 g, 10 mmol) and chloroacetylchloride (2.30 g, 20 mmol) in 20 ml of dioxane was refluxed for 45 min. The mixture was allowed to cool to room temperature then poured onto cold water. The obtained solid was collected by filtration and crystallized from methanol to give pale pink crystals (93% yield), m.p. 105°C; IR (KBr) ν (cm^{-1}): 3118 (NH) and 1700 (C=O); ^1H NMR (DMSO- d_6) δ (ppm): 4.58 (s, 4H, 2CH₂), 8.10–8.30 (m, 3H, pyr-H), 8.50 (s, 2H, 2NH); ^{13}C NMR (DMSO- d_6) δ (ppm): 190.5 (2CO), 154.2 (C-2 and C-6 pyridine), 149.3 (C-3 and C-5 pyridine), 138.5 (C-4 pyridine), 53.23 (CH₂); MS: m/z = 262 [M^+]; Anal. Calcd. for C₉H₉N₃Cl₂O₂ (262.09): C, 41.24; H, 3.46; N, 16.03; Cl, 27.05. Found: C, 41.35; H, 3.47; N, 16.25; Cl, 27.35.

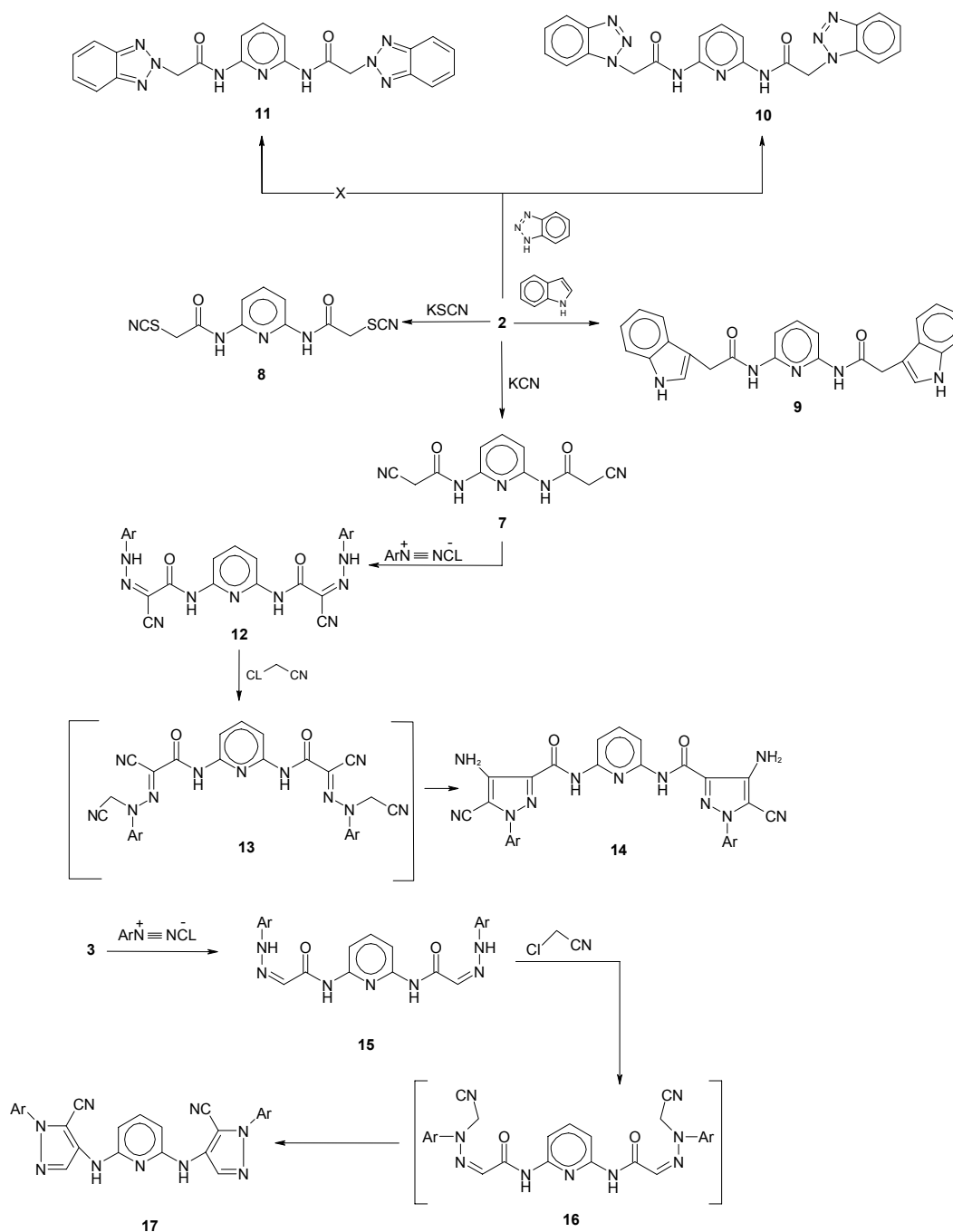
2,6-Bis-(acetamido-N-yl) pyridine (3): Reflux gently 1 g of **1** and 3 ml of acetic anhydride for 15 min. Pour in 20 ml of cold water then boil to destroy any excess of acetic anhydride. Filter the precipitate, wash with a little cold water and dry in air. Crystallization from ethanol afforded 0.18 g of a creamy crystals (95% yield), m.p. 95°C; IR (KBr) ν (cm^{-1}): 3225 (NH), 1700 (C=O); ^1H NMR (DMSO- d_6) δ ppm: 1.5 (s, 6H, 2CH₃), 8.10–8.30 (m, 3H, pyr-H), 8.55 (s, 2H, 2NH); ^{13}C NMR (DMSO- d_6) δ (ppm): 184.5 (2CO), 153.5 (C-2 and C-6 pyridine), 148.4 (C-3 and C-5 pyridine), 138.7 (C-4 pyridine), 24.15 (CH₃); MS: m/z = 193 [M^+]; Anal. Calcd. for C₉H₁₁N₃O₂ (193.21): C, 55.95; H, 5.74; N, 21.75. Found: C, 55.90; H, 5.76; N, 21.90.

2,6-Bis (5-cyano-4-hydroxythiazol-3-yl-2-thione) pyridine (5): To a solution of **1** (1.09 g, 0.01 mol) in 30 ml of DMF, carbon disulphide (1.52 g, 0.02 mol) and potassium hydroxide (1.12 g, 0.02 mol) in 10 ml of water were added. The whole reaction mixture was heated in a boiling water bath for 1 h then left to cool till 20°C. To a cold solution of the reaction mixture (3.84 g, 0.02 mol) of ethyl α -bromocynoacetate was added. The reaction mixture was stirred at room temperature for one night. The solid product, formed upon acidification with hydrochloric acid, was collected by filtration and crystallized from dioxane to give orange crystals (87% yield), m.p. 150°C; IR (KBr) ν (cm^{-1}): 3480–3340 (OH), 2225 (2 CN), 1210–1195 (2 C=S); ^1H NMR (DMSO- d_6) δ (ppm): 7.90–8.25 (m, 3H, pyr-H), 10.33 (s, 2H, 2OH); ^{13}C NMR (DMSO- d_6) δ (ppm): 164.5 (2C=S), 153.2 (C-2 and C-6 pyridine), 150.2 (C-4 and C-4' thiazole), 148.1 (C-3 and C-5 pyridine), 140.8 (C-5 and C-5' thiazole), 138.1 (C-4 pyridine), 119.7 (2CN); MS: m/z = 391 [M^+]; Anal. Calcd. for C₁₃H₅N₅S₄O₂

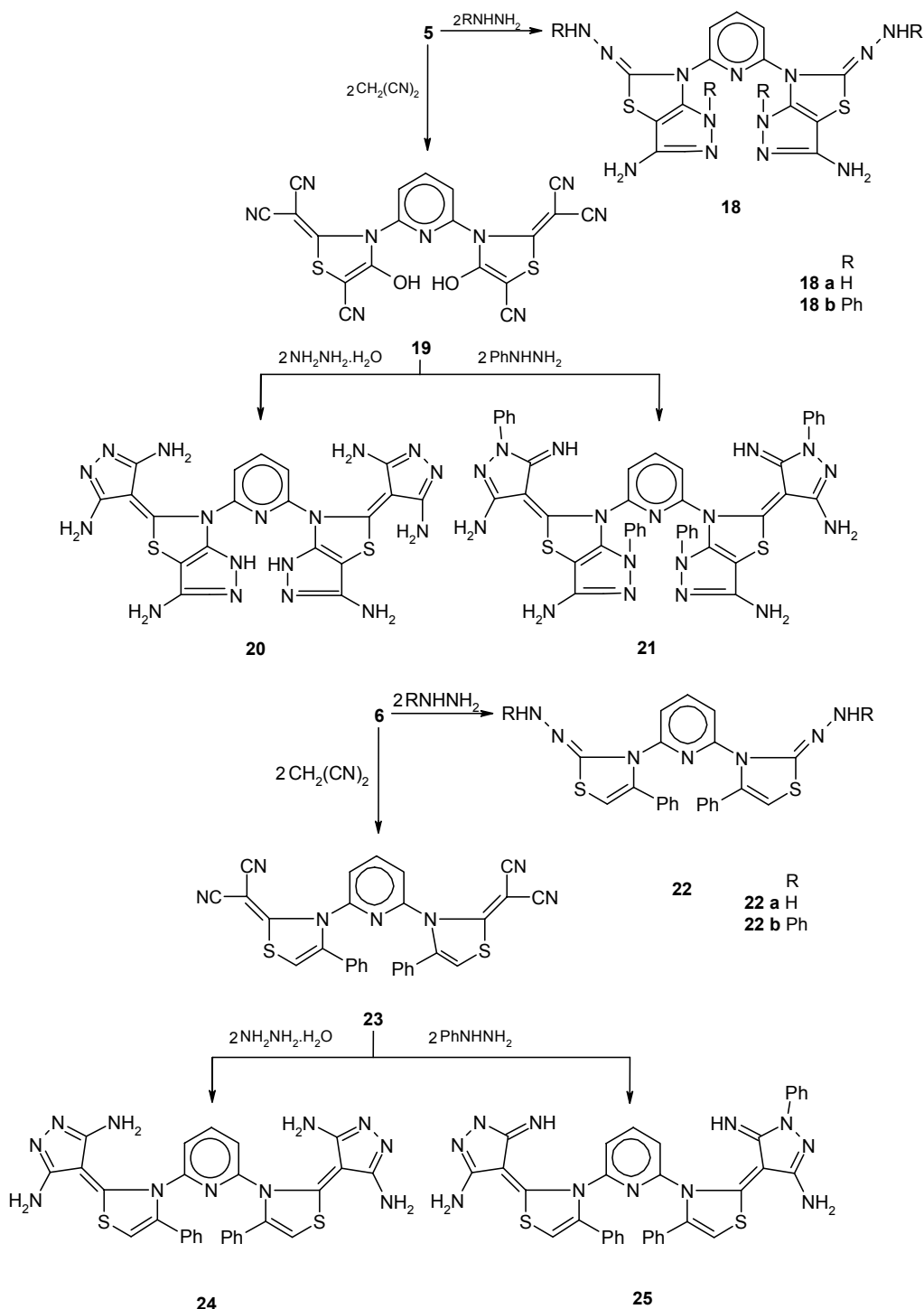
(391.47): C, 39.89; H, 1.29; N, 17.89; S, 32.76.
 Found: C, 39.95; H, 1.31; N, 18.01; S, 32.80.

2,6-Bis-(4-phenylthiazol-3-yl-2-thione)pyridine (6):
 To a solution of **1** (1.09 g, 0.01 mol) in 30 ml of DMF, (1.52 g, 0.02 mol) of carbon disulphide and (1.12 g, 0.02 mol) of potassium hydroxide in 10 ml of water were added. The whole reaction mixture was heated in boiling water bath for 1 h then left to cool down to 20°C; (3.96 g, 0.02 mol) of phenacyl-bromide was added to this cold solution. The reaction mixture was stirred at room temperature for one night. The solid product formed upon acidification with hydrochloric acid was collected by filtration.

Crystallization from dioxane gave red crystals (80% yield), m.p. 99°C; IR (KBr) ν (cm⁻¹): 3060 (CH aromatic), 1200–1190 (C=S); ¹H NMR (DMSO-d₆) δ (ppm): 6.95 (s, 2H, thiazole H-5), 7.32–7.55 (m, 10H, 2C₆H₅), 7.95–8.30 (m, 3H, pyr-H); ¹³C NMR (DMSO-d₆) δ (ppm): 180.4 (C-5 and C-5' thiazole), 164.1 (2C=S), 153.4 (C-2 and C-6 pyridine), 148.8 (C-3 and C-5 pyridine), 146.5 (C-4 and C-4' thiazole), 138.5 (C-4 pyridine), 152.1, 143.2, 132.1, 129.5, 128.5, 126.2 (C-arom.); MS: m/z = 461 [M⁺]; Anal. Calcd. for C₂₃H₁₅N₃S₄ (461.65): C, 59.84; H, 3.28; N, 9.10; S, 27.78. Found: C, 59.80; H, 3.27; N, 9.11; S, 27.82.



Scheme 2.



Scheme 3.

2,6-Bis-(cyanoacetamido-N-yl) pyridine (7): To a warmed solution of **2** (1.31 g, 5 mmol) in 10 ml benzene, were added (0.78 g, 12 mmol) of potassium cyanide in 10 ml of water. The reaction mixture was stirred at 50°C (bath temperature) for 1 h, then the aqueous layer was separated and poured onto acidified cooled water. The product, so formed, was collected by filtration and dried. Crystallization from acetic acid gave creamy crystals (95% yield), m.p. 235°C; IR (KBr) ν (cm⁻¹): 2252 (CN), 3220 (NH),

1638 (C=O); ¹H NMR (DMSO-d₆) δ (ppm): 4.48 (s, 4H, 2 CH₂), 8.10–8.30 (m, 3H, pyr-H), 9.45 (s, 2H, 2NH); MS: $m/z = 243$ [M⁺]; Anal. Calcd. for C₁₁H₉N₅O₂ (243.23): C, 54.32; H, 3.73; N, 28.79. Found: C, 54.37; H, 3.74; N, 28.84.

2,6-Bis-(thiocyanate acetamido-N-yl)pyridine (8): To a warmed solution of **2** (1.13 g, 5 mmol) in 10 ml acetonitrile, were added (0.92 g, 12 mmol) of potassium thiocyanate. The reaction mixture was stirred at 50°C (bath temperature) for 1 h, then

poured onto ice cold water. The product, so formed, was collected by filtration, crystallized from ethanol to give faint pink crystals (95% yield), m.p. 130°C; IR (KBr) ν (cm⁻¹): 3220 (NH), 2157 (SCN), 1696 (C=O); ¹H NMR (DMSO-d₆) δ (ppm): 4.48 (s, 4H, 2CH₂), 8.10–8.30 (m, 3H, pyr-H), 9.20 (s, 2H, 2NH); MS: m/z = 307 [M⁺]; Anal. Calcd. for C₁₁H₉N₅S₂O₂ (307.35): C, 42.99; H, 2.95; N, 22.79; S, 20.86. Found: C, 43.01; H, 2.98; N, 23.01; S, 20.88.

General procedure for the synthesis of compounds 9 and 10

A mixture of **2** (2.62 g, 10 mmol), (2.34 g, 20 mmol) of indole or (2.38 g, 20 mmol) of benzotriazole and 2 ml triethylamine (20 mmol) in 15 ml of toluene was refluxed for 2 h. The solvent was removed in vacuum and the remaining residue was triturated with 5% sodium hydroxide. The solid product, so formed, was collected by filtration.

2,6-Bis-[2-(1[H]-indol-3-yl)acetamido-N-yl] pyridine (9): Crystallization from ethanol gave white crystals (78% yield), m.p. 162°C; IR (KBr) ν (cm⁻¹): 3225 (NH), 1700 (C=O); ¹H NMR (DMSO-d₆) δ (ppm): 4.60 (s, 4H, 2CH₂), 7.38–7.75 (m, 8H, 2C₆H₄), 8.10–8.30 (m, 3H, pyr-H), 8.44 (d, 2H, two indole H-2), 9.43 (s, 2H, 2NH), 11.92 (br s, 2H, two indole NH); MS: m/z = 423 [M⁺]; Anal. Calcd. for C₂₅H₂₁N₅O₂ (423.48): C, 70.91; H, 4.99; N, 16.54. Found: C, 70.94; H, 4.98; N, 16.78.

2,6-Bis-[2-(1,2,3-benzotriazol-1-yl)acetamido-N-yl] pyridine (10): Crystallization from ethanol gave white solid (75% yield), m.p. 175°C; IR (KBr) ν (cm⁻¹): 3225 (NH), 1700 (C=O); ¹H NMR (DMSO-d₆) δ (ppm): 4.58 (s, 4H, 2CH₂), 7.33–7.80 (m, 8H, 2C₆H₄), 8.10–8.30 (m, 3H, pyr-H), 9.33 (s, 2H, 2NH); MS: m/z = 427 [M⁺]; Anal. Calcd. for C₂₁H₁₇N₉O₂ (427.43): C, 59.01; H, 4.01; N, 29.49. Found: C, 59.05; H, 4.00; N, 29.55.

General procedure for the synthesis of compounds 12 and 15

To a stirred solution of (0.01 mol) of **7** or **3** in 20 ml of dioxane containing 10 g of sodium acetate, was added benzene diazonium salt (prepared from 20 mmol of aniline and the appropriate quantities of sodium nitrite and hydrochloric acid). The solid product separated on standing was collected by filtration.

2,6-Bis-(2-cyano-2-phenylhydrazonocetamido-N-yl)pyridine (12): Crystallization from dioxane gave yellow crystals (75% yield), m.p. 261°C; IR (KBr) ν (cm⁻¹): 3440, 3234 (NH), 2215 (CN), 1700 (C=O); ¹H NMR (DMSO-d₆) δ (ppm): 7.11–7.25 (m, 10H, 2C₆H₅), 8.10–8.30 (m, 3H, pyr-H), 9.35 (s, 2H, 2NH), 12.04 (br, 2H, hydroazonyl NH); MS: m/z =

451 [M⁺]; Anal. Calcd. for C₂₃H₁₇N₉O₂ (451.451): C, 61.19; H, 3.79; N, 27.92. Found: C, 61.23, H, 3.77; N, 28.15.

2,6-Bis-(1-oxo-2-phenylhydrazonoethanoneamido-N-yl)pyridine (15): Crystallization from dioxane gave yellow crystals (78% yield), m.p. 255°C; IR (KBr) ν (cm⁻¹): 3440, 3230 (NH), 1700 (C=O); ¹H NMR (DMSO-d₆) δ (ppm): 7.11–7.45 (m, 10H, 2C₆H₅), 7.56 (s, 2H, olefinic CH), 8.10–8.30 (m, 3H, pyr-H), 9.30 (s, 2H, 2NH), 12.04 (br, 2H, two hydrazone NH); MS: m/z = 401 [M⁺]; Anal. Calcd. for C₂₁H₁₉N₇O₂ (401.43): C, 62.83; H, 4.77; N, 24.42. Found: C, 62.85; H, 4.74; N, 24.46.

General procedure for the synthesis of compounds 14 and 17

To a solution of (5 mmol) of **12** or **15** in a 2 ml of DMF and 10 ml of triethylamine, was added (1.3 ml, 20 mmol) of chloroacetonitrile. The reaction mixture was refluxed for 1 h and then left to cool to room temperature. The obtained residual product was triturated with ethanol to give a solid product that was collected by filtration, washed with water and crystallized from the proper solvent.

2,6-Diamido-bis-(4-amino-5-cyano-1-phenylpyrazol-3-yl) pyridine (14): Crystallization from ethanol gave faint brown crystals (75% yield), m.p. 268–270°C; IR (KBr) ν (cm⁻¹): 1700 (C=O), 3450 (NH₂), 3200 (NH), 2220 (CN), 1650 (C=N); ¹H NMR (DMSO-d₆) δ (ppm): 6.52(s, 4H, 2NH₂), 7.31–7.65 (m, 10H, 2C₆H₅), 8.10–8.30 (m, 3H, pyr-H), 8.90 (s, 2H, 2NH); MS: m/z = 529 [M⁺]; Anal. Calcd. for C₂₇H₁₉N₁₁O₂ (529.53): C, 61.24; H, 3.62; N, 29.10. Found: C, 61.25; H, 3.61; N, 29.40.

2,6-Diamino-bis-(5-cyano-1-phenylpyrazol-4-yl) pyridine (17): Crystallization from ethanol gave faint brown crystals (85% yield), m.p. 230°C; IR (KBr) ν (cm⁻¹): 3200(NH), 2220 (CN), 1600 (C=C), 1650 (C=N); ¹H NMR (DMSO-d₆) δ (ppm): 7.30 (s, 2H, pyrazolyl H-3), 7.41–7.65 (m, 10H, 2C₆H₅), 8.10–8.30 (m, 3H, pyr-H), 8.35 (s, 2H, 2NH); MS: m/z = 443 [M⁺]; Anal. Calcd. for C₂₅H₁₇N₉ (443.48): C, 67.71; H, 3.86; N, 28.43. Found: C, 67.72; H, 3.84; N, 28.44.

2,6-Bis-(5-cyano-2-dicyanomethino-4-hydroxythiazol-N-yl)pyridine (19): A solution of **5** (3.91g, 0.01 mol) in 40 ml of DMF containing piperidine 0.5 ml, (1.32 ml, 0.02 mol) of malonitrile was added. The reaction mixture was heated under reflux for 10 h, then evaporated *in vacuo*. The remaining product was triturated with ethanol and the formed solid product was collected by filtration. Crystallization from dioxane gave brown crystals (75% yield), m.p. > 360°C; IR (KBr) ν (cm⁻¹): 3490 (OH), 2225, 2220, 2215 (CN), 1655 (C=C); ¹H NMR

(DMSO- d_6) δ (ppm): 8.10–8.30 (m, 3H, pyr-H), 10.44 (s, 2H, 2OH); MS: m/z = 455 [M^+]; Anal. Calcd. for $C_{19}H_5N_9S_2O_2$ (455.44): C, 50.11; H, 1.11; N, 27.68; S, 14.08. Found: C, 50.15; H, 1.09; N, 27.72; S, 14.12.

General procedure for the synthesis of compounds 18a, b, 20, 21 and 22a, b

To a solution of **5**, **19** or **6** (0.01 mol) in 30 ml of DMF, hydrazine hydrate or phenylhydrazine (0.04 mol) or (0.02 mol) were added, respectively. The reaction mixture was heated under reflux for 6–8 h then poured into ice/water mixture containing few drops of hydrochloric acid and the formed solid product was collected by filtration.

2,6-Bis-(3-amino-1[H]-5-hydrazonopyrazolo[4,5-d]thiazol-N-yl) pyridine (18a): Crystallization from ethanol gave pale yellow crystals (68% yield), m.p. > 360°C; IR (KBr) ν (cm^{-1}): 3465–3365 (NH, NH_2), 1660 (exocyclic C=N), 1645 (C=C); 1H NMR (DMSO- d_6) δ (ppm): 4.46, 5.35 (2s, 8H, 4 NH_2), 8.10–8.30 (m, 3H, pyr-H), 8.44 (s, 2H, 2NH); MS: m/z = 415 [M^+]; Anal. Calcd. for $C_{13}H_{13}N_{13}S_2$ (415.46): C, 37.58; H, 3.15; N, 43.83; S, 15.44. Found: C, 37.56; H, 3.16; N, 43.85; S, 15.43.

2,6-Bis-(3-amino-1-phenyl-5-phenylhydrazono-pyrazolo[4,5-d]thiazol-N-yl)pyridine (18b): Crystallization from dioxane gave yellow crystals (70% yield), m.p. > 360°C; IR (KBr) ν (cm^{-1}): 3450–3370 (NH_2 , NH), 1665 (exocyclic C=N), 1650 (C=C); 1H NMR (DMSO- d_6) δ (ppm): 5.32 (s, 4H, 2 NH_2), 7.36–7.48 (m, 20H, 4 C_6H_5), 8.10–8.30 (m, 3H, pyr-H), 8.45 (s, 2H, 2NH); MS: m/z = 719 [M^+]; Anal. Calcd. for $C_{37}H_{29}N_{13}S_2$ (719.86): C, 61.74; H, 4.06; N, 25.29; S, 8.91. Found: C, 61.75; H, 4.04; N, 25.3; S, 8.90.

2,6-Bis[3-amino-1[H]-5-(3',5'-diaminopyrazolo-4'-ylidino) pyrazolo [4,5-d]thiazol-N-yl] pyridine (20): Crystallization from ethanol gave white crystals (68% yield), m.p. > 360°C; IR (KBr) ν (cm^{-1}): 3460–3370 (NH_2 , NH), 1660 (C=N), 1655 (C=C); 1H NMR (DMSO- d_6) δ (ppm): 5.31, 5.36, 7.42 (3s, 12H, 6 NH_2), 8.10–8.30 (m, 3H, pyr-H), 8.41 (s, 2H, 2NH); MS: m/z = 547 [M^+]; Anal. Calcd. for $C_{19}H_{17}N_{17}S_2$ (547.59): C, 41.68; H, 3.13; N, 43.48; S, 11.71. Found: C, 41.65; H, 3.14; N, 43.52; S, 11.69.

2,6-Bis-[3-amino-1-phenyl-5-(3'-amino-5'-imino-1'-phenylpyrazolo-4'-ylidino) pyrazolo[4,5-d] thiazol-N-yl] pyridine (21): Crystallization from dioxane gave pale brown crystals (74% yield), m.p. > 360°C; IR (KBr) ν (cm^{-1}): 3460–3365 (NH_2 , NH), 1670 (exocyclic C=N), 1660 (C=N), 1645 (C=C); 1H NMR (DMSO- d_6) δ (ppm): 4.82, 5.45 (2s, 8H, 4 NH_2), 7.30–7.46 (m, 20H, 4 C_6H_5), 8.10–8.30 (m,

3H, pyr-H), 8.33 (s, 2H, 2NH); MS: m/z = 851 [M^+]; Anal. Calcd. for $C_{43}H_{33}N_{17}S_2$ (851.94): C, 60.62; H, 3.90; N, 27.95; S, 7.53. Found: C, 60.60; H, 3.91; N, 27.99; S, 7.50.

2,6-Bis-(2-hydrazono-4-phenylthiazol-N-yl)pyridine (22a): Crystallization from dioxane gave buff crystals (75% yield), m.p. 125°C; IR (KBr) ν (cm^{-1}): 3460 (NH_2), 1665 (exocyclic C=N), 1650 (C=C); 1H NMR (DMSO- d_6) δ (ppm): 6.35 (s, 4H, 2 NH_2), 6.37 (s, 2H, thiazolyl H-5), 7.32–7.37 (m, 10H, 2 C_6H_5), 8.10–8.30 (m, 3H, pyr-H); MS: m/z = 457 [M^+]; Anal. Calcd. for $C_{23}H_{19}N_7S_2$ (457.59): C, 60.37; H, 4.19; N, 21.43; S, 14.01. Found: C, 60.39; H, 4.17; N, 21.55; S, 13.89.

2,6-Bis-(2-phenylhydrazono-4-phenylthiazol-N-yl) pyridine (22b): Crystallization from dioxane gave pale yellow crystals (73% yield), m.p. 120°C; IR (KBr) ν (cm^{-1}): 3460–3375°C (NH), 1665 (exocyclic C=N), 1650 (C=C); 1H NMR (DMSO- d_6) δ (ppm): 6.37 (s, 2H, thiazolyl H-5), 7.32–7.48 (m, 20H, 4 C_6H_5), 8.10–8.30 (m, 3H, pyr-H), 8.33 (s, 2H, 2NH); MS: m/z = 609 [M^+]; Anal. Calcd. for $C_{35}H_{27}N_7S_2$ (609.78): C, 68.94; H, 4.46; N, 16.08; S, 10.52. Found: C, 68.97; H, 4.44; N, 16.10; S, 10.49.

2,6-Bis-(2-dicyanomethino-4-phenylthiazol-N-yl) pyridine (23): To a solution of **6** (4.61 g, 0.01 mol) in 30 ml of DMF, (1.32 ml, 0.02 mol) of malononitrile was added. The mixture was heated under reflux for 6 h (till the evolution of H_2S was ceased). The solid product formed upon pouring into water was collected by filtration. Crystallization from dioxane gave brown crystals (80% yield), mp 145°C; IR (KBr) ν (cm^{-1}): 2225–2220 (CN), 1655 (C=C); 1H NMR (DMSO- d_6) δ (ppm): 6.34 (s, 2H, thiazolyl H-5), 7.34–7.45 (m, 10H, 2 C_6H_5), 8.10–8.30 (m, 3H, pyr-H); MS: m/z = 525 [M^+]; Anal. Calcd. for $C_{29}H_{15}N_7S_2$ (525.62): C, 66.27; H, 2.88; N, 18.65; S, 12.20. Found: C, 66.28; H, 2.87; N, 18.66; S, 12.19.

General procedure for the synthesis of compounds 24 and 25

To a solution of **23** (5.01 g, 0.01 mol) in 40 ml of dioxane, hydrazine hydrate or phenyl hydrazine (0.02 mol) was added. The reaction mixture was heated under reflux for 3–4 h, then left to cool. The solid product formed upon standing was collected by filtration.

2,6-Bis-[2-(3',5'-diaminopyrazolo-4'-ylidino)-4-phenyl thiazol-N-yl] pyridine (24): Crystallization from DMF gave white crystals (70% yield), m.p. 323°C; IR (KBr) ν (cm^{-1}): 3465 (NH_2), 1645 (C=C), 1660 (C=N); 1H NMR (DMSO- d_6) δ (ppm): 4.44, 5.03 (2s, 8H, 4 NH_2), 6.42 (s, 2H, thiazolyl H-5), 7.35–7.58 (m, 10H, 2 C_6H_5), 8.10–8.30 (m, 3H, pyr-H); MS: m/z = 589 [M^+]; Anal. Calcd. for

C₂₉H₂₃N₁₁S₂ (589.71): C, 59.07; H, 3.93; N, 26.13; S, 10.87. Found: C, 59.05; H, 3.94; N, 26.17; S, 10.84.

2,6-Bis-[2-(3'-amino-5'-imino-1'-phenylpyrazolo-4'-ylidino)-4-phenylthiazol-N-yl] pyridine (25): Crystallization from ethanol afforded pale yellow crystals (65% yield), m.p. > 360°C; IR (KBr) ν (cm⁻¹): 3465, 3390 (NH₂, NH), 1660 (C=N), 1645 (C=C); ¹H NMR (DMSO-d₆) δ (ppm): 4.43 (s, 4H, 2NH₂), 6.43 (s, 2H, thiazolyl H-5), 7.30–7.64 (m, 20H, 4C₆H₅), 8.10–8.30 (m, 3H, pyr-H), 8.37 (s, 2H, 2NH); MS: m/z = 741 [M⁺]; Anal. Calcd. for C₄₁H₃₁N₁₁S₂ (741.91): C, 66.38; H, 4.21; N, 20.77; S, 8.64. Found: C, 66.40; H, 4.20; N, 20.80; S, 8.60.

REFERENCES

1. R. M. Mohareb, S. M. Sherif, F. A. M. Abdel-Aal, N. I. Abdel-Sayed, *Leibigs Ann. Chem.*, 1143 (1990).
2. N. I. Abdel-Sayed, *Women's College Ann. Rev.*, **16**, 12 (1991).
3. R. M. Mohareb, N. I. Abdel-Sayed, S. M. Sherif, *Phosphorus, Sulfur and Silicon*, **63**, 119 (1991).
4. R. M. Mohareb, S. I. Aziz, N. I. Abdel-Sayed, H. Z. Shams, *J. Chin. Chem. Soc.*, **39**, 181 (1992).
5. R. M. Mohareb, N. I. Abdel-Sayed, *Collect. Czech. Chem. Commun.*, **57**, 1758 (1992).
6. R. M. Mohareb, S. M. Sherif, A. Habashi, N. I. Abdel-Sayed, S. S. Osman, *Collect. Czech. Chem. Commun.*, **60**, 1578 (1995).
7. S. M. Sherif, N. I. Abdel-Sayed, S. M. El Kousy, R. M. Mohareb, *Monatsh. Chem.*, **126**, 601 (1995).
8. R. M. Mohareb, Y. M. Elkholy, N. I. Abdel-Sayed, *Phosphorus, Sulfur and Silicon*, **106**, 193 (1995).
9. R. M. Mohareb, S. I. Aziz, N. I. Abdel-Sayed, A. H. El-Banna, *J. Chem. Res.*, (S) 10 (1999); *Ibid.*, (M) 0101 (1999).
10. N. I. Abdel-Sayed, *Egypt. J. Chem.*, **42**, 175 (1999).
11. P. Nussbaumer, G. Petranyi, A. Stutz, *J. Med. Chem.*, **34**, 65 (1991).
12. N. J. P. Broom, J. S. Elder, P. C. T. Hannan, J. E. Pons, P. J. O'Hanlon, G. Walker, J. Wilson, P. Woodall, *J. Antibiotic*, **48**, 1336 (1995).
13. M. Nakanishi, H. Imamura, Y. Maruyama, H. Hoshino, *J. Pharm. Soc. Jpn.*, **90**, 272 (1970).
14. D. Briel, *Pharmazie*, **45**, 236 (1995).
15. M. Yamaguchi, N. Maruyama, T. Koga, K. Kamei, M. Akima, T. Kuroki, M. Hamana, N. Ohi, *Chem. Pharm. Bull.*, **43**, 236 (1995).
16. R. E. Boyd, J. B. Press, C. R. Rasmussen, R. B. Raffa, E. E. Codd, C. D. Connelly, Q. S. Li, R. P. Martinez, M. A. Lewis, B. J. Almond, *J. Med. Chem.*, **44**, 863 (2001).
17. M. T. Cocco, C. Congiu, V. Onnis, *J. Heterocyclic Chem.*, **32**, 463 (1995).

НОВИ СИНТЕЗИ НА НОВИ СИМЕТРИЧНИ БИС-ХЕТЕРОЦИКЛЕНИ СЪЕДИНЕНИЯ: СИНТЕЗ НА БИС-ТИАЗОЛ-, БИС-ПИРАЗОЛ-, БИС-БЕНЗОТРИАЗОЛ-, БИС-ИНДОЛ- И БИС-ПИРАЗОЛИЛТИАЗОЛ-2,6-ДИАМИНПИРИДИНОВИ ПРОИЗВОДНИ

Н. И. Абдел-Сайед

*Департамент по химия, Девически факултет по изкуства, наука и образование, Университет Айн Шамс,
Хелиополис, п.к. 11757, Кайро, АР Египет*

Постъпила на 25 декември 2008 г.; Преработена на 8 юни 2009 г.

При реакция на 2,6-диаминопиридин с хлорацетилхлорид се получава 2,6-бис-(2-хлорацетамид-N-ил)пиридин. Реакцията на продукта поотделно с KCl, KSCN, индол и бензотриазол води съответно до 2,6-бис-(цианацетамид-N-ил)пиридин (продуктът при купелуване с бензендиазониев хлорид дава бис-цианфенилхидразоновото производно и чрез дестилация на последното съединение с обратен хладник и хлорацетонитрил се получава 2,6-диамин-5-циан-1-фенилпиразол-3-ил)пиридин), 2,6-бис-(тиоцианат ацетамид-N-ил)пиридин, 2,6-бис-[2-(1-[H]-индол-3-ил)ацетамид-N-ил]пиридин и 2,6-бис-[2-(1,2,3-бензотриазол-1-ил)ацетамид-N-ил]пиридин. Ацетиране на 2,6-диаминопиридин с оцетен анхидрид води до 2,6-бис-(ацетамид-N-ил)пиридин, който при купелуване с бензендиазониев хлорид дава бис-фенилхидразоново производно. При реакцията на последното с хлорацетонитрил се получава 2,6-диамино-бис-(5-циан-1-фенил-пиразол-N-ил)пиридин. В алкална среда реакцията на 2,6-диаминопиридин с CS₂ последвана поотделно с стил- α -бромцианоацетат и фенацилбромид дава съответно 2,6-бис-(5-циан-4-хидроксипиразол-3-ил-2-тионил)пиридин и 2,6-бис-(4-фенил-тиазол-3-ил-2-тионил)пиридин. При кондензация на получените съединения поотделно с малонитрил се получават дицианметинтиазолови производни. При реакция на хидразинхидрат или фенилхидразин с тиазолилтенови производни или с дицианметинтиазолови производни води съответно до хидразонтиазолови и пиразолови производни.

Oxidative cleavage of salbutamol with *N*-bromosuccinimide in acidic and alkaline media: A kinetic and mechanistic study

P. M. Ramdas Bhandarkar, K. N. Mohana*

Department of Studies in Chemistry, University of Mysore, Manasagangothri, Mysore- 570006, India

Received February 17, 2009; Revised June 17, 2009

Salbutamol sulfate (SBL) is a β_2 -adrenergic receptor agonist used for the relief of bronchospasm in conditions such as asthma and chronic obstructive pulmonary disease (COPD). The kinetic study of oxidation of this bioactive compound is of much use in understanding the mechanistic profile in redox reactions. Consequently, the kinetics of oxidative degradation of SBL with *N*-bromosuccinimide (NBS) in HClO_4 and NaOH media has been studied at 308 K. The experimental rate laws obtained are $-d[\text{NBS}]/dt = [\text{NBS}][\text{SBL}]^x[\text{H}^+]^y$ in acidic medium and $-d[\text{NBS}]/dt = [\text{NBS}][\text{SBL}]^x[\text{OH}^-]$ in alkaline medium, where x and y are less than unity. The reactions were subjected to changes in concentration of succinimide, the reduction product of NBS, concentration of added neutral salt, dielectric permittivity and ionic strength of the medium. Solvent isotope effect has been studied using D_2O . The stoichiometry of the reaction has been determined and oxidation products were identified and characterized in both media. Activation parameters for the overall reactions have been computed from Arrhenius plot. $(\text{CH}_2\text{CO})_2 \text{N}^+\text{HBr}$ and OBr^- have been postulated as the reactive oxidizing species in acidic and alkaline media, respectively. The oxidation reaction fails to induce polymerization of added acrylonitrile. It was found that the reaction was faster in alkaline medium in comparison with acidic medium. The observed results have been explained by plausible mechanisms and the relative rate laws have been deduced.

Key words: *N*-bromosuccinimide, salbutamol sulfate, oxidation kinetics, acidic and alkaline media.

INTRODUCTION

N-bromosuccinimide (NBS) is a source of positive halogen, and this reagent has been exploited as an oxidant for a variety of substrates [1–5] in both acidic and alkaline solutions. This potent oxidizing agent has been used in the determination of various pharmaceutical compounds [6–9]. However, a little information exists in the literature on oxidation kinetics of substrates particularly with respect to pharmaceuticals [10, 11], which may throw some light on the mechanism [12] of metabolic conversions in the biological system. In view of these facts, there is a considerable scope for the study of reactions with NBS to get better in sight of the speciation of NBS reaction models and to understand its redox chemistry in solutions.

Salbutamol sulfate (SBL) is a β_2 -adrenergic receptor agonist used for the relief of bronchospasm in condition such as asthma and COPD. Salbutamol is a relevant medication for the treatment of asthma. It acts quickly on the nerves that control the airway muscles and causes them to relax and dilating the airways. It also relieves swelling of the airways that can be caused by the allergic response and helps to clear mucous that may contribute to asthmatic

symptoms. SBL is specifically used for the following conditions such as acute asthma, certain conditions involving hyperkalemia. It is also used in obstetrics as a tocolytic to delay premature labor. It was therefore found to be of interest to investigate the mechanism of oxidation of this drug with *N*-bromosuccinimide. There was a need for understanding the oxidation mechanism of this drug, so that, the study could throw some light on the fate of the drug in the biological system.

In the light of available information and our continued interest on mechanistic studies on haloamietric reactions in general and bioactive compounds in particular, the present investigation was undertaken. The present paper reports for the first time on the detailed kinetics of oxidation of SBL with NBS in HClO_4 and NaOH media. The work was carried out with a view to elucidate the mechanism of the reactions, put forward appropriate rate laws, identify the oxidation products of reactions, ascertain the reactive species of oxidant and compare the kinetic results and oxidative behaviour of NBS in acidic and alkaline solutions.

EXPERIMENTAL

Materials

An aqueous solution of NBS was prepared afresh

* To whom all correspondence should be sent:
E-mail: knmsvp@yahoo.com

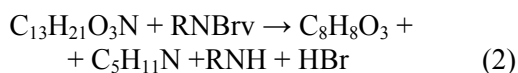
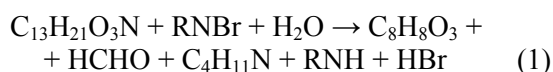
each day from a G.R. Merck sample of the reagent, and its strength was checked by the iodo-metric method [13]. Analar grade SBL (Medrich, India) was used as received. All other reagents used were of analytical grade. Doubly distilled water was used throughout the investigations.

Kinetic measurements

All kinetic measurements were performed in glass stoppered pyrex boiling tubes coated black to eliminate photochemical effects. The reactions were carried out under pseudo-first-order conditions by taking a known excess of $[SBL]_0$ over $[NBS]_0$ at 308 K. Appropriate amounts of SBL, $HClO_4$ or NaOH solutions, mercuric acetate, sodium perchlorate, and water to keep the total volume constant were equilibrated at constant temperature (± 0.1 deg). A measured amount of NBS solution also pre-equilibrated at the same temperature was rapidly added to the mixture. The progress of the reaction was monitored by estimating the amount of unconsumed NBS at regular time intervals iodometrically. The course of reaction was studied for atleast two half-lives. The pseudo-first-order rate constants (k_{obs}) calculated from the linear plots of $\log[NBS]$ vs. time were reproducible within $\pm 4\%$. Regression analysis of the experimental data to obtain regression coefficient, r , was performed using MS Excel.

Stoichiometry and product analysis

Reaction mixtures containing varying ratios of NBS and SBL in presence of $0.1 \text{ mol}\cdot\text{dm}^{-3}$ $HClO_4$ or $0.01 \text{ mol}\cdot\text{dm}^{-3}$ NaOH at 308 K were kept aside for 48 h, so that the substrate was completely converted into products. Estimation of the unreacted NBS showed that one mole of substrate utilized one mole of oxidant in both acidic and alkaline media, confirming the following stoichiometry:



where $R = (CH_2CO)_2$.

The reaction products were neutralized with acid/alkali and extracted with ether. The combined ether extract was evaporated and subjected to column chromatography on silica gel using gradient elution (chloroform). The reduction product of NBS, succinimide (RNH) was detected by spot tests [14] and confirmed by IR absorption bands. The oxidation products of SBL were found to be 3-hydroxy-4-(hydroxymethyl)benzaldehyde, formaldehyde and *t*-butyl amine in acidic medium, and 3-

hydroxy-4-(hydroxymethyl)benzaldehyde, methylene-*N-t*-butylamine in the case of alkaline medium and were detected by spot tests [14]. 3-hydroxy-4-(hydroxymethyl)benzaldehyde was further confirmed by IR absorption bands. RNH: a broad band at 3450 cm^{-1} for NH stretching mode and a sharp band at 1698 cm^{-1} for C=O stretching mode. 3-hydroxy-4-(hydroxymethyl)benzaldehyde: 1705 cm^{-1} (C=O stretch), 2848 cm^{-1} (aldehydic C-H stretch) and 3473 cm^{-1} (O-H stretch).

RESULTS

The kinetics of oxidation of SBL with NBS has been kinetically investigated at different initial concentrations of reactants in the presence of $HClO_4$ or NaOH at 308 K. In the present investigations we could not establish the identical experimental conditions for acidic and alkaline media. The salient features obtained in these two media are discussed separately.

Kinetics of oxidation in acidic medium

Under pseudo-first-order conditions ($[SBL] \gg [NBS]$) at constant $[HClO_4]$ and temperature, plots of $\log[NBS]$ vs. time were linear ($r \geq 0.996$) indicating a first-order dependence of rate on $[NBS]_0$. The pseudo-first-order rate constant (k_{obs}) calculated is given in Table 1. Further, the values of k_{obs} calculated from these plots are unaltered with variation of $[NBS]_0$ confirming the first-order dependence on $[NBS]_0$.

Table 1. Effect of varying concentrations of oxidant, substrate and $HClO_4$ on the reaction rate at 308 K; $[Hg(OAC)_2] = 1 \times 10^{-3} \text{ mol}\cdot\text{dm}^{-3}$; $\mu = 0.2 \text{ mol}\cdot\text{dm}^{-3}$.

$[NBS] \times 10^4$ ($\text{mol}\cdot\text{dm}^{-3}$)	$[SBL] \times 10^3$ ($\text{mol}\cdot\text{dm}^{-3}$)	$[HClO_4] \times 10$ ($\text{mol}\cdot\text{dm}^{-3}$)	$k_{obs} \times 10^4$ (s^{-1})
1.0	8.0	1.0	3.30 ± 0.0351
3.0	8.0	1.0	3.37 ± 0.0350
5.0	8.0	1.0	3.36 ± 0.0450
7.0	8.0	1.0	3.31 ± 0.0458
9.0	8.0	1.0	3.38 ± 0.0503
5.0	4.0	1.0	2.20 ± 0.0405
5.0	6.0	1.0	2.90 ± 0.0350
5.0	10.0	1.0	3.99 ± 0.0360
5.0	12.0	1.0	4.36 ± 0.0362
5.0	8.0	0.6	2.29 ± 0.0430
5.0	8.0	0.8	2.88 ± 0.0356
5.0	8.0	1.2	3.99 ± 0.0358
5.0	8.0	1.4	4.46 ± 0.0430
5.0 ^a	8.0	1.0	3.34 ± 0.0442
5.0 ^b	8.0	1.0	3.37 ± 0.0353

^a $\mu = 0.25 \text{ mol}\cdot\text{dm}^{-3}$; ^b $\mu = 0.3 \text{ mol}\cdot\text{dm}^{-3}$.

The rate increased with increase in $[SBL]_0$ (Table 1). A plot of $\log k_{obs}$ vs. $\log[SBL]$ was linear (Fig. 1; $r = 0.998$) with a slope of 0.62 indicating fractional order dependence of the rate on $[SBL]_0$. The rate

increased with increase in $[\text{HClO}_4]$ (Table 1) and a plot of $\log k_{\text{obs}}$ vs. $\log[\text{HClO}_4]$ was linear (Fig. 2; $r = 0.999$) with a slope of 0.78 indicating fractional order with respect to $[\text{H}^+]$. At constant $[\text{H}^+]$, addition of chloride ions in the form of NaCl does not change the rate of reaction.

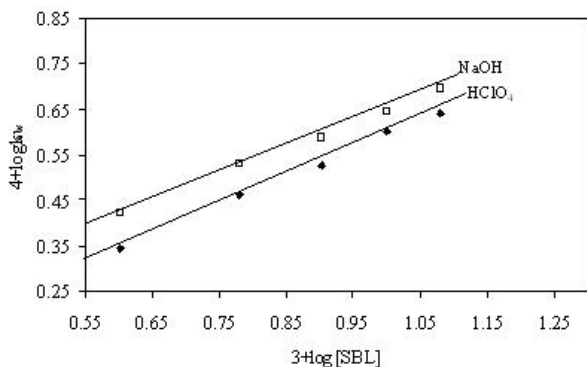


Fig. 1. Plot of $4 + \log k_{\text{obs}}$ vs. $3 + \log[\text{SBL}]$.

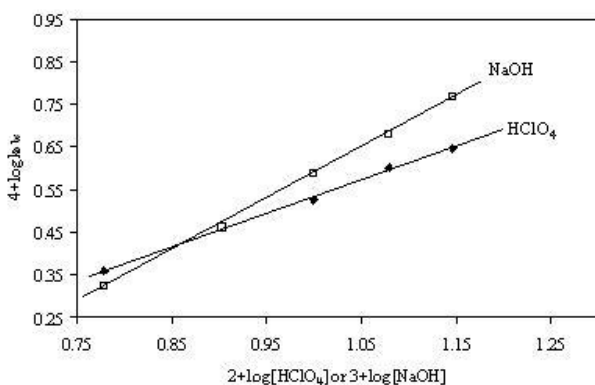


Fig. 2. Plot of $2 + \log[\text{HClO}_4]$ or $3 + \log[\text{NaOH}]$ vs. $4 + \log k_{\text{obs}}$.

Addition of succinimide (0.0002 – $0.001 \text{ mol}\cdot\text{dm}^{-3}$) to the reaction mixture, variation of ionic strength of the medium (0.2 – $0.3 \text{ mol}\cdot\text{dm}^{-3}$) and addition of mercuric acetate (0.001 – $0.005 \text{ mol}\cdot\text{dm}^{-3}$) had no significant effect on the rate. The rate increased with increasing CH_3CN content (0 – 20% v/v) and the results are shown in Table 2.

Table 2. Effect of varying dielectric permittivity of the medium on the reaction rate at 308 K.

CH ₃ CN (% v/v)	<i>D</i>	$k_{\text{obs}} \times 10^4 \text{ (s}^{-1}\text{)}$	
		Acidic ^a	Alkaline ^b
0	73.6	3.36 ± 0.0450	3.87 ± 0.0340
5	71.8	4.38 ± 0.0501	3.48 ± 0.0355
10	70.0	6.06 ± 0.0525	2.88 ± 0.0345
15	68.2	7.79 ± 0.0460	2.51 ± 0.0430
20	66.5	10.28 ± 0.0380	2.14 ± 0.0501

^a $[\text{NBS}] = 5 \times 10^{-4} \text{ mol}\cdot\text{dm}^{-3}$; $[\text{SBL}] = 8 \times 10^{-3} \text{ mol}\cdot\text{dm}^{-3}$; $[\text{HClO}_4] = 0.1 \text{ mol}\cdot\text{dm}^{-3}$; $\mu = 0.2 \text{ mol}\cdot\text{dm}^{-3}$; $[\text{Hg}(\text{OAC})_2] = 1 \times 10^{-3} \text{ mol}\cdot\text{dm}^{-3}$;

^b $[\text{NBS}] = 5 \times 10^{-4} \text{ mol}\cdot\text{dm}^{-3}$; $[\text{SBL}] = 8 \times 10^{-3} \text{ mol}\cdot\text{dm}^{-3}$; $[\text{NaOH}] = 1 \times 10^{-2} \text{ mol}\cdot\text{dm}^{-3}$; $\mu = 0.1 \text{ mol}\cdot\text{dm}^{-3}$; $[\text{Hg}(\text{OAC})_2] = 1 \times 10^{-3} \text{ mol}\cdot\text{dm}^{-3}$.

Plot of $\log k_{\text{obs}}$ vs. $1/D$ was linear ($r = 0.998$) with a positive slope. The values of permittivity (D) for CH_3CN – H_2O mixtures are calculated from the equation $D = D_w V_w + D_A V_A$ where D_w and D_A are the dielectric permittivities of pure water and acetonitrile and V_w and V_A are the volume fractions of components, water and acetonitrile in the total mixture. Blank experiments performed indicated that CH_3CN was not oxidized with NBS under the experimental conditions employed. Solvent isotope study in D_2O medium was made. The value of $k_{\text{obs}}(\text{H}_2\text{O})$ is 3.36 and that of $k_{\text{obs}}(\text{D}_2\text{O})$ is 2.40 leading to solvent isotope effect of $k_{\text{obs}}(\text{H}_2\text{O})/k_{\text{obs}}(\text{D}_2\text{O}) = 1.40$. Proton inventory studies were made in H_2O – D_2O mixtures and the results are shown in Table 3. The corresponding proton inventory plot for the rate constant k_{obs} in a solvent mixture containing deuterium atom fraction (n) is given in Fig. 3.

Table 3. Proton inventory studies in H_2O – D_2O mixture at 308 K

Atom fraction of D_2O (<i>n</i>)	$k_{\text{obs}} \times 10^4 \text{ (s}^{-1}\text{)}$	
	Acidic ^a	Alkaline ^b
0.0	3.36 ± 0.0450	3.87 ± 0.0340
0.25	3.19 ± 0.0353	3.37 ± 0.0405
0.50	2.98 ± 0.0424	3.03 ± 0.0371
0.75	2.70 ± 0.0503	2.80 ± 0.0455
0.95	2.40 ± 0.0362	2.30 ± 0.0358

^a $[\text{NBS}] = 5 \times 10^{-4} \text{ mol}\cdot\text{dm}^{-3}$; $[\text{SBL}] = 8 \times 10^{-3} \text{ mol}\cdot\text{dm}^{-3}$; $[\text{HClO}_4] = 0.1 \text{ mol}\cdot\text{dm}^{-3}$; $\mu = 0.2 \text{ mol}\cdot\text{dm}^{-3}$; $[\text{Hg}(\text{OAC})_2] = 1 \times 10^{-3} \text{ mol}\cdot\text{dm}^{-3}$;

^b $[\text{NBS}] = 5 \times 10^{-4} \text{ mol}\cdot\text{dm}^{-3}$; $[\text{SBL}] = 8 \times 10^{-3} \text{ mol}\cdot\text{dm}^{-3}$; $[\text{NaOH}] = 1 \times 10^{-2} \text{ mol}\cdot\text{dm}^{-3}$; $\mu = 0.1 \text{ mol}\cdot\text{dm}^{-3}$; $[\text{Hg}(\text{OAC})_2] = 1 \times 10^{-3} \text{ mol}\cdot\text{dm}^{-3}$.

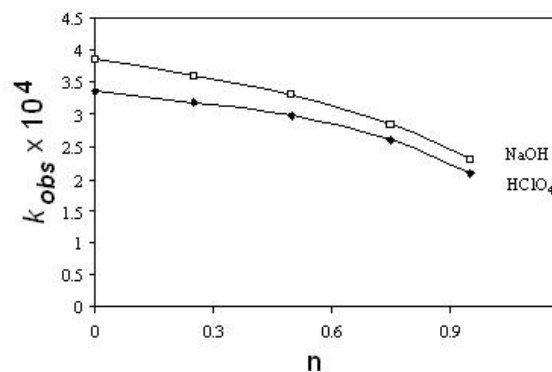


Fig. 3. Plot of k_{obs} vs. n .

The reaction was studied at different temperatures (300 – 318 K) keeping other experimental conditions constant. From the linear Arrhenius plot of $\log k_{\text{obs}}$ vs. $1/T$ (Fig. 4; $r = 0.999$), the values of activation parameters for the overall reaction were computed. The results are compiled in Table 4. The absence of free radicals during the course of oxidation was confirmed when no polymerization was initiated with addition of acrylonitrile solution to the reaction mixture.

Kinetics of oxidation in alkaline medium

With substrate in excess at constant [NaOH] and temperature, the [NBS]₀ was varied. Plots of log[NBS] vs. time were linear ($r \geq 0.998$) indicating a first-order dependence of the rate on [NBS]₀. The pseudo-first-order rate constant (k_{obs}) obtained is listed in Table 5. The values of k_{obs} increased with increase in [SBL] (Table 5) and a plot of $\log k_{\text{obs}}$ vs. $\log[\text{SBL}]$ (Fig. 1; $r = 0.999$) gave a slope of 0.58 indicating fractional-order dependence of the rate on [SBL]₀. The higher [NaOH], i.e. [OH⁻] leads to higher k_{obs} (Table 5) and from the linear plot of $\log k_{\text{obs}}$ vs. $\log[\text{NaOH}]$, (Fig. 2; $r = 0.996$) an order of 1.02 was obtained showing first-order dependence of the rate on [NaOH].

Table 4. Effect of varying temperature on the reaction rate and activation parameters for the oxidation of SBL.

Temperature (K)	$k_{\text{obs}} \times 10^4$ (s ⁻¹)	
	Acidic ^a	Alkaline ^b
300	1.38 ± 0.0475	1.90 ± 0.0370
304	2.18 ± 0.0510	2.69 ± 0.0358
308	3.36 ± 0.0450	3.87 ± 0.0340
313	6.45 ± 0.0550	5.45 ± 0.0430
318	11.49 ± 0.0515	8.51 ± 0.0425
E_a (kJ·mol ⁻¹)	94.54	66.07
ΔH^\ddagger (kJ·mol ⁻¹)	91.97	63.51
ΔG^\ddagger (kJ·mol ⁻¹)	95.86	95.72
ΔS^\ddagger (JK ⁻¹ ·mol ⁻¹)	-12.60	-104.36

^a [NBS] = 5×10^{-4} mol·dm⁻³; [SBL] = 8×10^{-3} mol·dm⁻³; [HClO₄] = 0.1 mol·dm⁻³; $\mu = 0.2$ mol·dm⁻³; [Hg(OAC)₂] = 1×10^{-3} mol·dm⁻³;
^b [NBS] = 5×10^{-4} mol·dm⁻³; [SBL] = 8×10^{-3} mol·dm⁻³; [NaOH] = 1×10^{-2} mol·dm⁻³; $\mu = 0.1$ mol·dm⁻³; [Hg(OAC)₂] = 1×10^{-3} mol·dm⁻³.

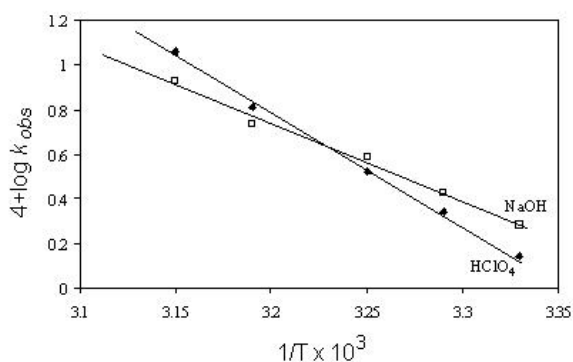


Fig. 4. Arrhenius plot of $4 + \log k_{\text{obs}}$ vs. $10^3/T$.

Addition of succinimide (0.0002 – 0.001 mol·dm⁻³) to the reaction mixture, variation of ionic strength of the medium (0.1 – 0.3 mol·dm⁻³) and addition of mercuric acetate (0.001 – 0.005 mol·dm⁻³) had no significant effect on the rate. The rate decreased with increasing CH₃CN content (0 – 20% v/v) and the results are shown in Table 2. Plot of $\log k_{\text{obs}}$ vs. $1/D$ was linear ($r = 0.998$) with a negative slope. Solvent isotope study in D₂O medium was made. The value of $k_{\text{obs}}(\text{H}_2\text{O})$ is 3.87 and that of $k_{\text{obs}}(\text{D}_2\text{O})$ is 2.30

leading to solvent isotope effect $k_{\text{obs}}(\text{H}_2\text{O})/k_{\text{obs}}(\text{D}_2\text{O}) = 1.68$. Proton inventory studies were made in H₂O–D₂O mixtures, and the results are shown in Table 3. The corresponding proton inventory plot for the rate constant k_{obs} in a solvent mixture containing deuterium atom fraction (n) is given in Fig. 3. Kinetic and thermodynamic parameters were calculated by studying the reaction at different temperatures (300 – 318 K) and from the linear Arrhenius plot of $\log k_{\text{obs}}$ vs. $1/T$. (Fig. 4; $r = 0.999$). These results are given in Table 4. Absence of free radicals in the reaction mixture has been demonstrated by the acrylonitrile test.

Table 5. Effect of varying concentrations of oxidant, substrate and NaOH on the reaction rate at 308 K; [Hg(OAC)₂] = 1×10^{-3} mol·dm⁻³; $\mu = 0.1$ mol·dm⁻³.

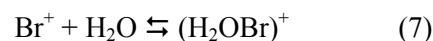
[NBS] × 10 ⁴ (mol·dm ⁻³)	[SBL] × 10 ³ (mol·dm ⁻³)	[NaOH] × 10 ² (mol·dm ⁻³)	$k_{\text{obs}} \times 10^4$ (s ⁻¹)
1.0	8.0	1.0	3.86 ± 0.0355
3.0	8.0	1.0	3.89 ± 0.0351
5.0	8.0	1.0	3.87 ± 0.0340
7.0	8.0	1.0	3.81 ± 0.0360
9.0	8.0	1.0	3.80 ± 0.0470
5.0	4.0	1.0	2.64 ± 0.0503
5.0	6.0	1.0	3.38 ± 0.0458
5.0	10.0	1.0	4.41 ± 0.0430
5.0	12.0	1.0	4.95 ± 0.0356
5.0	8.0	0.6	2.10 ± 0.0442
5.0	8.0	0.8	2.88 ± 0.0353
5.0	8.0	1.2	4.78 ± 0.0503
5.0	8.0	1.4	5.87 ± 0.0358
^a 5.0	8.0	1.0	3.82 ± 0.0362
^b 5.0	8.0	1.0	3.85 ± 0.0405

^a $\mu = 0.15$ mol·dm⁻³; ^b $\mu = 0.2$ mol·dm⁻³.

DISCUSSION AND MECHANISMS

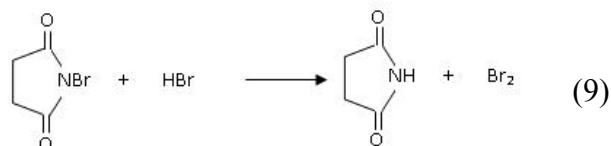
Reactive species of NBS

NBS is a double equivalent oxidant which oxidizes many substrates through NBS itself or Br⁺ or RN⁺HBr or hypobromite anion. The reactive species responsible for the oxidizing character may depend on the pH of the medium [3]. Depending on the pH of the medium, NBS furnishes different types of reactive species in solutions [15–17] as shown in the following equations:



where R = (CH₂CO)₂.

In acidic medium, the probable reactive species of NBS are NBS itself or Br^+ or protonated NBS (RN^+HBr), and the reactive species in alkaline solutions are NBS itself or HOBr or OBr^- . It may be pointed out that, all kinetic studies have been made in presence of mercury(II) acetate in order to avoid any possible bromine oxidation which may be produced as follows:

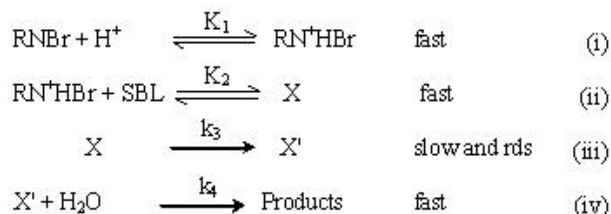


Mercuric acetate acts as a capture agent for any Br^- formed in the reaction and exists as HgBr_4^{2-} or unionized HgBr_2 and ensures that oxidation takes place purely through NBS [18, 19].

Mechanism and rate law in acidic medium

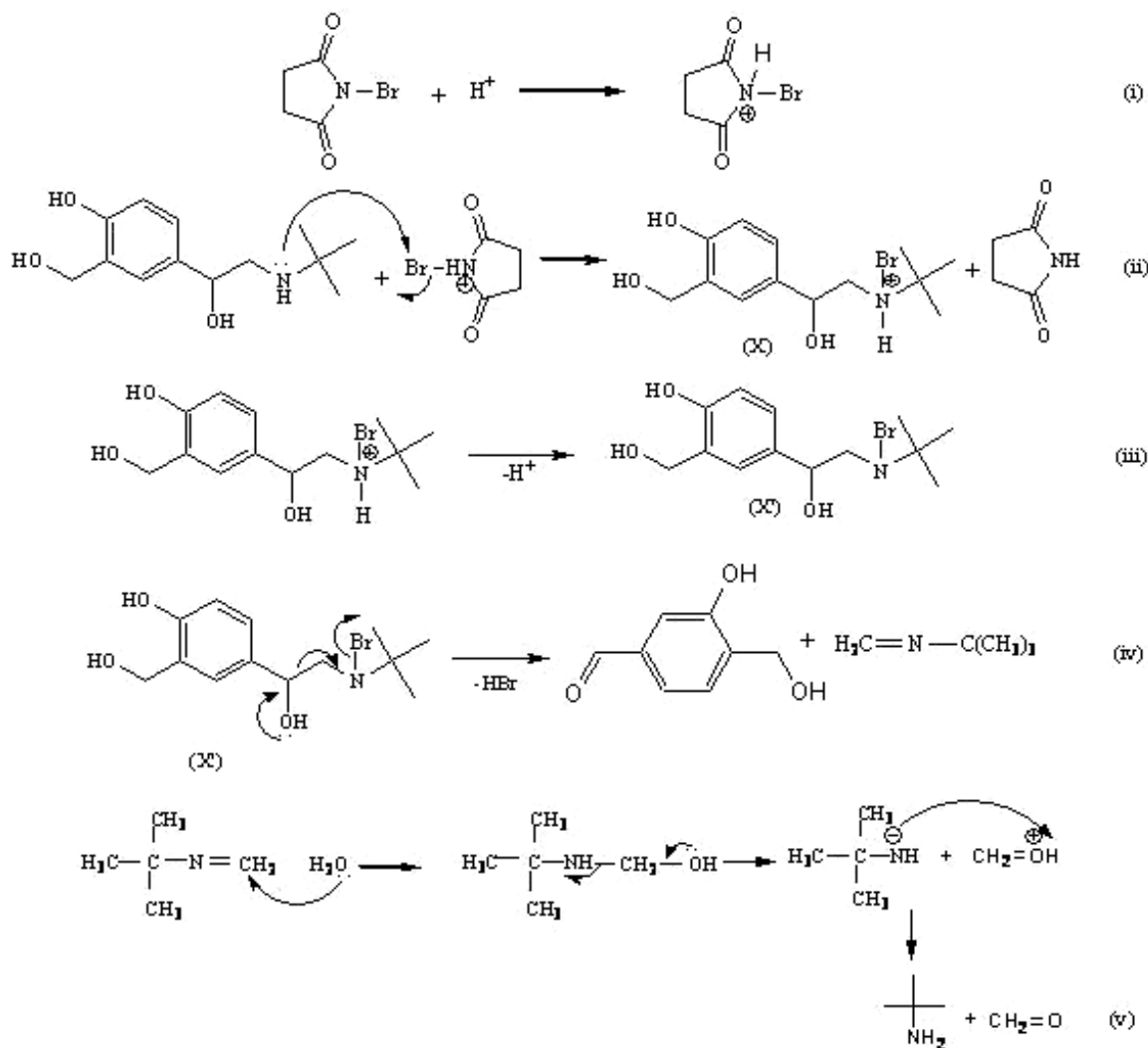
Most investigations of NBS oxidations of organic substrates have assumed that, the molecular NBS acts only through its positive polar end [20, 21]. In

the present investigation, acceleration of the rate by increasing concentration of H^+ , assumes that protonated species of NBS, i.e., RN^+HBr is the most likely oxidizing species. Further, the insignificant effect of initially added product succinimide, (RNH) allows us to take RN^+HBr as the active oxidizing species. The protonated NBS reacts with SBL to form a complex which further undergo hydrolysis and intramolecular rearrangement to form products.



Scheme 1.

In Scheme 1, X and X' are the intermediate species whose structures are shown in Scheme 2, where a detailed mechanistic interpretation of SBL oxidation with NBS in acid medium is proposed.



Scheme 2.

Step (iii) of Scheme 1 determines the overall rate:

$$rate = \frac{-d[RNBr]}{dt} = k_3[X]. \quad (10)$$

If $[RNBr]_t$ represents the total effective concentration of NBS in solution, then

$$[RNBr]_t = [RNBr] + [RN^+HBr] + [X] \quad (11)$$

From step (i) of Scheme 1

$$[RNBr] = [RN^+HBr]/K_1[H^+] \quad (12)$$

From step (ii) of Scheme 1

$$[RN^+HBr] = [X]/K_2[SBL] \quad (13)$$

Substituting Eqns. (12) and (13) in Eqn. (11) one obtains:

$$[X] = \frac{K_1K_2[RNBr]_t[SBL][H^+]}{1 + K_1[H^+] + K_1K_2[SBL][H^+]} \quad (14)$$

By substituting for $[X]$ from Eqn. (14) in Eqn. (10), the following rate law can be obtained:

$$rate = \frac{K_1K_2k_3[RNBr]_t[SBL][H^+]}{1 + K_1[H^+] + K_1K_2[SBL][H^+]} \quad (15)$$

Since $rate = k_{obs}[RNBr]_t$, Eqn. (15) can be transformed into Eqns. (16) and (17):

$$k_{obs} = \frac{K_1K_2k_3[SBL][H^+]}{1 + K_1[H^+][1 + K_2[SBL]]} \quad (16)$$

$$\frac{1}{k_{obs}} = \frac{1}{K_1K_2k_3[SBL][H^+]} + \frac{1}{K_2k_3[SBL]} + \frac{1}{k_3}$$

$$\frac{1}{k_{obs}} = \frac{1}{K_2k_3[SBL]} \left\{ \frac{1}{K_1[H^+]} + 1 \right\} + \frac{1}{k_3} \quad (17)$$

Based on Eqn. (17), plot of $1/k_{obs}$ vs. $1/[SBL]$ (Fig. 5; $r = 0.998$) at constant $[H^+]$ and temperature has been found to be linear. From the intercept of the above plot, the value of k_3 was found to be $7.64 \times 10^{-4} \text{ s}^{-1}$.

The change in solvent composition by varying the CH_3CN content in $\text{CH}_3\text{CN-H}_2\text{O}$ affects the reaction rate. For limiting case of zero angle of approach between two dipoles or an ion-dipole system, Amis [22] has shown that a plot of $\log k_{obs}$ vs. $1/D$ gives a straight line, with a positive slope for a reaction involving a positive ion and a dipole and a negative slope for a negative ion-dipole or dipole-dipole interactions. In the present investigation a plot of $\log k_{obs}$ vs. $1/D$ was linear with a positive slope. This observation indicates the ion-dipole nature of the rate determining step in the reaction

sequence and also points to extending of charge to the transition state.

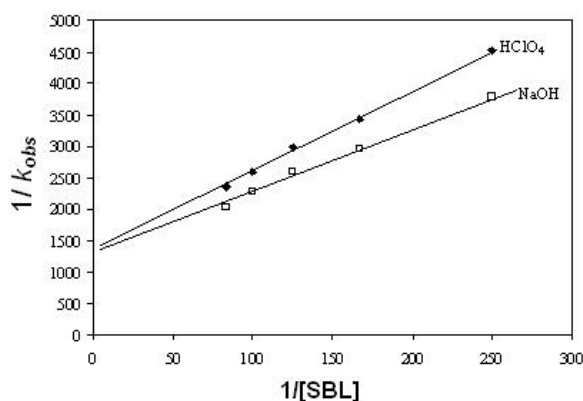


Fig. 5. Plot of $1/k_{obs}$ vs. $1/[SBL]$.

The observed solvent isotope effect supports the proposed mechanism and the derived rate law. For a reaction involving a fast equilibrium H^+ or OH^- ion transfer, the rate increases in D_2O medium, since D_3O^+ and OD^- are stronger acid and stronger base respectively than H_3O^+ and OH^- ions [23, 24]. In the present case, the observed solvent isotope effect of $k_{obs}(\text{H}_2\text{O})/k_{obs}(\text{D}_2\text{O}) > 1$ is due to the protonation step followed by hydrolysis involving the OH bond scission. The retardation of rate in D_2O is due to the hydrolysis step which tends to make the normal kinetic isotope effect. The proton inventory studies made in $\text{H}_2\text{O-D}_2\text{O}$ mixture could throw light on the nature of the transition state. The dependence of the rate constant, k_{obs} on the deuterium atom fraction 'n' in the solvent mixture is given by the following form of Gross-Butler equation [25]:

$$\frac{k'_o}{k'_n} = \frac{\pi\text{TS}(1-n+n\phi_i)}{\pi\text{RS}(1-n+n\phi_j)} \quad (18)$$

where ϕ_i and ϕ_j are isotope fractionation factor for isotopically exchangeable hydrogen sites in the transition state (TS) and in the ground/reactant state (RS), respectively. The Gross-Butler equation permits the evaluation of ϕ_i when the value of ϕ_j is known. However, the curvature of proton inventory plot could reflect the number of exchangeable proton in the reaction [25]. Plot of k_{obs} versus n is a curve in the present case, and this, in comparison with the standard curves, indicate the involvement of a single proton or H-D exchange in the reaction sequence [26]. This proton exchange is indicative of the participation of hydrogen in the formation of transition state.

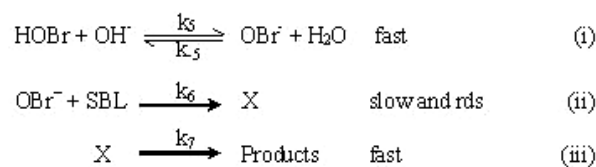
The negligible influence of added succinimide and halide ions on the rate are in agreement with the proposed mechanism. The proposed mechanism is also supported by the high values of energy of

activation and other thermodynamic parameters. The fairly high positive value of ΔH^\ddagger indicates that, the transition state is highly solvated.

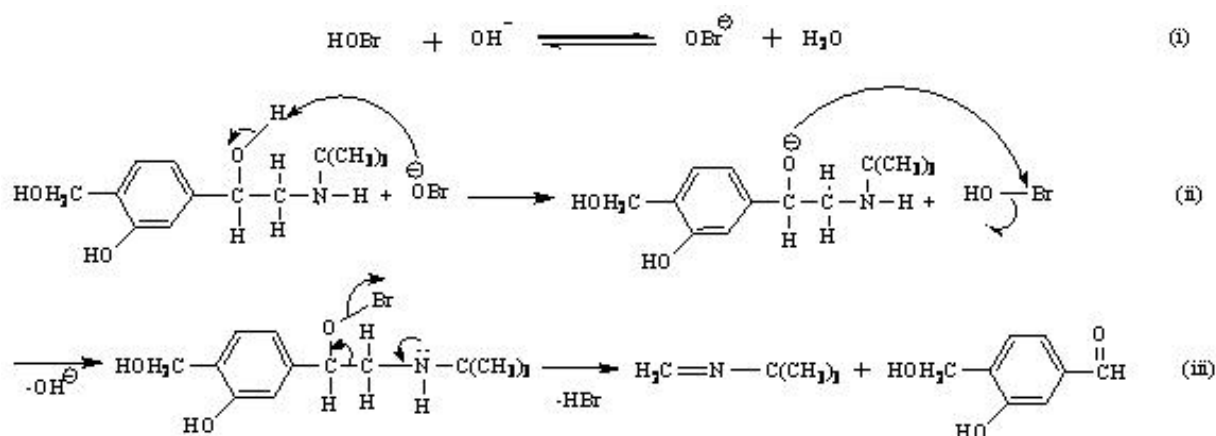
Mechanism and rate law in alkaline medium

NBS is a double equivalent oxidant, which oxidizes many substrate through NBS itself, or hypobromite anion [27, 28]. The reaction exhibits 1:2 stoichiometry of SBL and NBS with unit order dependence on [NBS]. Increase in rate with increasing $[\text{OH}^-]$ can be well explained [29] by the formation of oxidant species OBr^- according to the equilibria (5) and (8). Insignificant effect of added

succinimide on the rate can be attributed to the involvement of OBr^- according to the equilibrium step (5). Hence OBr^- reacts with the substrate to form a complex (X) in the rate determining step, which then undergoes decomposition in the fast step to give products as shown in Scheme 3. A detailed mechanistic interpretation is shown in Scheme 4.



Scheme 3.



Scheme 4.

From the slow step of Scheme 3

$$\text{rate} = \frac{-d[\text{RNBr}]}{dt} = k_6[\text{OBr}^-][\text{SBL}] \quad (19)$$

Applying steady state condition for OBr^- , it can be shown that

$$[\text{OBr}^-] = \frac{k_5[\text{HOBr}][\text{OH}^-]}{k_{-5}[\text{H}_2\text{O}] + k_6[\text{SBL}]} \quad (20)$$

On substituting Eqn. (20) in Eqn. (19), the following rate law (Eqn. (21)) is obtained:

$$\text{rate} = \frac{k_5 k_6 [\text{HOBr}][\text{OH}^-][\text{SBL}]}{k_{-5}[\text{H}_2\text{O}] + k_6[\text{SBL}]} \quad (21)$$

Since $\text{rate} = k_{\text{obs}}[\text{NBS}]$, Eqn. (21) can be transferred into Eqns. (22) and (23):

$$k_{\text{obs}} = \frac{k_5 k_6 [\text{OH}^-][\text{SBL}]}{k_{-5}[\text{H}_2\text{O}] + k_6[\text{SBL}]} \quad (22)$$

$$\frac{1}{k_{\text{obs}}} = \frac{k_{-5}[\text{H}_2\text{O}]}{k_5 k_6 [\text{OH}^-][\text{SBL}]} + \frac{1}{k_5 [\text{OH}^-]} \quad (23)$$

Based on Eqn. (23), a plot of $1/k_{\text{obs}}$ vs $1/[\text{SBL}]$ (Fig. 5, $r = 0.997$) at constant $[\text{OH}^-]$ and temperature has been found to be linear. From the slope and intercept of the above plot, the values of k_5 and k_{-5}/k_6 were found to be $0.0816 \text{ mol}^{-1}\cdot\text{dm}^3\cdot\text{s}^{-1}$ and 1.513×10^{-4} respectively, with $[\text{H}_2\text{O}] = 55.5 \text{ mol}\cdot\text{dm}^{-3}$. The proposed Scheme 3 and rate law (Eqn. (21)) are also substantiated by the experimental results discussed below.

The negligible influence of the added succinimide and variation of ionic strength of the medium is consistent with the proposed mechanism. The dielectric effect observed in the present case indicates ion-dipole interaction in the rate limiting step. The sign and magnitude of ΔS^\ddagger observed suggested that the activated complex is more compact than the ground state. The positive free energy of activation shows that the transition state is highly solvated.

The solvent isotope effect $k_{\text{obs}}(\text{H}_2\text{O})/k_{\text{obs}}(\text{D}_2\text{O}) > 1$ is noticed in alkaline medium supports the proposed mechanism. The magnitude of retardation in D_2O medium can be attributed to the first-order depend-

ence on $[\text{OH}^-]$ and may be due to the involvement of hydrolysis step in the rate limiting step.

CONCLUSIONS

In conclusion, the stoichiometry of oxidation of salbutamol with NBS is same in both acidic and alkaline media. Kinetic studies in acidic medium reveal that, $(\text{CH}_2\text{CO})_2\text{N}^+\text{HBr}$ as active oxidant species which oxidizes the substrate to the corresponding aldehyde. In alkaline medium the reaction takes place between the substrate and OBr^- to form the corresponding aldehyde. The magnitude of the two activation energies indicates that, the reaction is faster in alkaline medium compared to acidic medium. The different active oxidizing species involved in the two media are responsible for the difference in activity. Hence, the kinetics of oxidation of SBL with NBS is more facile in alkaline medium in comparison with acidic medium.

Acknowledgement: The authors are thankful to the University of Mysore, Mysore for the financial support.

REFERENCES

1. R. Filler, *Chem. Rev.*, **63**, 21 (1963).
2. S. K. Mavalangi, M. R. Kembhavi, S. T. Nandibewoor, *Turk. J. Chem.*, **25**, 355 (2001).
3. G. Gopalakrishnan, J. L. Hogg, *J. Org. Chem.*, **50**, 1206 (1985).
4. A. K. Singh, S. Rahmani, V. Singh, V. Gupta, B. Singh, *Oxid. Commun.*, **23**, 55 (2000).
5. C. P. Kathari, P. D. Pol, S. T. Nandibewoor, *Inorg. React. Mech.*, **3**, 213 (2002).
6. K. Basavaiah, U. R. Anil Kumar, *Bull. Chem. Soc. Ethiopia*, **22**, 135 (2008).
7. K. Basavaiah, U. R. Anil Kumar, *Proc. Nat. Acad. Sci. USA*, **77A**, 301 (2007).
8. K. Basavaiah, U. R. Anil Kumar, V. Ramakrishna, *Indian J. Chem. Technol.*, **14**, 313 (2007).
9. K. Basavaiah, V. Ramakrishna, B. Somashekara, *Acta Pharm.*, **57**, 87 (2007).
10. R. Ramachandrappa, Puttaswamy, S. M. Mayanna, N. M. Made Gowda, *Int. J. Chem. Kinet.*, **30**, 407 (1998).
11. K. N. Mohana, P. M. Ramdas Bhandarkar, *J. Chin. Chem. Soc.*, **54**, 1223 (2007).
12. K. J. Isselbacher, E. Braunwald, J. D. Wilson, J. B. Martin, A. S. Fauci, D. L. Kasper, Harrison's Principles of Internal Medicine, 13th edition, McGraw-Hill Inc, New York, 1994.
13. N. K. Mathur, C. R. Narang, The Determination of Organic Compounds with N-bromosuccinimide, Academic Press, New York, 1975.
14. F. Feigl, V. Anger, Spot Tests in Organic Analysis, Elsevier, New York, 1975.
15. C. P. Kathari, R. M. Mulla, S. T. Nandibewoor, *Oxid. Commun.*, **28**, 579 (2005).
16. B. Singh, L. Pandey, J. Sharma, S. M. Pandey, *Tetrahedron*, **38**, 169 (1982).
17. B. Thimmegowda, J. Iswara Bhat, *Indian J. Chem.*, **28A**, 43 (1989).
18. A. K. Singh, S. Rahmani, V. K. Singh, V. Gupta, D. Kesarwani, B. Singh, *Indian J. Chem.*, **40A**, 519 (2001).
19. G. Gopalakrishnan, B. R. Pai, N. Venkatasubramanian, *Indian J. Chem.*, **19B**, 293 (1980).
20. J. M. Antelo, F. Arce, J. Crugeiras, M. Parajo, *J. Phys. Org. Chem.*, **10**, 631 (1997).
21. N. Venkatasubramanian, V. Thiagarajan, *Can. J. Chem.*, **47**, 694 (1969); *Indian J. Chem.*, **8**, 809 (1970).
22. E. S. Amis, Solvent Effects on Reaction Rates and Mechanisms, Academic Press, New York, 1966.
23. C. J. Collins, N. S. Bowman, Isotope Effects in the Chemical Reactions, Van Nostrand Reinhold, New York, 1970.
24. K. B. Wiberg, *Chem. Rev.*, **55**, 713 (1955); K. B. Wiberg, Physical Organic Chemistry, Wiley, New York, 1964.
25. W. J. Albery, M. H. Davies, *J. Chem. Soc. Faraday Trans.*, **68**, 167 (1972).
26. N. S. Isaacs, Physical Organic Chemistry, Wiley, New York, 1987.
27. R. B. Chougale, D. L. Kamble, S. T. Nandibewoor, *Polish J. Chem.*, **71**, 986 (1997).
28. S. K. Mavalangi, M. Nirmala, N. Halligudi, S. T. Nandibewoor, *React. Kinet. Catal. Lett.*, **72**, 391 (2001).
29. D. L. Kamble, G. H. Hugar, S. T. Nandibewoor, *Indian J. Chem.*, **35A**, 144 (1996).

ИЗСЛЕДВАНЕ НА КИНЕТИКАТА И МЕХАНИЗМА НА ОКИСЛИТЕЛНО РАЗПАДАНЕ НА САЛБУТАМОЛ С *N*-БРОМСУКЦИНАМИД В КИСЕЛА И АЛКАЛНА СРЕДА

П. М. Рамдас Бхандаркар, К. Н. Мохана*

Департамент по химически изследвания, Университет на Майсур, Манасаганготри, Майсур 570006, Индия

Постъпила на 17 февруари 2009 г.; Преработена на 17 юни 2009 г.

(Резюме)

Салбутамол сулфат (SBL) е β_2 -адренергичен рецептор агонист използван за облекчаване на бронхоспазми при астма и хронична обструктивна белодробна болест (COPD). Кинетичното изследване на окислението на това биологично активно съединение се използва за изясняване на механизма на редокс реакции. Затова кинетиката на окислително разлагане на SBL с *N*-бромсукцинимид (NBS) в среда от HClO₄ или NaOH е изследвано при 308 K. Експериментално получените уравнения за скоростта са $-d[\text{NBS}]/dt = [\text{NBS}][\text{SBL}]^x[\text{H}^+]^y$ в кисела среда и $-d[\text{NBS}]/dt = [\text{NBS}][\text{SBL}]^x[\text{OH}^-]$ в алкална среда, където x и y са по-малки от единица. Реакциите са провеждани при промени в концентрацията на сукцинимид, продукта на редукция на NBS, концентрацията на добавените неутрални соли, диелектричната проводимост и йонната сила на средата. Изотопния ефект на разтворителя е изследван като е използвана D₂O. Определена е стехиометрията на реакцията и са идентифицирани и охарактеризирани продуктите на окисление в двете среди. Параметрите на активация за сумарните реакции са изчислени от Арениусовите зависимости. Като реакционни окислителни форми са приети (CH₂CO)₂ N⁺HBr и OBr⁻ съответно в кисела или алкална среда. Реакцията на окисление не води до полимеризация на добавен акрилонитрил. Намерено е, че реакцията е по-бърза в алкална среда отколкото в кисела среда. Предложени са механизми за обяснение на получените резултати и съответни уравнения за скоростта на реакциите.

Chemical composition and antibacterial activity of essential oil from leaves, stems and flowers of *Prangos ferulacea* (L.) Lindl. grown in Iran

M. T. Akbari¹, A. Esmaili^{2*}, A. H. Zarea³, N. Saad³, F. Bagheri³

¹Department of Chemistry, Islamic Azad University, Khomeini Shahr, Esfhan, Iran

²Department of Chemical Engineering, North Tehran Branch, Islamic Azad University, Tehran, Iran

³Pharmaceutical Sciences Branch, Islamic Azad University, Tehran, Iran

Received December 31, 2008; Revised July 27, 2009

Essential oils from the leaves, stems and flowers of *Prangos ferulacea* (family *Umbelliferae*) growing in Esfahan, Iran, were obtained by hydrodistillation using a Clevenger-type apparatus and their chemical composition and antibacterial activity analysed by GC-MS. All the oils consisted mainly of oxygenated monoterpenes and a small percentage of sesquiterpene compounds. In the oil from the leaf, 10 components were identified, dominated by oxygenated monoterpenes. The three major constituents identified (representing 65.1% of the oil) were linalool (36.7%), caryophyllene oxide (16.3%) and α -pinene (12.1%). In the stem oil, 11 compounds were identified, with oxygenated monoterpenes again predominating. The two major constituents identified (representing 29.3% of the oil) were 1,8-cineole (19.0%) and α -pinene (10.3%). Of the 17 compounds found in the flower oil, the five main components identified (representing 74.1% of the oil) were oxygenated monoterpenes: linalool (19.0%), lavandulyl acetate (16.0%), 1,8-cineole (14.5%), α -pinene (12.4%) and geranyl isobutyrate (12.2%). The oils were tested against four Gram-positive or Gram-negative bacteria. Antibacterial activity was measured using a dilution method. It was found that oil from leaves, stems and flowers of *P. ferulacea*, and especially that of leaves, exhibited interesting antibacterial activity.

Key words: *Prangos ferulacea*, umbelliferae, essential oil, linalool, antibacterial activity.

INTRODUCTION

Of the fifteen species of the genus *Prangos* (family *Umbelliferae*) found in Iran, five are endemic: *P. gaubae*, *P. crossoptera*, *P. tuberculata*, *P. cheilanthifolia* and *P. cattigonoides* [1, 2]. A survey of the literature revealed that the oil composition of *P. latiloba* [3], *P. pabularia* [4], *P. hissarica*, *P. seraiwschanica*, *P. fedtschenkoi* [5], *P. ferulacea* [6, 7], *P. uechtritzi* [8, 9], *P. bornmuelleri* [10], *P. heyniae* [11], *P. uloptera* [12], *P. asperula* [13] and *P. platychlaena* [14] have been reported. The main constituents of the aerial parts of *P. uloptera* were found to be β -caryophyllene (18.2%), germacrene D (17.2%) and limonene (8.7%), whereas the seed oil comprised mainly α -pinene (41.5%) and β -cedrene (4.0%) [12]. Analysis of the aerial parts of *P. asperula* showed δ -3-carene (16.1%), β -phellandrene (14.7%), α -pinene (10.5%), α -humulene (7.8%), germacrene-D (5.4%), δ -cadinene (4.2%) and terpinolene (4.0%) to be the major components of the oil [13]. Aerial parts of *P. uechtritzi* contained δ -carene (3.39%) and *p*-cymene (3.38%) [8, 9], while α -pinene (40.82%), nonene (17.03%), phellandrene (11.14%), δ -carene (7.39%),

and *p*-cymene (4.90%) were identified as major components of *P. platychlaena* [14]. Study of the chemical composition and antibacterial activity of essential oil from aerial parts of *P. ferulacea* (L.) Lindl grown in Iran showed its primary constituents to be α -pinene (36.6%), β -pinene (31.9%) and β -phellandrene (11.7%) [15]. Some *Prangos* species have been used in folk medicine as emollient, carminative [16], tonic, antifatulent, anthelmintic, antifungal and antibacterial agents [17, 18]. Chemical investigations on the components of the genus *Prangos* have resulted in the isolation of various coumarins, alkaloids, flavonoids and terpenoids [19]. According to the literature, leaves, stems and flowers of *P. ferulacea* have not been the subject of any investigation, and this paper is the first such phytochemical study on this plant.

EXPERIMENTAL

Plant material

The sample of *Prangos ferulacea* was collected during the flowering stage in June 2005 from the Province of Esfahan, in the centre of Iran. Voucher specimens were deposited at the Herbarium (Voucher No. 6014) of the Research Institute of Forests and Rangelands (TARI), Tehran, Iran.

* To whom all correspondence should be sent:
E-mail: akbaresmaeili@yahoo.com

Oil isolation

Fresh leaves (80 g), stems (90 g) and flowers (70 g) of *P. ferulacea* were subjected to separate hydro-distillation for 3 h using a Clevenger-type apparatus. After decanting and drying over anhydrous sodium sulphate, the corresponding yellowish coloured oils were recovered from the leaves, stems and flowers in yields of 0.9, 0.8 and 1.1% (w/w), respectively.

Analysis

GC analysis of the oils was performed on a Shimadzu 15A gas chromatograph equipped with a split/splitless injector (250°C). N₂ was used as carrier gas (1 mL/min), and the capillary column used was DB-5 (50 m × 0.2 mm, film thickness 0.32 µm). The column temperature was maintained at 60°C for 3 min and then heated to 220°C with a 5°C/min rate and kept constant at 220°C for 5 min.

GC/MS analysis was performed using a Hewlett-Packard 6890/5973 with an HP-5MS column (30 m × 0.25 mm, film thickness 0.25 µm). The column temperature was maintained at 60°C for 3 min and programmed to 220°C at a rate of 5°C/min, and kept constant at 220°C for 5 min. The flow rate of helium as the carrier gas was 1 mL/min. MS was taken at 70 eV.

Identification of the constituents of each oil was made by comparison of their mass spectra and retention indices (RI) with those given in the literature and the authentic samples [20–22]. Relative percentage amounts were calculated from the peak area using a Shimadzu C-R4A Chromatopac without correction factors.

Antibacterial activity

A collection of four microorganisms was used, including the Gram-positive bacteria *Staphylococcus aureus* (ATCC 1112), *Staphylococcus epidermidis* (ATCC 1114) and *Bacillus cereus* (ATCC 1015) and the Gram-negative bacteria *Pseudomonas aeruginosa* (ATCC 1310), identified by the Research Centre of Science and Industry, Tehran, Iran.

Microorganisms (obtained from enrichment culture of the microorganisms in 1 mL of Mueller-Hinton broth, incubated at 37°C for 12 h) were cultured on Mueller-Hinton agar medium.

The following method was used to measure antibacterial activity: 40 µL of diluted essential oil (40 µL oil in 2 mL DMSO 10%) was added to a 200 µL microbial suspension (1 loop from medium in physiological serum that compared with a 0.5 McFarland standard) in well 1 in a microplate, and 100 µL from this well was added to a 100 µL

microbial suspension in well 2, and this continued until 8 wells in the microplate were filled. Microplates were incubated at 37°C for 24 h [23].

RESULTS AND DISCUSSION

Chemical components identified in the three oils of *P. ferulacea* and their percentage compositions are listed in Table 1.

Table 1. Percentage composition of the leaf, stem and flower oils of *Prangos ferulacea*.

Compound	RI*	Leaf Oil	Stem Oil	Flower Oil
α-pinene	953	12.1	10.3	12.4
sabinene	970	0.5	0.4	1.4
p-cymene	1014	-	-	1.4
1,8-cineole	1033	8.9	19.0	14.5
linalool	1087	36.7	3.7	19.0
α-campholenal	1126	2.3	0.7	7.0
camphor	1136	1.6	-	1.3
α-terpineol	1189	-	2.8	-
myrtenal	1190	-	0.5	0.5
lavandulyl acetate	1289	1.2	-	16.0
β-caryophyllene	1410	-	-	0.6
γ-elemene	1433	-	-	0.6
germacrene D	1480	-	0.5	1.6
δ-cadinene	1524	-	-	1.4
geranyl isobutyrate	1530	1.2	-	12.2
germacrene B	1556	-	-	0.3
caryophyllene oxide	1581	16.3	4.2	-
β-eudesmol	1648	-	0.7	-
α-cadinol	1650	-	-	6.4
kusinol	1674	0.9	0.5	1.6

* Retention indices as determined on a DB-5 column using the homologous series of *n*-alkane.

The leaf oil consisted of 10 identified compounds representing 81.7% of the oil composition. The main compounds were linalool (36.7%), caryophyllene oxide (16.3%) and α-pinene (12.1%). Another notable constituent was 1,8-cineole (8.9%).

In the stem oil, 11 compounds were identified, representing 43.3% of the oil composition. The main compounds were 1,8-cineole (19.0%) and α-pinene (10.3%).

Linalool (19.0%), lavandulyl acetate (16.0%), 1,8-cineole (14.5%), α-pinene (12.4%) and geranyl isobutyrate (12.2%) were the main compounds among the 17 constituents representing 98.2% of the total components detected in the flower oil.

Oxygenated monoterpenes represented the most abundant constituent of the oil of leaves, stems and flowers (63.3%, 37.4% and 74.7%, respectively). Linalool was the main constituent of the leaf and flower oils (36.7% and 19.0%, respectively), and 1,8-cineole (19.0%) of the stem oil.

The literature survey of the chemical composition of *P. asperula* showed δ -3-carene, β -phellandrene, α -pinene and α -humulene to be the major components of the oil [13].

Dried aerial parts of *Prangos uechtritzi* contained δ -carene (3.39%) and *p*-cymene (3.38%) [8, 9], while α -pinene (40.82%), nonene (17.03%), phellandrene (11.14%), δ -carene (7.39%), and *p*-cymene (4.90%) were identified as major components of *P. platychnaena* [14]. The main compounds of the *P. ferulacea* aerial parts were α -pinene (36.6%), β -pinene (31.9%) and β -phellandrene (11.7%) [15]. In our previous investigation [24] the oil of *P. ferulacea* collected from north of Tehran, Iran, contained α -pinene, δ -3-carene, β -pinene and epi- α -bisabolol as main compounds and was found to be rich in sesquiterpenes hydrocarbons, while in the present study, the stem, leaf and flower oils of the plant, collected from Lorestan Province, Iran, contained mostly oxygenated monoterpenes.

The oil of *P. ferulacea* aerial parts collected from Lorestan province, Iran, and of *P. acaulis* from Iran were rich in regard to oxygenated monoterpenes (77.8% and 86.2%, respectively) [15,25]. Our results, compared with our previous investigation on oils of the *Prangos* genus, also showed the oils of these parts to be dominated by oxygenated monoterpenes.

The antibacterial assays showed that the oils of leaves, stems and flowers of *P. ferulacea* inhibited the growth of all the bacteria. Leaves, stems and flowers of *P. ferulacea* were further tested for Gram-positive and Gram-negative bacteria. The results of the bioassays (Table 2) showed that the three oils exhibited moderate to strong differences in antimicrobial activity.

Table 2. Antibacterial activity of leaves, stems and flowers of *Prangos ferulacea* oils based on dilution method and using DMSO*.

Bacterial Species	Gram +/-	Leaf Oil	Stem Oil	Flower Oil	DMSO
Staphylococcus aureus ATCC 1112	+	0.5	2	0.5	>4
Staphylococcus epidermidis ATCC 1114	+	0.25	0.5	>4	>4
Bacillus cereus ATCC 1015	+	1	2	0.5	>4
Pseudomonas aeruginosa ATCC 1310	-	0.0625	0.5	1	>4

* Values are the mean MIC (ppm).

In the antimicrobial screening, the oil of *P. ferulacea* leaves exhibited particularly strong activity, especially for the Gram-positive organisms,

although that of stem and flower oils was also interesting. (Leaf-oil MIC values for *Pseudomonas aeruginosa*, *Staphylococcus epidermidis*, *Staphylococcus aureus* and *Bacillus cereus* were 0.0625 ppm, 0.25 ppm, 0.50 ppm and 1.00 ppm, respectively.) In previous studies, antibacterial activity of the essential oils of aerial parts of *P. ferulacea* in Iran appeared strong for Gram-positive bacteria, especially *Staphylococcus aureus* [15], while the *P. ferulacea* in Turkey was active against *Staphylococcus aureus* [23]. Our previous article addressed the antibacterial activity of leaf oils against a Gram-negative strain.

CONCLUSIONS

1. The chemical composition and antibacterial activity of essential oil from leaves, stems and flowers of *Prangos ferulacea* (L.) Lindl grown in Iran were investigated by hydrodistillation using a Clevenger-type apparatus and analysed by GC-MS.

2. The leaf oil consisted of 10 identified compounds representing 81.7% of the oil composition. The main compounds were linalool (36.7%), caryophyllene oxide (16.3%) and α -pinene (12.1%). Another notable constituent was 1,8-cineole (8.9%).

In the stem oil, 11 compounds were identified, representing 43.3% of the oil composition. The main compounds were 1,8-cineole (19.0%) and α -pinene (10.3%).

Linalool (19.0%), lavandulyl acetate (16.0%), 1,8-cineole (14.5%), α -pinene (12.4%) and geranyl isobutyrate (12.2%) were the main components among the 17 constituents characterized in the flower oil, representing 98.2 % of the total components detected.

3. Oxygenated monoterpenes represented the most abundant constituents of the oil of leaves, stems and flowers (63.3%, 37.4% and 74.7%, respectively).

4. The oils were tested against four Gram-positive or negative bacteria using a dilution method. It was found that oils from leaves, stems and flowers of *P. ferulacea*, and especially that of leaves, exhibited interesting antibacterial activity.

5. Comparing these results with investigations on oils of other species of the *Prangos* genus showed they are also dominated by oxygenated monoterpenes.

Acknowledgements: We are grateful to Dr. V. Mozaffarian (Research Institute of Forest and Rangelands, Tehran) for his helpful assistance in the botanical identification.

REFERENCES

1. K. H. Rechinger, in: Flora Iranica, Umbelliferae, vol. 162, K. H. Rechinger, I. C. Hedge, (eds), Akademische Druck und Verlagsanstalt, Graz, 1987, p. 196.
2. V. A. Mozaffarian, Dictionary of Iranian Plant Names, Farhang Moaser, Tehran, 1996.
3. S. Masoudi, Z. Aghjani, M. Yari, A. Rustaiyan, *J. Essent. Oil Res.*, **11**, 767 (1999).
4. S. K. Koul, R. S. Thakur, *J. Essent. Oil Res.*, **22**, 284 (1978).
5. G. A. Kuznetsova, Yu. N. Yor'er, L. V. Kuzmina, G. G. Senchenko, L. I. Shagova, *Rast. Resur.*, **9**, 388 (1973).
6. A. Menghini, M. R. Cagiotti, L. Montanarella, F. C. Fischerand, R. Bos, *J. Essent. Oil Res.*, **57**, 34 (1987).
7. K. H. C. Baser, N. Ermin, N. Adiguzel, Z. Aytac, *J. Essent. Oil Res.*, **8**, 297 (1996).
8. M. Özcan, Y. Bagci, A. Akgül, M. Durai, J. Novak, *J. Essent. Oil Res.*, **12**, 183 (2000).
9. K. H. C. Baser, B. Demirci, F. Demiroi, E. Bedir, P. Weyerstahl, H. Marschall, H. Duman, Z. Aytac, M. T. Hamann, *Planta Med.*, **66**, 674 (2000).
10. K. H. C. Baser, M. Kurkuoglaand, H. Duman, *J. Essent. Oil Res.*, **11**, 151 (1999).
11. K. H. C. Baser, T. Ozek, B. Demirci, H. Duman, *Flav. Fragr. J.*, **15**, 47 (2000).
12. H. Mazloomifar, M. Bigdeli, M. Saber-Tehrani, A. Rustaiyan, *J. Essent. Oil Res.*, **9**, 415 (2004).
13. S. E. Sajjadi, I. Mehregan, *DARU*, **11**, 2 (2003).
14. A. Uzel, T. Dirmenci, A. Celik, T. Arabaci, *Chem. Nat. Compd.*, **42** (2), 169 (2006).
15. H. Amri, *J. Med. Plants*, **21**, 36 (2006).
16. A. Zargari, Medicinal Plants, vol. 12, Tehran University Publications, Tehran, 1988.
17. K. H. C. Baser, B. Demirci, E. D. Bedri, P. Weyersthal, H. Marschall, H. Duman, Z. Aytac, M. T. Hamann, *Planta Med.*, **66**, 6747 (2000).
18. A. Ulubelen, G. Topcv, N. Tan, S. Olcal, S. Tamer, *J. Ethnopharm.*, **45**, 193 (1995).
19. J. Buckingham, Dictionary of Natural Products, Chapman and Hall, London, 1998, p. 737.
20. Eight Peak Index of Mass Spectra, Unwin Brothers, Surrey, 1991.
21. R. P. Adams, Identification of Essential Oil Components by Gas Chromatography/Quadrupole Mass Spectroscopy, Allured Publishing, Carol Stream, IL, 2001.
22. D. Joulain, W. A. König, The Atlas of Spectral Data of Sesquiterpene Hydrocarbons, E. B. - Verlag, Hamburg, 1998.
23. A. Barry, The antimicrobial Susceptibility Test: Principles and Practices, Lea and Febiger, Philadelphia, 1976.
24. F. Sefidkon, *J. Med. Plants*, **5**, 47-50 (2000).
25. H. Hadavand Mirzaei, M. H. Meshkatsadat, S. Soheilvand, *Pak. J. Appl. Sci.*, **7**, 2535 (2007).

ХИМИЧЕН СЪСТАВ И АНТИБАКТЕРИАЛНА АКТИВНОСТ НА ЕТЕРИЧНИ МАСЛА ОТ ЛИСТА, СТЬБЛА И ЦВЕТОВЕ ОТ *Prangos ferulacea* (L.) Lindl. ОТ ИРАН

М. Т. Акбари¹, А Есмаели^{2*}, А. Х. Зареа³, Н. Саад³, Ф. Багери³

¹ Департамент по химия, Ислямски университет Азад, Хомейни Шахр, Исфahan, Иран

² Департамент по инженерна химия, Отдел Северен Техеран, Ислямски университет Азад, Техеран, Иран

³ Отдел по фармацевтични науки, Ислямски университет Азад, Техеран, Иран

Постъпила на 31 декември 2008 г.; Преработена на 27 юли 2009 г.

(Резюме)

Получени са етерични масла от листа, стъбла и цветове от *Prangos ferulacea* (L.) Lindl. растящи в Исфahan, Иран чрез хидродестилация с използване на оборудване тип Clevenger и е анализиран техния химичен състав чрез ГХ-МС и е изследвана антибактериалната им активност. Всички масла се състоят главно от кислородсъдържащи монотерпени и малък процент от сескитерпенови съединения. В маслото от листа са идентифицирани 10 компонента с преобладаване на кислородсъдържащи монотерпени. Идентифицираните три главни съставки (представляващи 65.1% от маслото) са линалол (36.7%), кариофилен оксид (16.3%) и α -пинен (12.1%). В маслото от стъбла са идентифицирани 11 съединения като отново преобладават кислородсъдържащи монотерпени. Двете главни идентифицирани съставки (представляващи 29.3% от маслото) са 1,8-цинелол (19.0%) α -пинен (10.3%). От 17-те съединения намерени в маслото от цветове, петте главни идентифицирани компоненти (представляващи 74.1% от маслото) са кислородсъдържащи монотерпени: линалол (19.0%), лавандулилacetат (16.0%), 1,8-цинелол (14.5%), α -пинен (12.4%) и геранилизобутират (12.2%). Маслата бяха тествани срещу грам-положителни и грам-отрицателни бактерии. Антибактериалната активност е измерена използвайки метода на разреждане. Намерено е, че маслото от листа, стъбла и цветове от *Prangos ferulacea* и особено това от листа показва интересна антибактериална активност.

Synthesis and evaluation of novel carbazole derivatives as free radical scavengers

N. Naik*, H. Vijay Kumar, H. Swetha

Department of Studies in Chemistry, University of Mysore, Manasagangothri, Mysore-570 006, Karnataka, India

Received July 29, 2009

A series of carbazole conjugated with different aminophenols and substituted aminophenols were synthesized by base catalyzed condensation reaction. The key intermediate 1-(9H-carbazol-9-yl)-2-chloroethanone, was obtained by N-acylation of carbazole with chloroacetyl chloride. The newly synthesized compounds were characterized by spectral and elemental analysis data and studied for their radical scavenging activity using 2,2-diphenyl-1-picrylhydrazyl (DPPH) assay. Butylated hydroxy anisole (BHA) was used as a reference antioxidant compound and the comparative study with newly synthesized compounds was also done. Among the analogues, 1-(9H-carbazole-9-yl)-2-(4-hydroxy-3-methoxyphenylamino)ethanone, bearing electron donating methoxy substituent in the phenolic moiety, showed predominant activity.

Key words: carbazole, 1-(9H-carbazol-9-yl)-2-chloroethanone and radical scavenging activity.

INTRODUCTION

Free radicals, which are generated in many bioorganic redox processes, may induce oxidative damage in various components of the body (e.g. lipids, proteins and nucleic acids) and may also be involved in processes leading to the formation of mutations, were recently reported [1]. Reactive oxygen species have been recognized to play an important role in the initiation and or progression of various diseases such as ischemia-reperfusion injury, atherosclerosis, and inflammatory injury [2]. There is a growing interest on natural and synthetic antioxidants as a protective strategy against these diseases by block or removal of oxidative stress [3]. Free radical formation is associated with the normal natural metabolism of aerobic cells. The oxygen consumption inherent in cell growth leads to the generation of a series of oxygen free radicals. The interaction of these species with lipid molecules produces new radicals: hydroperoxides and different peroxides [4–5]. This group of radicals (superoxide, hydroxyl and lipid peroxides) may interact the biological systems in a cytotoxic manner. Free radicals and their uncontrolled production, in fat, are responsible for several pathological processes, such as certain tumors (prostate and Colon cancers) and coronary heart diseases [6]. The reducing properties of diarylamines make them very important as antioxidants, especially as radical scavengers [7]. In fact most representative examples of antioxidants are hindered phenols and diphenylamine derivatives [8]. The reaction of RO_2^{\cdot} radicals with secondary amine

seems to proceed according to the mechanism proposed by Thomas [9], the H-transfer reaction from the N–H bond to peroxy radical occurring in a first step leads to aminyl radical (RR_1N^{\cdot}), which react again with RO_2^{\cdot} radical giving nitroxide radicals (RR_1NO^{\cdot}) in a second step.

Antioxidants are now forged as the drug candidate to combat several diseases. In the literature some tricyclic amines and their chemical structure showed antioxidant neuroprotective activity *in vitro* [10]. Recently, radical scavenging activity of amino acid analogues of 10-methoxy-5H-dibenz[b,f]azepine, a tricyclic amine has been reported [11]. Herein, carbazole belonging to the same class of compound is taken as model compound. Carbazole is one of the aromatic heterocyclic organic compound and its derivatives are known as alkaloids from plants, and many of these show antioxidative and biological activities, such as antitumor, psychotropic, anti-inflammatory, antihistaminic, and antibiotic activities [12–15]. Owing to the widespread applications, synthetic and biological activity evaluation of carbazole and their derivatives has been subject of intense investigations. In the course of the development of new antioxidants, we have interested in novel carbazole derivatives based on the preliminary findings that carbazole has an antioxidant properties.

CHEMISTRY

Carbazole was synthesized by applying known method [15]. The active sites for the coupling of different aminophenols and substituted aminophenols to the basic molecule was very less thus, we select the N-acylation reaction in order to obtain the

* To whom all correspondence should be sent:
E-mail: drnaik_chem@yahoo.co.in

key intermediate in which the coupling of different aminophenols and substituted aminophenols can be done very easily with simple experiment protocol with good yield. The selection of aminophenols and substituted aminophenols was done on the basis of its chemical feasibility. The synthesis of carbazole analogues conjugated with different aminophenols and substituted aminophenols was realized in two steps. In the first step, the key intermediate 1-(9H-carbazol-9-yl)-2-chloroethanone was prepared in good yield by N-acylation of carbazole with chloroacetyl chloride in the presence of triethylamine as base (Scheme 1). In the second step, further coupling of respective aminophenols and substituted aminophenols to the intermediate was done by base condensation reaction to obtain the novel carbazole analogues (Scheme 2).

EXPERIMENTAL

Materials and Methods

DPPH was purchased from Sigma Aldrich, chloroacetyl chloride, triethylamine, benzene, diethyl ether, ethyl acetate, *n*-hexane, tetrahydrofuran, anhydrous potassium carbonate, methanol, chloroform, sodium bicarbonate, anhydrous sodium sulphate and aminophenols like 2-aminophenol, 3-aminophenol, 4-aminophenol, substituted aminophenols like 4-nitro-2-aminophenol and 4-methoxy-2-aminophenol were all of analytical grade and procured from Merck. TLC aluminium sheets - Silica gel 60 F₂₅₄ was also purchased from Merck. All the reported melting points were taken in open capillaries and are reported uncorrected. The IR spectra were recorded on a FT-IR021 model in KBr disc. The ¹H NMR spectra were recorded on Jeol GSX 400 MHz spectrophotometer using CDCl₃ as a solvent and the chemical shift (δ) are in ppm relative to internal standard. The Mass spectra were recorded on Waters-Q-TOF Ultima spectrometer.

Synthesis of 1-(9H-carbazol-9-yl)-2-chloroethanone (2)

To the well stirred solution of carbazole (2 mM) and triethylamine (2.2 mM) in 50 ml benzene, chloroacetyl chloride (2.2 mM) in 25 ml benzene

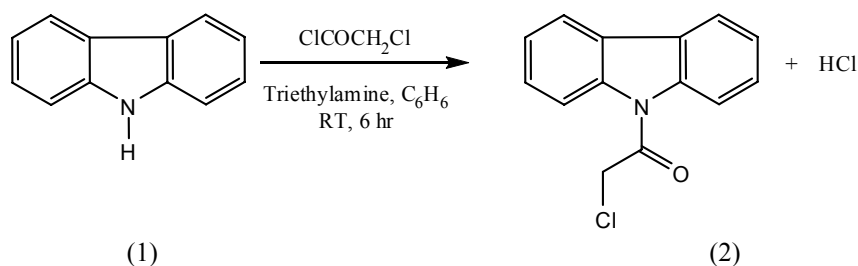
was added drop by drop for about 30 min. Then the reaction mixture is stirred at room temperature for about 6 hr. Progress of the reaction is monitored by TLC using 9:1 hexane:ethyl acetate mixture as mobile phase. After the completion of reaction, the reaction mass was quenched in ice cold water and extracted in diethyl ether. The ether layer was washed twice with 5% NaHCO₃ solution followed by distilled water. Finally the ether layer is dried over anhydrous Na₂SO₄. The pale yellow solid product was obtained by desolventation through rotary evaporator at 35°C.

Carbazole (1). Light yellow solid, yield 73%, melting point 218–220°C, IR (KBr) ν_{\max} (cm⁻¹): 3418.21 (N–H), 2360.4–2922.59 (Ar–H); ¹H NMR (CDCl₃) δ: 10.2 (s, N–H, 2H), 7.2–8.33 (m, Ar–H, 8H). Mass (m/z, %): M⁺ 167.8; Anal. calcd. for C₁₂H₉N: C, 86.20; H, 5.43; N, 8.38%; Found: C, 86.21; H, 5.42; N, 8.37%.

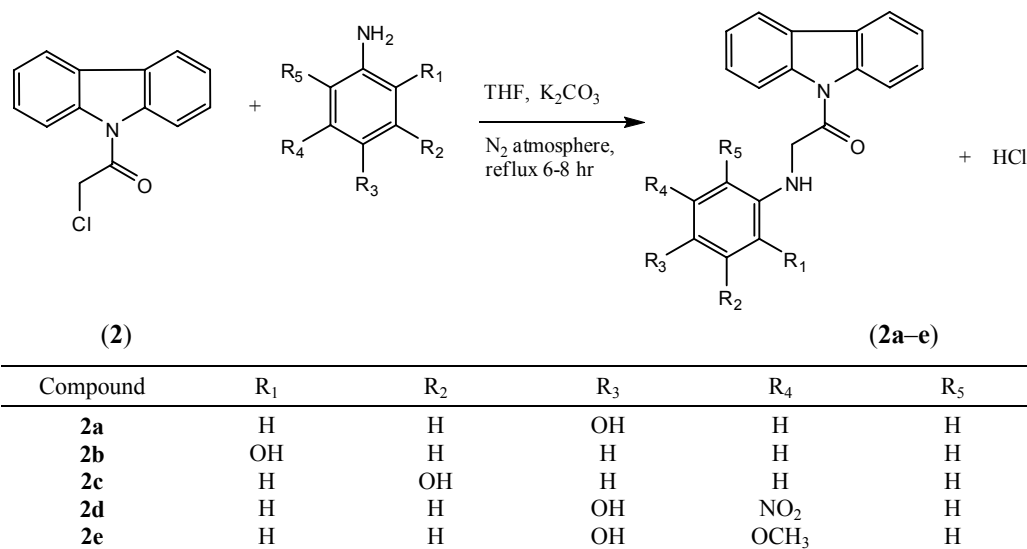
1-(9H-carbazol-9-yl)-2-chloroethanone (2): Light yellow solid, yield 85%, melting point 209–212°C, IR (KBr) ν_{\max} (cm⁻¹): 1600.8 (C=O), 2378.4–2872.9 (Ar–H); ¹H NMR (CDCl₃) δ (ppm): 4.36 (d, CH₂–C=O, 2H), 7.78–8.33 (m, Ar–H, 8H). Mass (m/z, %): M⁺ 243; Anal. calcd. for C₁₄H₁₀ClNO: C, 69.00; H, 4.14; N, 5.75%; Found: C, 69.01; H, 4.16; N, 5.73%.

General procedure for the synthesis of 1-(9H-carbazol-9-yl)-2-chloroethanone conjugated with different aminophenols and substituted aminophenols (2a–e).

2-aminophenol (1.2 mM) in THF (25 mL) was treated with K₂CO₃ (600 mg) under N₂ atmosphere. Later the solution of 1-(9H-carbazol-9-yl)-2-chloroethanone (1 mM) in THF (25 mL) was added drop by drop for 30 min. The reaction mixture was refluxed for 6–8 hr. The progress of the reaction mixture was monitored by TLC. The reaction mixture was then desolventized in rotary evaporator and the compound is extracted in ethyl acetate. The ethyl acetate layer was washed with water and dried over anhydrous Na₂SO₄. The yellow semisolid was obtained by further desolventation in rotary evaporator at 50°C.



Scheme 1.



Scheme 2.

1-(9H-carbazol-9-yl)-2-chloroethanone derivatives conjugated with 3-aminophenol, 4-aminophenol, substituted aminophenols like 4-nitro-2-aminophenol and 4-methoxy-2-aminophenol were obtained by following same procedure. The analogues were separated and purified by column chromatography by using mixture of chloroform/methanol = 85:15. The products were characterized by IR, mass, ¹H NMR and elemental analysis.

1-(9H-Carbazole-9-yl)-2-(4-hydroxy phenylamino)ethanone (2a). Light yellow solid, yield 74%, melting point 222–224°C, IR (KBr) ν_{\max} (cm⁻¹): 3413.21 (N–H), 1600.8 (C=O), 2364.5–2922.59 (Ar–H), 3201.3–3412.6 (Ph–OH); ¹H NMR (CDCl₃) δ (ppm): 4.34 (d, CH₂–C=O, 2H), 7.71–8.32 (m, Ar–H, 8H), 6.2 (s, NH, 1H), 6.7–6.8 (m, Ph–Ar–H, 4H), 10 (s, Ph–OH, 1H). Mass (m/z, %): M⁺ 316; Anal. calcd. for C₂₀H₁₆N₂O₂: C, 75.93; H, 5.10; N, 8.86%; Found: C, 75.91; H, 5.12; N, 8.88%.

1-(9H-Carbazole-9-yl)-2-(2-hydroxy phenylamino)ethanone (2b). Light yellow solid, yield 71%, melting point 178–182°C, IR (KBr) ν_{\max} (cm⁻¹): 3401.21 (N–H), 1601.8 (C=O), 2360.4–2921.5 (Ar–H), 3378.2–3446.6 (Ph–OH); ¹H NMR (CDCl₃) δ (ppm): 4.35 (d, CH₂–C=O, 2H), 7.76–8.33 (m, Ar–H, 8H), 6.3 (s, NH, 1H), 6.5–7.2 (m, Ph–Ar–H, 4H), 10.1 (s, Ph–OH, 1H); Mass (m/z, %): M⁺ 316; Anal. calcd. for C₂₀H₁₆N₂O₂: C, 75.93; H, 5.10; N, 8.86%; Found: C, 75.91; H, 5.12; N, 8.88%.

1-(9H-Carbazole-9-yl)-2-(3-hydroxy phenylamino)ethanone (2c). Light yellow solid, yield 66%, melting point 200–202°C, IR (KBr) ν_{\max} (cm⁻¹): 3412.21 (N–H), 1600.6 (C=O), 2362.4–2920.9 (Ar–H), 3377.3–3456.4 (Ph–OH); ¹H NMR (CDCl₃) δ (ppm): 4.33 (d, CH₂–C=O, 2H), 7.73–8.36 (m, Ar–H, 8H), 6.1 (s, NH, 1H), 6.0–7.2 (m, Ph–Ar–H, 4H),

9.8 (s, Ph–OH, 1H). Mass (m/z, %): M⁺ 316; Anal. calcd. for C₂₀H₁₆N₂O₂: C, 75.93; H, 5.10; N, 8.86%; Found: C, 75.91; H, 5.12; N, 8.88%.

1-(9H-Carbazole-9-yl)-2-(4-hydroxy-3-nitro phenylamino)ethanone (2d). Light brown solid, yield 77.6%, melting point 220–224°C, IR (KBr) ν_{\max} (cm⁻¹): 3411.21 (N–H), 1600.5 (C=O), 2368.4–2922.5 (Ar–H), 3360.3–3455.3 (Ph–OH); ¹H NMR (CDCl₃) δ (ppm): 4.31 (d, CH₂–C=O, 2H), 7.77–8.39 (m, Ar–H, 8H), 6.2 (s, NH, 1H), 7.1–7.9 (m, Ph–Ar–H, 3H), 10.3 (s, Ph–OH, 1H); Mass (m/z, %): M⁺ 361; Anal. calcd. for C₂₀H₁₅N₃O₄: C, 68.48; H, 4.18; N, 11.63%; Found: C, 68.46; H, 4.19; N, 11.64%.

1-(9H-Carbazole-9-yl)-2-(4-hydroxy-3-methoxy phenylamino)ethanone (2e). White solid, yield 83.4%, melting point 189–193°C, IR (KBr) ν_{\max} (cm⁻¹): 3412.21 (N–H), 1613.9 (C=O), 2361.4–2932.5 (Ar–H), 3377.3–3455.6 (Ph–OH); ¹H NMR (CDCl₃) δ (ppm): 4.30 (d, CH₂–C=O, 2H), 7.71–8.31 (m, Ar–H, 8H), 6.4 (s, NH, 1H), 7.0–7.7 (m, Ph–Ar–H, 3H), 9.8 (s, Ph–OH, 1H), 3.5 (s, OCH₃, 3H). Mass (m/z, %): M⁺ 346; Anal. calcd. for C₂₁H₁₈N₂O₃: C, 72.82; H, 5.24; N, 8.09%; Found: C, 72.83; H, 5.21; N, 8.07%.

RADICAL SCAVENGING ACTIVITY

The newly synthesized compounds were screened for their radical scavenging activity using a stable free radical, 2,2-diphenyl-1-picrylhydrazyl (DPPH).

The compounds under studies were dissolved in distilled ethanol (50 mL) to prepare 1000 μ M solution. Solutions of different concentrations (10, 25, 50, 100, 200 and 500 μ M) were prepared by serial dilution and the free radical scavenging activity was studied.

DPPH radical scavenging activity

The DPPH (2,2-diphenyl-2-picrylhydrazyl) radical scavenging effect was carried out according to the method first employed by Blois [16]. Compounds of different concentrations were prepared in distilled ethanol, 1 mL of each compound solutions having different concentrations (10, 25, 50, 100, 200 and 500 μM) were taken in different test tubes, 4 mL of a 0.1 mM ethanol solution of DPPH was added and shaken vigorously. The tubes were then incubated in the dark room at RT for 20 min. A DPPH blank was prepared without compound, and ethanol was used for the baseline correction. Changes (decrease) in the absorbance at 517 nm were measured using a UV-visible spectrophotometer and the remaining DPPH was calculated. The percent decrease in the absorbance was recorded for each concentration, and percent quenching of DPPH was calculated on the basis of the observed decreased in absorbance of the radical. The radical scavenging activity was expressed as the inhibition percentage and was calculated using the formula:

$$\text{Radical scavenging activity} = [(A_0 - A_1)/A_0] \times 100 (\%)$$

Where A_0 is the absorbance of the control (blank, without compound) and A_1 is the absorbance of the compound. The radical scavenging activity of BHA and ascorbic acid was also measured and compared with that of the newly synthesized compound.

RESULTS AND DISCUSSION

N-Acylation of carbazole was affected initially by using Na_2CO_3 as a base and benzene as solvent. Only poor yields was achieved. Instead, when triethylamine was used as base the yield of the product improved significantly (i.e., about 85%) in stirring mode at about 30–35°C.

Scheme 1 shows the reaction pathway of the N-acylation of carbazole (**1**) in the presence of triethylamine as base affords key intermediate 1-(9H-carbazol-9-yl)-2-chloroethanone (**2**). Further base condensation with different aminophenols and substituted aminophenols were carried out to get the target analogues (**2a–e**) (Scheme 2).

The obtained analogues were characterized by various spectroscopic techniques like IR, Mass, ^1H NMR and elemental analysis.

The IR spectra of key intermediate showed the absence of N–H stretching at 3418 cm^{-1} and addition of C=O stretching at 1600 cm^{-1} respectively. ^1H NMR reveals the absence of N–H proton at 11.2 ppm and the presence of $-\text{CH}_2$ protons as doublet at 4.36 ppm. All the respective aromatic protons were

signaled at 7.78–8.33 ppm. These data reveals the N-acylation of carbazole was successful under our experimental protocol.

Further the coupling of various aminophenols and substituted aminophenols was done by base condensation reaction in the presence of K_2CO_3 as base. The IR spectra of all the target analogues showed broad stretching at a region at $3201\text{--}3456\text{ cm}^{-1}$ for phenolic $-\text{OH}$, all the conjugated analogues showed N–H stretching at $3401\text{--}3413\text{ cm}^{-1}$. ^1H NMR spectra of all 1-(9H-carbazol-9-yl)-2-chloroethanone derivatives (**2a–2e**) showed multiplet for Ar–H proton at δ 6.0–8.39 ppm. All the conjugated analogues showed sharp singlet peak at δ 9.8–10.3 ppm corresponding to phenolic $-\text{OH}$. Compound (**2e**) showed sharp singlet peak at δ 3.5 ppm corresponding to $-\text{OCH}_3$ group.

All the analogues showed mass according to their M^+ ions.

The radical scavenging effects of newly synthesized compounds were examined in the present study using radicals generated by DPPH.

Radical scavengers reacts with DPPH, which is a stable free radical and convert it to 2,2-diphenyl-1-picrylhydrazine. The degree of discoloration indicates the scavenging potentials of the compounds. The percentage DPPH activities of all the newly synthesized compounds are showed in the Figure 1.

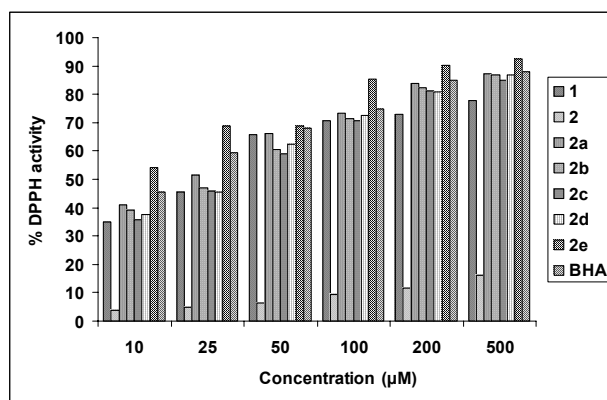


Fig. 1. % DPPH radical scavenging activity of carbazole and newly synthesized analogues. Each value represents the mean \pm SD ($n = 3$).

From the figure, all the compound showed DPPH activity in concentration dependent manner. On the other hand, the half inhibition concentration (IC_{50}) for all the newly synthesized analogues including the reference antioxidant BHA was calculated graphically using a linear regression algorithm and showed in Table 1.

Initially, the key intermediate (**2**) showed negligible activity, but coupling of different aminophenols and substituted aminophenols (**2a–2e**) increases the activity. All the analogues demonstrated signi-

ficant radical scavenging effect. Among them, the methoxy substituted analogues (**2e**) was found to be more potent followed by *p*-aminophenol analogue (**2a**).

Table 1. 50% Inhibition of DPPH radical by the carbazole and its analogues. where – corresponds to no 50% inhibition.

Compound	IC ₅₀ (μM)
1	60.34 ± 1.94
2	–
2a	18.32 ± 0.56
2b	21.67 ± 0.86
2c	25.55 ± 1.11
2d	20.87 ± 0.94
2e	15.12 ± 0.43
BHA	16.23 ± 1.23

The presence of electron donating methoxy substituent in the phenolic compounds is known to increase the stability of the radical and hence, the antioxidant activity [17]. Thus the introduction of a methoxy group to aminophenol increases the hydrogen donation ability and therefore increases the radical scavenging capacity. But the introducing of electron withdrawing NO₂ group slightly decreases the scavenging capacity.

The radical scavenging activity of all the newly synthesized analogues was compared with the standard antioxidant i.e., BHA. 1-(9H-carbazole-9-yl)-2-chloro ethanone conjugated with methoxy substituted aminophenol (**2e**) showed dominant activity than the BHA, whereas all the analogues showed less activity than the BHA.

The increased DPPH radical scavenging activity of all the newly synthesized compounds is as follows **2e** > BHA > **2a** > **2d** > **2b** > **2c** > **1** > **2**

CONCLUSION

We have synthesized a ray of carbazole analogues conjugated with different aminophenols and substituted aminophenols. The synthetic protocol proposed by us, reproduces the convenient way for the target compounds. The synthesized compounds were evaluated for their DPPH radical scavenging activity. Initially, the key intermediate 1-(9H-carbazole-9-yl)-2-chloro ethanone (**2**) showed negligible activity, whereas coupling of different aminophenols and substituted aminophenols enhance the radical scavenging activity. Among the analogues carbazole

conjugated with 4-methoxy-2-aminophenol exhibited more potent inhibition of DPPH radical scavenging activity and also more potent than the standard BHA.

Our study provides evidence that carbazole derivative bearing different aminophenols and substituted aminophenols exhibits interesting DPPH radical scavenging activity. These analogues may be useful in the treatment of pathologies, in which free radical oxidation plays a fundamental role. This may warrant further in depth biological evolutions. Work is in progress to design, synthesize and evaluate addition compound in this and related systems.

REFERENCES

1. G. C. Yen, H. Y. Chen, *J. Agric. Food Chem.*, **43**, 27 (1995).
2. J. M. Braughler, E. D. Hall, *Free Radical Biol. Med.*, **6**, 289 (1989).
3. (a). G. Marcinik, M. A. Petty, *Drugs Future*, **21**, 1037 (1996). (b) S. C. Hasrison, J. J. Lynch, K. Rose, D. W. Choi, *Brain Res.*, **102**, 639 (1994) (c) R. D. Saunders, L. L. Dugan, P. Demediuk, E. D. Means, L. A. Horrocks, D. K. Anderson, *J. Neurochem.*, **49**, 24 (1987).
4. S. D. Aust, B. A. Sringen, in: *Free Radicals in Biology*, W. A. Pryor (ed.) Academic Press, New York, 1982, p. 1–287.
5. W. A. Pryor, J. W. Lightsey, D. G. Prier, in: *Lipid Peroxides in Biology and Medicine*, K. Yagi (ed.), Academic Press, New York, 1982.
6. B. Halliwell, *Ann. Rev. Nutr.*, **16**, 33 (1996).
7. M. A. Esteves, N. Narendar, M. J. Marcelo-Curto, B. J. Gigante, *Nat. Prod.*, **64**, 76 (2001).
8. G. Scott, *Bull. Chem. Soc. Jpn.*, **61**, 165 (1988).
9. J. R. Thomas, *J. Am. Chem. Soc.*, **82**, 5955 (1960).
10. L. Chirtian Beh, B. Moosmann, *Free Radical Biol. Med.*, **33**, 182 (2000).
11. H. Vijay Kumar, C. R. Gnanendra, D. Chenne Gowda, Nagaraja Naik, *Bulg. Chem. Commun.*, **41**, 72 (2009).
12. D. P. Chakarabarty, *The Alkaloids*, **44**, 257 (1993).
13. D. P. Chakarabarty, R. S. Roy, *Prog. Chem. Org. Nat. Prod.*, **57**, 71 (1991).
14. Y. Tachibana, H. Kikuzaki, N. H. Lajis, N. Nakatani, *J. Agric. Food Chem.*, **49**, 5589 (2001).
15. S. Stolc, *Life Sci.*, **65**, 1943 (1999).
16. H. T. Bucherer, F. Seyde, *J. Prakt. Chem.*, **77**, 403 (1980).
17. M. S. Blois, *Nature*, **26**, 1199 (1958).
18. P. Rajan, I. Vedrnikova, P. Cos, V. D. Berghe, K. Augustunsa, A. Haemersa, *Bioorg. Med. Chem. Lett.*, **11**, 215 (2001).

СИНТЕЗ И ПРЕЦЕНКА НА НОВИ КАРБАЗОЛОВИ ПРОИЗВОДНИ КАТО АНТИОКСИДАНТИ

Н. Наик*, Х. Виджай Кумар, Х. Суита

*Департамент по химични изследвания, Университет на Майсур, Манасаганготри,
Майсур 570006, Карнатака, Индия*

Постъпила на 29 юли 2009 г.

(Резюме)

Синтезирани е серия съединения от карбазол спрегнат с различни аминофеноли и заместени аминофеноли чрез алкална каталитична реакция на кондензация. Ключовото междинно съединение 1-(9Н-карбазол-9-ил)-2-хлоретанон е получено чрез N-ацилиране на карбазол с хлорацетилхлорид. Новосинтезираните съединения са охарактеризирани чрез спектрални и елементен анализи и е изследвана тяхната активност като антиоксиданти с 2,2-дифенил-1-пикрилхидразил (DPPH). Направено е сравнително изследване на новосинтезираните съединения като антиоксиданти в сравнение с бутилхидроксианизол (ВНА). От анализите по-висока активност показва 1-(9Н-карбазол-9-ил)-2-(4-хидрокси-3-метоксифениламино)етанона, който има електронодобен метокси заместител във фенолната част.

Acceleration and increase of hydrogen production by simultaneous fermentation of *Clostridium butyricum* and *Rhodobacter sphaeroides* on wine-vinasse substrate

M. Krysteva^{1*}, I. Lalov¹, V. Beschkov²

¹ Department of Biotechnology, University of Chemical Technology and Metallurgy
8 Kliment Ohridski Blvd., 1756 Sofia, Bulgaria

² Institute of Chemical Engineering, Bulgarian Academy of Sciences,
Acad. G. Bonchev St., Block 103, 1113 Sofia, Bulgaria

Received February 9, 2009; Revised August 12, 2009

A fermentation process for hydrogen production as a result of the simultaneous effect of *Rhodobacter sphaeroides* and *Clostridium butyricum* on a wine-vinasse substrate was realized in a single illuminated bioreactor. The kinetics of the cooperative process indicates rapid and enhanced production of hydrogen showing yield of 65.41 mmol/l vinasse with a mixed culture as compared to processes using the two bacteria separately that have yields of 27.41 and 25.49 mmol/l vinasse for *Rhodobacter* and *Clostridium*, respectively. The experiment with a mixture of the two bacteria revealed co-operative assimilation of almost all components studied in the following sequence: malic acid > lactic acid > residual sugars > tartaric acid > citric acid. The use of vinasse substrate for hydrogen production would be a significant ecological energy resource for enterprises producing wine brandies together with waste utilization.

Key words: hydrogen production, mixed fermentation, *Rhodobacter sphaeroides*, *Clostridium butyricum*, renewable energy resource, wine-vinasse.

INTRODUCTION

In the nearest future hydrogen is expected to find a wide application in both industry and transport because water is the only product of its burning. In addition to the labour-consuming and expensive methods of its chemical preparation, biological methods became very popular during the past years.

Methods based on photo-fermentation and dark-fermentation H₂-producing bacteria on various substrates proved very important. One of the main problems with these bacterial processes is the substrate material which is, in most cases, an agricultural waste product, waste water, whey, etc., needing sometimes additional pre-treatment before being thrown away [1, 2]. The utilization of these products aimed at hydrogen production would result in cheap and pure energy, the polluting waste products being eliminated. Some studies used carbohydrate-containing substrates and dark-fermentation with the participation of bacteria, above all of the kind *Clostridium* [3, 4] as well as photo bacteria acting on substrates which contain mainly organic acids were carried out [5, 6]. Combination of the two processes has been achieved by successive utilization of a glucose-containing substrate with *Enterobacter cloacae* followed by photofermen-

tation with *Rhodobacter sphaeroides* of the metabolites from the dark process which contain, mainly acetic acid and other products. This combination of the two processes significantly increases the hydrogen yield and the utilization of the substrate chemical energy. The hydrogen yield of the combined processes is found to be higher than that of a single process [7]. The development of an integrated biological hydrogen production process is described on the basis of unicellular green algae, which are driven by the visible portion of the solar spectrum, coupled with purple photosynthetic bacteria, which are driven by the near infrared portion of spectrum [8].

In the present study, we tried to obtain hydrogen by simultaneous photo fermentation and dark fermentation in a single bioreactor with combined action of *Chlostridium butyricum* and *Rodobacter sphaeroides* on the waste substrate. The latter, called wine-vinasse, was a waste product formed during wine distillation before obtaining brandy as a final product. This product is rich in organic acids and residual sugars, amino acids and small amounts of other compounds coming from the grapes.

MATERIALS AND METHODS

Cultivation of Rhodobacter sphaeroides and Clostridium butyricum

Clostridium butyricum 1389 strain was supplied from the National Bank of Industrial Microorga-

* To whom all correspondence should be sent:
E-mail: krysteva@uctm.edu

nisms and Cell Culture in Sofia. The initial *Rhodobacter sphaeroides* strain was bought from the firm NCIMB, UK with an authentic certificate.

Rhodobacter sphaeroides was cultivated in M₂₂ medium [9] containing sodium lactate, succinate, glutamate and aspartic acid as carbon and nitrogen sources as well as minerals and vitamins. Cultivation was performed under anaerobic conditions in light at a temperature of 30°C and pH 6.5. The cells grown were colored in red. Prior to its use, the culture was adapted in vinasse, at first in a 1:1 ratio, and then on pure vinasse.

Clostridium butyricum was precultured at 37°C in a basal medium (pH 7.0) containing (g/l) casein hydrolyzate 15 g, L-cystein 0.5 g, glucose 5.0 g, yeast extract 5 g, sodium thioglycolate 0.5 g, sodium chloride 2.5 g and agar 0.75 g. Before using the culture to obtain hydrogen from vinasse, it was adapted in a nutrient medium and vinasse in a 1:1 ratio, after which it was transferred to pure vinasse.

Vinasse substrate was prepared by distillation of white wines and consisted mainly of tartaric acid, citric, malic and lactic acids, amino acids, residual sugars as well as other compounds of lower contents. When vinasse from red wines were used, the residue after the alcohol distillation was decoloured with active carbon in order to eliminate dyeing substances.

Assays

Analysis of acids were performed with a HPLC chromatography (HPLC Waters column Lichrosper 100, RP-C₁₈). The sugars were determined spectrophotometrically as reducing substances by means of 3,5-dinitrosalicylic acid [10]. Quantitative estimation was made on the basis of a standard straight line obtained using glucose and the above method.

The cell concentration in this case was also determined nephelometrically at 600 nm and then recalculated per mg dry weight with the use of a standard calibrating curve.

Hydrogen gas was estimated using an electrochemical gas sensor TGS-FIGARO Engineering Inc., based on tin dioxide as sensing material. The output signal displayed the percentage volume of H₂ in a biogas mixture. The system was calibrated once in two days using pure hydrogen calibration gas.

Procedure of hydrogen production

Hydrogen is produced from both single pure cultures and the mixed cultures in the laboratory installation shown in Fig. 1.

Vinasse substrate (150 ml) was placed in a glass bioreactor with a volume of 200 ml and flat walls ensuring better illumination. Inoculated and adapted

Rhodobacter sphaeroides culture was added during the single experiments in amounts of 20 ml so that the final concentration in the total working volume was about 0.4 mg/ml dry cells. In the case of *Clostridium butyricum*, an inoculate of its cells adapted to wine-vinasse in a volume of 20 ml was added to 150 ml of the substrate with a view to achieving a final concentration of about 0.2 mg·ml⁻¹ dry cells in the working volume of the reactor. The biomass concentration in the mixed culture of the two microorganisms was the same as with the experiments with one bacterial kind (*R. sphaeroides* 0.4 mg·ml⁻¹ *C. butyricum* 0.2 mg·ml⁻¹, i.e. a ratio of 2:1 between them taking into consideration that organic acids content is higher in vinasse than reducing sugar compounds). With both kinds of experiments the pH value was 6.5 and this value was maintained during the whole process at a temperature of 30°C. Immediately after introducing the inoculate, the whole system was blown through with argon for 15 min to ensure an anaerobic medium. After this procedure, the halogen lamp of 500 W was switched on in order to illuminate the reactor. The bioreactor content was stirred with a magnetic stirrer and the adsorption of carbon dioxide before hydrogen accumulation proceeded in a 10% Ca(OH)₂ solution.

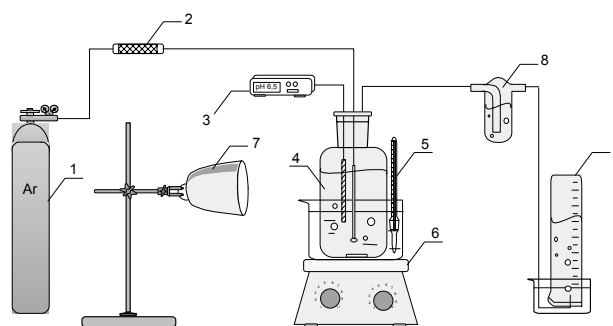


Fig. 1. Laboratory scheme for photo production of hydrogen by *Clostridium butyricum* and *Rhodobacter sphaeroides*. 1 - argon; 2 - microbial filter; 3 - pH-meter; 4 - photobioreactor; 5 - temperature control; 6 - magnetic stirrer; 7 - halogen lamp; 8 - CO₂ trap (10% Ca(OH)₂); 9 - gasholder.

RESULTS AND DISCUSSION

Photo fermentation process for hydrogen production using *Rhodobacter sphaeroides* and waste wine-vinasse substrate

Fig. 2. shows the kinetics of hydrogen production in a periodic photo fermentation process.

Hydrogen evolution was observed for 115 h. Hydrogen generation began approximately during the fifth hour from the process beginning and had its highest rate of 163.79 μmol·h⁻¹ until the 23th hour,

then continued with a rate of $49.05 \mu\text{mol}\cdot\text{h}^{-1}$ up to the 68th h. After that, the rate of biohydrogen production gradually dropped until abating of the process 96 h after its start probably due to exhaustion of the substrate. During these 96 h the volume of hydrogen amounted to 5.612 mmoles, i.e. the mean rate of its generation was $59.03 \mu\text{mol}\cdot\text{h}^{-1}$. Along with the fermentation process, the increase in biomass was also followed. The cell biomass introduced with the inoculate, was found to grow from $0.42 \text{ mg}\cdot\text{ml}^{-1}$ to $0.997 \text{ mg}\cdot\text{ml}^{-1}$ in the exponential phase of the growth curve, these investigations being also presented in Fig. 2. The productivity curve (Fig. 2) shows the maximum in the late exponential phase of the microbial growth followed by sharp decrease, with a relatively low productivity in the stationary phase.

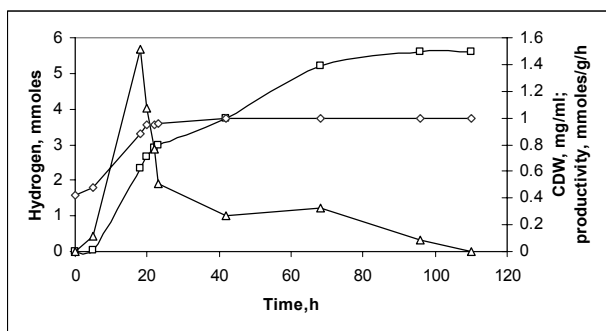


Fig. 2. Kinetics of hydrogen production, microbial growth and productivity at photo fermentation process with *Rhodobacter sphaeroides* and vinasse as a substrate. (-◇-) – CDW (cell dry weight); (-△-) – hydrogen; (-□-) – productivity.

Hydrogen production using *Clostridium butyricum* and waste wine-vinasse substrate

The batch fermentation process of hydrogen production by means of *Clostridium butyricum* was realized under conditions identical to those of the above process, however without illumination. Fig. 3, illustrating the process kinetics, evidences noticeable hydrogen production about the 10th h. The process continued with a constant high rate of $120.55 \mu\text{mol}\cdot\text{h}^{-1}$ till the 32th h, after which a rapid rate drop was noticed. The process preserved its intensity till the 50th h (Fig. 3). The same plot demonstrates a biomass increase from $0.2 \text{ mg}\cdot\text{ml}^{-1}$ to $0.71 \text{ mg}\cdot\text{ml}^{-1}$ at the end of the process. For the strain *Clostridium butyricum* the maximum productivity was observed in the all phases of growth, with a maximum in the stationary one (Fig. 3)

Probably, for hydrogen production in the stationary phase a substrate available in the growth phase is necessary.

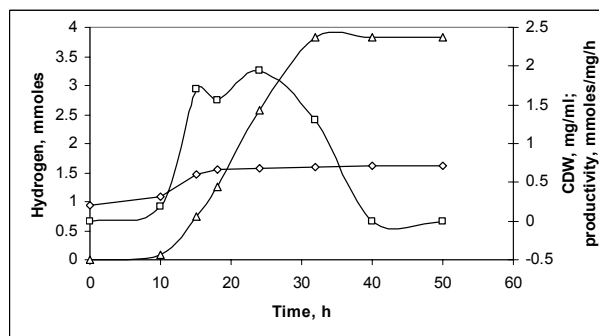


Fig. 3. Kinetics of hydrogen production and microbial growth at fermentation process with *Clostridium butyricum* and vinasse as a substrate. (-◇-) – CDW (cell dry weight); (-△-) – hydrogen; (-□-) – productivity.

A periodic photo fermentation process for hydrogen production using the joint effect of *Rhodobacter sphaeroides* and *Clostridium butyricum* on wine-vinasse as a substrate

Vinasse substrate in an amount as already used separately with the two microorganisms (*Rh. sphaeroides* and *C. butyricum*) was placed in the above reactor together with them taking into account the necessary condition of their having a 2:1 ratio in the working volume. The process was accompanied by illumination. Fig. 4 shows the kinetics of hydrogen production in the presence of both bacteria as well as biomass growth and productivity.

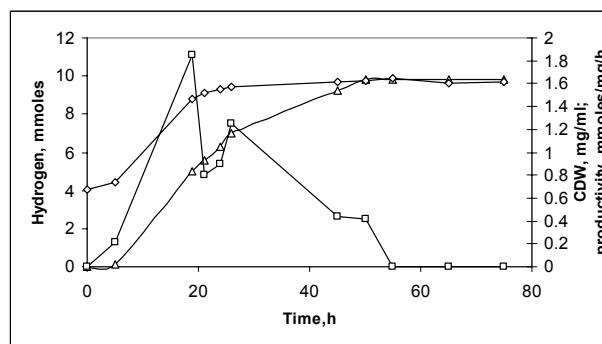


Fig. 4. Kinetics of hydrogen production and microbial growth at photo fermentation process with mixed culture of *Rhodobacter sphaeroides* and *Clostridium butyricum* and vinasse as a substrate. (-◇-) – CDW (cell dry weight); (-△-) – hydrogen; (-□-) – productivity.

Evidently, the production of hydrogen begins relatively soon (during the 5th h after the process beginning) and the rate increases quickly till the 26th h with an average rate of $326.74 \mu\text{mol}\cdot\text{h}^{-1}$. Hydrogen generation was observed for 50 h. but already with a lower rate of $117.64 \mu\text{mol}\cdot\text{h}^{-1}$. The total gas production was 9.811 mmoles, i.e. much more than the productions in the previous batch processes. During the 75th h the intensity of hydrogen production was still high.

It is obvious that hydrogen production takes place within the whole time for culture growth tending to zero when the substrate is probably exhausted. The results show the possibility of co-operating the two bacteria in order to enhance the hydrogen production and achieve better utilization of the vinasse substrate.

Analysis of the utilized components of the vinasse substrate

Table 1 shows some of the more important vinasse components followed separately in the presence of *Rhodobacter sphaeroides* and *Clostridium butyricum* as well as of mixed cultures during the fermentation processes. Some of the main vinasse components such as tartaric acid, lactic acid, malic acid and citric acid were subjected to analysis. The residual sugars were determined as reducing agents. *Rhodobacter sphaeroides* showed intense utilization of malic and lactic acids, and partial utilization of tartaric and citric acids. This bacterium was also found to use residual sugars relatively well. *Clostridium butyricum* was characterized by intense utilization of residual sugars as well as by consumption of some of the acids such as lactic and malic acids.

Table 1. Components content of initial vinasse and their residual concentrations at the end of different fermentation processes. In parentheses – the percentage molar consumption of a certain substrate; reducing substances are presented as glucose.

	Tartaric acid (g·l ⁻¹)	Lactic acid (g·l ⁻¹)	Malic acid (g·l ⁻¹)	Citric acid (g·l ⁻¹)	Reducing subst. (%)
Vinasse	1.77	0.077	0.893	0.168	5.5
<i>Rhodobacter sphaeroides</i>	1.578 (10.8%)	0.017 (77.9%)	0.103 (85.5%)	0.146 (13.1%)	1.3 (76%)
<i>Clostridium butyricum</i>	1.7 (4%)	0.031 (59.7%)	0.091 (90.8%)	0.16 (4.8%)	1.1 (80%)
<i>Rhodobacter</i> + <i>Clostridium</i>	0.74 (41.8%)	0.004 (94.8%)	0.017 (98.1%)	0.142 (15.4%)	0.5 (90.9%)

The experiment with a mixture of the two bacteria revealed co-operative assimilation of almost all components in the following sequence: malic acid > lactic acid > residual sugars > tartaric acid > citric acid

Taking into account the fact that *Rhodobacter* and *Clostridium* exist in nature as cooperative population in various kinds of habitats both in water basins and in soil [11] we assumed the probability for them to participate simultaneously in the fermentation processes, utilizing the components of the substrates used and showing mutual tolerance. On the one hand, our studies showed that waste

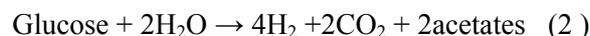
wine-vinasse was a suitable substrate for hydrogen production in the presence of both *Rhodobacter sphaeroides* and *Clostridium butyricum*, and on the other, organizing a fermentation process with the simultaneous participation of the two organisms, resulted in accelerated and increased hydrogen yield – 65.41 mmol/l vinasse in comparison with separated participation of *Rhodobacter* – 27.41 mmol/l vinasse and *Clostridium* – 25.49 mmol/l vinasse, respectively.

As it is known anoxygenic photosynthetic bacteria as *Rhodobacter sphaeroides* is photoheterotrophs that can grow anaerobically utilizing sunlight and short chain organic acids as substrate. Photosynthetic bacteria utilizing the enzyme nitrogenase, which catalyze to conversion of molecular nitrogen to ammonia as well as evolution of hydrogen according to the Eqn. (1):



In the absence of N₂ gas the enzyme acts as ATP-depending hydrogenase and simply reduce protons to generate H₂ [12].

On the other hand dark anaerobic fermentative bacteria like *Clostridium butyricum* utilize carbohydrate substrate and H₂ is one of the end products of their metabolism according to the Eqn. (2):



Depending of bacterial species and organic nutrients the fermentation results in generation of small organic acids as malate, lactate, acetate etc. [13, 14]

Based on analysis of the substrate components in our experiments, it may be assumed that they are not assimilated as a simple sum but, more probably, as a result of a cooperative process. Probably, *Rhodobacter sphaeroides* assimilates small organic acids in the substrate-vinasse as well as the metabolite products of *Clostridium butyricum*. The consumption of tartaric acid is of interest. Its assimilation by *Clostridium butyricum* is weak and that by *Rhodobacter sphaeroides*, medium. In the simultaneous presence of the two bacteria, however, drastic exhaustion of this acid is observed. This maybe due to its transformation into a metabolite which is assimilated quickly. The results obtained also showed that both anaerobic fermentations runs together and the light does not disturbs *C. butyricum* fermentation.

In an industrial scheme, the single hydrogen bioreactor with both bacteria can be placed in the same enterprise producing brandy and the illumination could be realized by sun.

CONCLUSION

The main advantages of the present investigation are:

- realization of a fermentation process yielding hydrogen with the use of the simultaneous effect of *Rhodobacter sphaeroidis* and *Clostridium butyricum* on waste vinasse substrate in a single bioreactor, leading to a quick and enhanced hydrogen production as compared to processes with the two bacteria used separately;
- simultaneous utilization of the substrate and the metabolite products by the microorganisms demonstrated the mutual tolerance between them;
- utilization of waste vinasse substrate for the production of hydrogen would be a significant ecological energy resource for wine processing enterprises.

Acknowledgements The authors are much obliged to Milena Ivanova and Tshvetan Tshvetkov diploma students at the Department of Biotechnology for their skilful assistance in carrying out the present investigations.

REFERENCES

1. S. Dunn, *Int. J. Hydrogen Energy*, **27**, 235 (2002).
2. D. Levin, L. Pitt, M. Love, *Int. J. Hydrogen Energy*, **29**, 173 (2004).
3. H. Zhang, M. A. Bruns, B. E. Logan, *Water Res.*, **40**, 728 (2006).
4. Y. Haruhiko, T. Tadafumi, H. Jun, H. Sachio, T. Yoshiyuki, *Biotechnol. Lett.*, **20**, 143 (1998).
5. M. Sunita, Ch. K. Mitra, *J. Biosci.*, **18**, 155 (1993).
6. H. Koku, I. Eroglu, U. Gunduz, M. Vucel, L. Turker, *Int. J. Hydrogen Energy*, **28**, 381 (2003).
7. N. Kaushik, A. Kumar, D. Das, *Appl. Microbiol. Biotechnol.*, **68**, 533 (2005).
8. A. Melis, M. R. Melinski, *Int. J. Hydrogen Energy*, **31**, 1563 (2006).
9. R. K. Clyton, *Biochim. Biophys. Acta*, **37**, 503 (1960).
10. G. C. Miller, *J. Assoc. Offic. Anal. Chemists*, **31**, 420 (1959).
11. R. Osinga, E. Armstrong, J. G. Burgess, F. Hoffmann, J. Reitner, G. Schumann-Kindel, *Hydrobiologia*, **461**, 55 (2001).
12. P. W. Ludden, G. P. Roberts, in: Anoxygenic Photosynthetic Bacteria, R. E. Blankenship, M. T. Madigan, C. E. Bauer, (Eds.), Kluwer Academic Publishers; Dordrecht, 1995, p. 929-47.
13. O. R. Zaborsky in: Biohydrogen, O. R. Zaborsky, J. R. Benemann, T. Matsunaga, J. Miyake, A. S. Pietro, (Eds.), Plenum Press, New York, 1998, p. 552.
14. K. Nath, D. Das, *Appl. Microbiol. Biotechnol.*; **65**, 520 (2004).

УСКОРЯВАНЕ И ПОВИШАВАНЕ НА ПРОДУКЦИЯТА НА ВОДОРОД С ЕДНОВРЕМЕННА ФЕРМЕНТАЦИЯТА НА *Clostridium butyricum* И *Rhodobacter Sphaeroides* ВЪРХУ СУБСТРАТ ОТ ВИНЕНА ВИНАСА

М. Кръстева^{1*}, И. Лалов¹, В. Бешков²

¹ Катедра „Биотехнология“, Химикотехнологичен и металургичен университет, бул. „Кл. Охридски“ № 8, 1756 София

² Институт по инженерна химия, Българска академия на науките, ул. „Акад. Г. Бончев“, Блок 103, 1113 София

Постъпила на 9 февруари 2009 г.; Преработена на 12 август 2009 г.

(Резюме)

Ферментационен процес за получаване на водород беше организиран като резултат от едновременния ефект на *Rhodobacter sphaeroides* и *Clostridium butyricum* в единичен реактор с осветяване и използване на винена винаса като субстрат. Кинетиката на кооперативния процес показва бърза и повишена продукция на водород с добив от 65.41 mmol/l винаса със смесената култура, в сравнение с процесите, където бактериите се използват поотделно и показват добиви от 27.41 и 25.49 mmol/l винаса, съответно за *Rhodobacter* и *Clostridium*. Експериментът със сместа от двете бактерии, показва кооперативно асимилиране на почти всичките изследвани компоненти в следния ред: ябълчена киселина > млечна киселина > остатъчни захари > винена киселина > лимонена киселина. Използването на винаса като субстрат за продукция на водород би представлявало значителен екологичен енергиен ресурс за предприятията, които произвеждат винено бренди, заедно с оползотворяването на отпадъка винаса.

Gas flow maldistribution in ceramic honeycomb packing

S. Darakchiev*, R. Darakchiev

*Institute of Chemical Engineering, Bulgarian Academy of Sciences,
Acad. G. Bonchev St., Block 103, 1113 Sofia, Bulgaria*

Received June 15, 2009; Revised October 22, 2009

Honeycomb packing is a type of structured packing with very good hydrodynamic, heat and mass transfer characteristics. A thorough study on its gas-flow distribution ability is carried out and has also shown very good results. Results are obtained for the maldistribution factor above and below the packing layers of different height and packing elements of different size. Also, results for the maldistribution factor at different flow rates are reported. Basic packing characteristics are determined, for example for packing No 1 the uniformity limit is 0.15 and penetration depth is about 0.4 m. For packing No 2 the uniformity limit is 0.13 and penetration depth is about 0.6 m.

Key words: packed columns, honeycomb packing, gas flow maldistribution, maldistribution factor, uniformity limit, penetration depth.

INTRODUCTION

Honeycomb packing is a structured packing with very good hydrodynamic, heat and mass transfer characteristics [1]. The body of a single packing element contains seven vertical hexagonal channels arranged like in a honey comb. In the column body, the packing is arranged in horizontal rows placed one over the other in a manner that the holes of each layer do not coincide with the holes of the layer below. This structure does not permit significant radial spreading of the gas flow in horizontal direction.

Previous studies on the gas flow velocity profile in such type of packing [2–4] have registered a good distribution. It is observed that in case of thicker

layers, the gas flow velocity does not affect the flow maldistribution.

It is interesting to study the flow maldistribution below and above the packing layer, which depends strongly on the type of gas inlet device. Determination of the uniformity limit and penetration depth for this type of packing is another task of this study.

EXPERIMENTAL

The experimental study of gas flow maldistribution in a layer of honey-comb packing has been done in a column 0.47 m in diameter with three types of gas inlet devices (Fig. 1): straight inlet ID1 (Fig. 1a), bevelled inlet ID2 (Fig. 1b) and bent-to-bottom inlet ID3 (Fig. 1c).

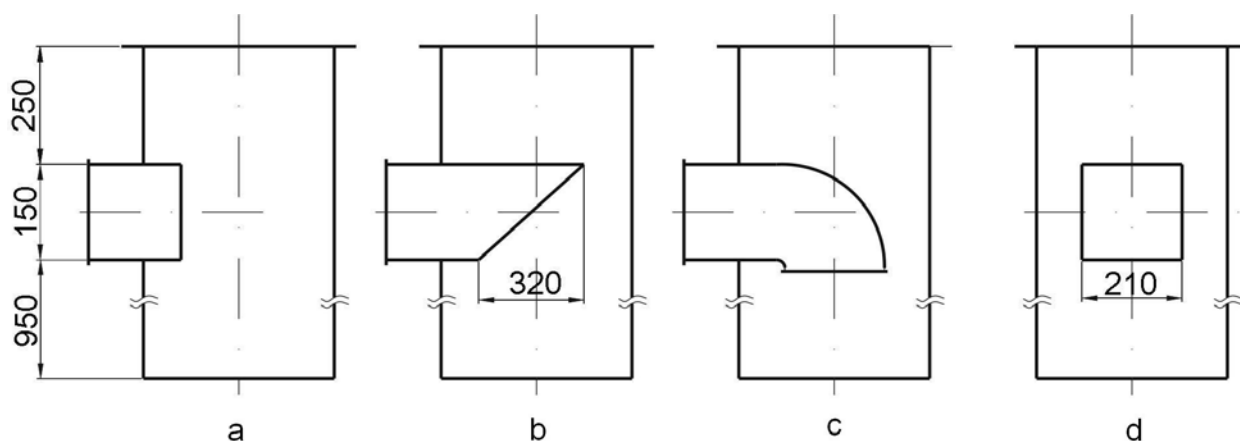


Fig. 1. Types of gas inlet devices (ID): a - straight inlet ID1; b - bevelled inlet ID2; c - bent-to-bottom inlet ID3; d - side look.

* To whom all correspondence should be sent:

E-mail: s_darakchiev@abv.bg

© 2010 Bulgarian Academy of Sciences, Union of Chemists in Bulgaria

Two packings have been studied. Their geometry parameters are rather similar and are given in previous publications [2, 4]. Packing No 1 has diameter of the circumference, inscribed in the packing hexagonal, equal to 21 mm and the height of the packing element is 66 mm. For packing No 2 these values are respectively 27 and 61 mm.

The packing elements have been arranged in rows over a supporting grid. It is mounted in the column lower part at 250 mm above the gas inlet upper end. The distance between the inlet and column bottom is 950 mm. Fig. 2 illustrates the arrangement of a packing row. The openings of every next row should not coincide with the openings of the row below.

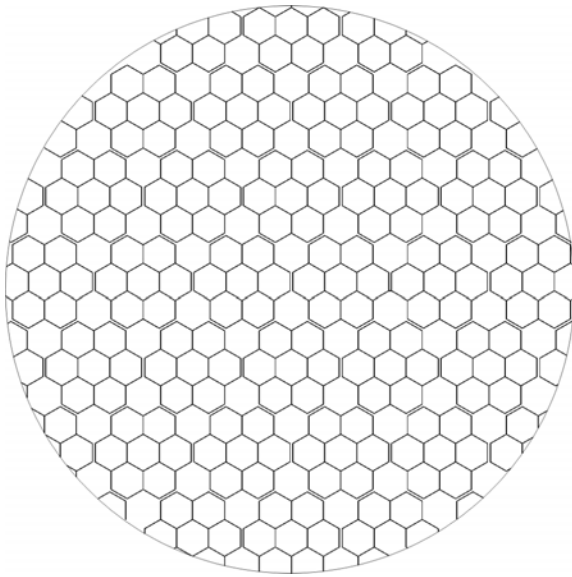


Fig. 2. Packed layer with blocks of ceramic honeycomb packing.

The measurement of gas flow velocity over the layer has been done by two schemes, depending on the height of column section filled with packing. When the section has been entirely filled (packing height 0.8 or 1.6 m), the measuring probe (thermoanemometer) has been placed directly on every packing hole over the cross-section (Fig. 2), and the maximal velocity over the corresponding hole is registered. When the column section has been partially filled, the velocity has been measured along two perpendicular directions – parallel and perpendicular to the axis of the inlet gas device.

The measured velocity profiles have been treated by the following equation in order to obtain the maldistribution factor M_f :

$$M_f = \sqrt{\frac{1}{n} \sum_{i=1}^n \left(\frac{W_i - W_0}{W_0} \right)^2} \quad (2)$$

In case of direct measurement over each hole the measuring probe (thermoanemometer) has been placed in the center of the hole and the registered velocity is the maximum one – $W_i = W_{\max,i}$ and $W_0 = W_{\max,0}$.

The velocity profile measurements below the packing layer have been made along two perpendicular diameters.

In parallel with velocity measurements, pressure drop of the packing layer has been measured with a sensitive differential manometer (precision 0.1 Pa).

All measurements have been done at varying the mean superficial flow velocity in the range 1.0–2.5 m/s.

RESULTS AND DISCUSSION

Fig. 3 represents the maldistribution factor above and below the layer for packing No 1 as depending on gas flow velocity. Some of the experimental data are given in [3]. The results are for two types of gas inlets (ID2 и ID3) and for packing height 0.26 m. Preliminary tests have shown that the non-uniformity created by inlet devices ID1 and ID2 are rather similar. The inlet device ID3 has demonstrated most favourable qualities. It is seen that the flow distribution in this case is significantly better even with such a small layer. This result is confirmed by our proper studies [2, 4, 5] and by these of other authors [6].

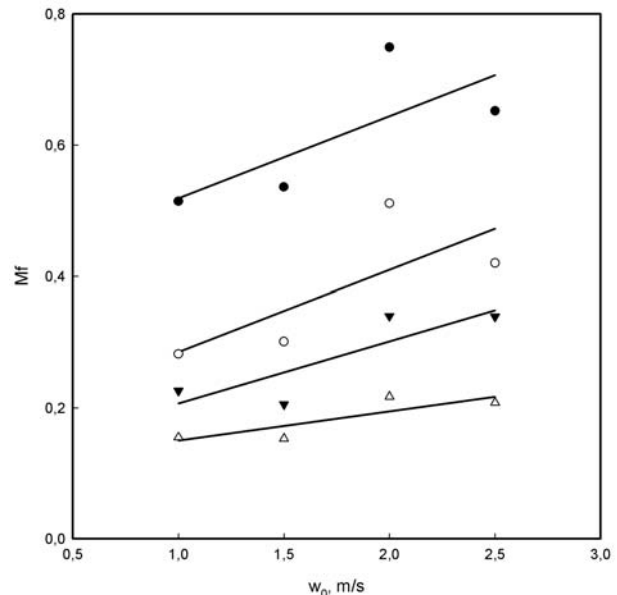


Fig. 3. Dependence of maldistribution factor on gas velocity in column below and over a layer height of 0.26 m for honeycomb No 1 and two types of inlets – ID2 and ID3; ● - below the packing and ID2; ○ - over the packing and ID2; ▼ - below the packing and ID3; △ - over the packing and ID3.

An interesting result is obtained with much higher layer of the same packing (Fig. 4). Two facts can be seen: The maldistribution factor at great layer height (1.6 m) is independent on gas flow velocity. Also, there is not significant difference in the maldistribution before and after the layer.

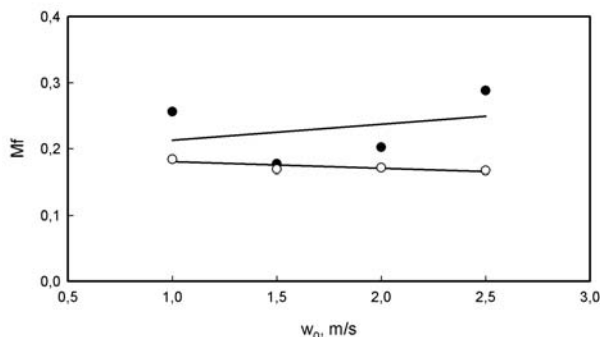


Fig. 4. Dependence of maldistribution factor on gas velocity in column below and under a layer height of 1.6 m for honeycomb No 1 and inlet ID3:

● - below the packing; ○ - over the packing.

Comparative studies on the maldistribution factor before and after the packing layer cannot be found in the literature. In all cases better flow distribution is observed above the layer. More detailed studies should be done, but one can say in advance that a better performance is related to packing structure, to its distribution ability, and probably to its pressure drop. The latter has been measured and the results are given on Fig. 5. Generally, it is not high and rather similar for both packings (Honeycomb No 1 and honeycomb No 2).

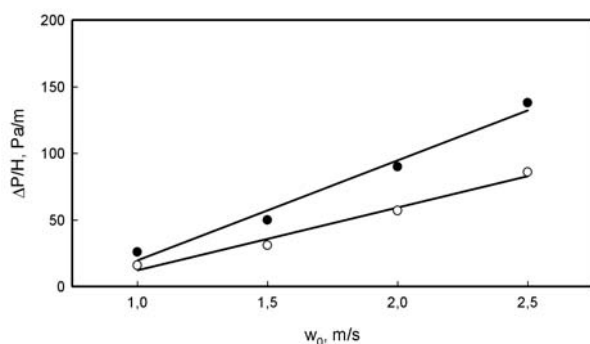


Fig. 5. Pressure drop as depending of gas velocity for honeycomb No 1 and honeycomb No 2: ● - honeycomb No 1 packing; ○ - honeycomb No 2 packing.

Analogous study on the maldistribution factor at different flow velocity has been carried out with packing honeycomb No 2 with gas inlet of type ID3 (Fig. 1c) and packing height 0.8 m. The results are reported on Fig. 6.

The evolution of maldistribution factor with the layer height is an important characteristic of the packing [5, 7]. Fig. 7 illustrates this dependence for

packing Honey-comb No 1 at four different flow velocities ($w_0 = 1.0, 1.5, 2.0$ and 2.5 m/s). As it is seen, at lower packing height ($H = 0.26$ and 0.8 m), the maldistribution factor varies in some range, while at larger packing height ($H = 1.2$ and 1.6 m) the values of M_f are very similar. This result confirms a previous estimation [3] that for thicker layers the maldistribution factor does not depend on gas flow velocity.

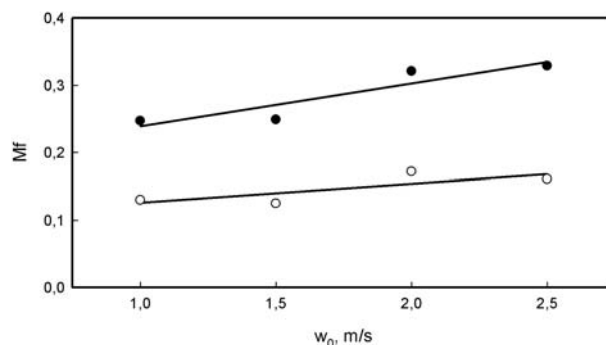


Fig. 6. Dependence of maldistribution factor on gas velocity in column below and under a layer height of 0.8 m for Honey-comb No 2 and inlet ID3:

● - below the packing; ○ - over the packing.

From Fig. 7 one can take information for penetration depth and uniformity limit [4, 7] of the ceramic honey-comb packing. For packing No 1 it is 0.4 and 0.15 correspondingly. Close to these values are the results for packing No 2 with uniformity limit 0.13 and penetration depth about 0.6 m.

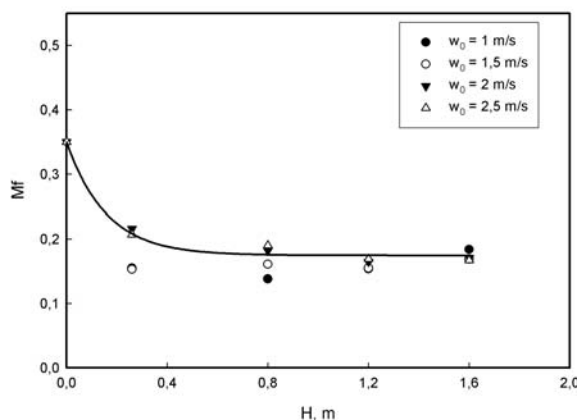


Fig. 7. Dependence of maldistribution factor on layer height of honeycomb No 1 packing ID3 gas inlet.

CONCLUSION

The structured ceramic packing honeycomb, besides its great hydrodynamic, heat and mass transfer characteristics, possess a very good distribution for the gas flow. Although the packing structure (packing made of ceramic blocks with hexagonal vertical holes) does not permit a radial gas spreading, the maldistribution factor M_f is suffi-

ciently low. For example, for packing No 1, uniformity limit equal to 0.15 and penetration depth about 0.4 m have been experimentally determined. Close to these values are the parameters of packing No 2, for which the uniformity limit is equal to 0.13 and penetration depth is about 0.6 m.

Symbols

ID	inlet device;
H	height of a packing, m;
M_f	maldistribution factor;
n	number of measuring point;
W_i	gas velocity in point i , m/s;
W_o	gas flow superficial velocity, m/s;
W_{maxi}	maximum gas flow velocity in point i , m/s;
W_{maxo}	mean maximum velocity in given cross-section, m/s.

REFERENCES

1. D. Elenkov, N. Kolev, R. Darakchiev, *Commun. Inst. Gen. Inorg. Chem., Bulg. Acad. Sci.* **5**, 65 (1967) (in Bulgarian).
2. Ch. V. Dodev, R. D. Darakchiev, *Bulg. Chem. Commun.*, **31**, 51 (1999).
3. R. D. Darakchiev, Ch. V. Dodev, *Bulg. Chem. Commun.*, **33**, 237 (2001).
4. R. Darakchiev, Ch. Dodev, *Chem. Eng. Process.*, **41**, 385 (2002).
5. R. Darakchiev, *Chem. Biochem. Eng. Q.*, **18**, 145 (2004).
6. X. Yuan, W. Li, *ICHEME Symp. Ser. No142*, part2, 931 (1997).
7. T. Petrova, S. Darakchiev, R. Darakchiev, *Bulg. Chem. Commun.*, **39**, 15 (2007).

НЕРАВНОМЕРНОСТ НА ГАЗОВОТО ТЕЧЕНИЕ В БЛОКОВ КЕРАМИЧЕН ПЪЛНЕЖ „ПЧЕЛНА ПИТА“

С. Даракчиев*, Р. Даракчиев

Институт по инженерна химия, Българска академия на науките, ул. „Г. Бончев“ бл. 103, 1113 София

Постъпила на 15 юни 2009 г.; Преработена на 22 октомври 2009 г.

(Резюме)

Блоковият керамичен пълнеж “Пчелна пита” е подреден тип пълнеж с много добри хидродинамични и топло- и масообменни характеристики. Подробното изследване на разпределителната му способност на газовото течение също показва много добри резултати. Показани са резултатите от изследване на фактора на неравномерност под и над пълнежния слой за пълнежи с различни размери на блока пълнеж и с различни височини на слоя пълнеж. Интересни са резултатите за фактора на неравномерност при различни скорости на течението и за измервания под и над слоя пълнеж. Установени са основни характеристики на пълнежа, като лимит на равномерност, който за пълнеж № 1 е 0.15 и дълбочина на проникване, която е около 0.4 m. За пълнеж “Пчелна пита” № 2 лимитът на неравномерност е 0.13, а дълбочината на проникване е около 0.6 m.

Batch reactor performance improvement for hexavalent chromium reduction by scrap iron using reciprocating perforated disc

A. H. Elshazly*

Chemical Engineering Department, Alexandria University, Egypt

Received June 15, 2009; Revised October 22, 2009

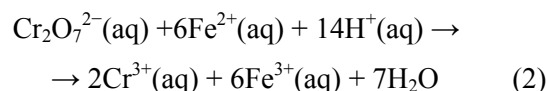
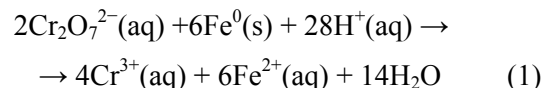
The aim of the present work is to improve the performance of a batch reactor used for the reduction of hexavalent chromium ions to trivalent ions by scrap iron shreds using reciprocating perforated disc. Many variables were investigated for its effect on the rate of reduction reaction such as frequency and amplitude of oscillation (vibration velocity), initial concentration of hexavalent chromium ions, phase ratio between the mass of solid scrap iron shreds and the volume of hexavalent chromium solution (m/v), and disc diameter. The results showed that the rate of hexavalent chromium ions reduction was increased by increasing the frequency and amplitude of oscillation (vibration velocity), increasing the phase ratio and increasing the disc diameter. On the other hand, the rate of reduction decreased by increasing the initial concentration of hexavalent chromium ions. It was found that the rate of mass transfer has increased by a factor ranging from 5 to 10 than the reduction without disc oscillation depending on vibration intensity of the disc oscillation. In addition mass transfer study of the process has revealed that the data fit the dimensionless equation $Sh_m = 0.032 Re_v^{1.12} Sc^{0.33}$. The importance of using the above equation in the design and operation of high productivity reactor was pointed out.

Key words: hexavalent chromium reduction, scrap iron, reciprocation, vibration, wastewater.

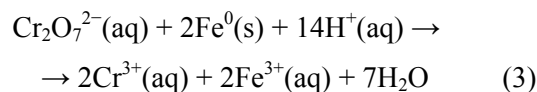
INTRODUCTION

Chromium is a common pollutant in the environment resulting from widespread industrial use such as, textile dyeing, tanneries, metallurgy, metal electroplating, cooling towers and wood preserving. The toxicity of chromium depends on its oxidation state. Chromium(VI) such as CrO_4^{2-} and $Cr_2O_7^{2-}$, is known to be toxic to humans, animals, plants and microorganisms, whereas trivalent chromium is essential for humans and less toxic than hexavalent chromium and easily removed by simple precipitation by lime as $Cr(OH)_3$ [1, 2]. Many techniques have been considered to reduce the content of chromium ion in waste water streams such as ion exchange and activated carbon adsorption [3–5], electrochemical techniques [6, 7] and chemical reduction using reducing agents such as SO_2 , $FeSO_4$, *etc.* and precipitation method [8, 9]. Although ion exchange and activated carbon adsorption have been successfully demonstrated on the laboratory scale, they have not been employed to any significant degree in full-scale operation and are only suitable for low concentrations of chromium ion (less than 100 ppm) [3–5]. On the other hand reduction of Cr(VI) to Cr(III) by different reducing agents such as $NaHSO_3$, FeS , $FeSO_4$, SO_2 , *etc.*, followed by chemical precipitation of Cr(III) by lime as $Cr(OH)_3$

has received a great attention [10–13], and was found to operate effectively with higher rate and higher % recovery at pH values 2–3. These methods are controlled by the cost of the chemicals used and the dosage required of each one. Typically it was found that, the chemical dosage required for Cr(VI) reduction is twice the stoichiometric required [13, 14]. With regard to cost considerations metallic Iron has received a great attention as a reducing agent for Cr(VI). In recent years, zerovalent iron was used for the in situ reduction of redox active metals from contaminated groundwater [15–18]. Previous investigators [19] have shown that Cr(VI) may be removed from solution via reduction to Cr(III) according to the following equations:



The net reaction for the reduction process can be written as:



The reduction of Cr (VI) to Cr (III) using a relatively pure iron wire was investigated by Gould [20], who concluded that iron surface is effective in

* To whom all correspondence should be sent:
E-mail: elshazly_a@yahoo.com

reducing Cr (VI) to Cr (III) under pH conditions of 2–3. Bowers *et al.* [21], have examined the use of scrap iron filings to treat Cr(VI) containing metal plating wastewaters and came to the conclusion that using iron filings to treat Cr(VI) containing solutions have the advantages that the chemical costs using scrap iron filings are substantially lower than conventional reducing agents such as SO_2 , NaHSO_3 , FeS , FeSO_4 , *etc.* also the dissolved iron provide a well conditioned sludge product. The indirect reduction of hexavalent chromium to trivalent chromium with scrap iron and simultaneous generation of electrical energy using a divided parallel plate cell and fixed bed electrodes was investigated by Abdo *et al.* [22], who came to the conclusion that this technique can reduce Cr(VI) to the permissible limit value effectively while it neither consumes energy nor expensive chemicals. Hou *et al.* [23], studied the effect of presence of different divalent cations on the reduction of hexavalent chromium by zerovalent iron and came to the conclusion that presence of copper ions and iron ions could improve the reduction process while calcium ions might inhibit the process.

Previous investigations for the reduction of Cr(VI) to Cr(III) on iron surface proved that the reduction reaction is a diffusion controlled one [19, 24]. From this point of view the rate of reaction can be increased using different techniques such solution circulation or agitation using mechanical tools. The aim of the present work is to implement mechanical vibration or reciprocation for enhancing the rate of reduction reaction. The application of vibrations, pulsation and or reciprocation has been recognized as effective process intensification techniques that enhances mass and heat transfer rates, and improves both process productivity and product quality [25–30]. Zaki *et al.* [31] suggested the possibility of using oscillating screen array as a catalytic reactor suitable for conducting liquid–solid diffusion controlled catalytic reactions such as removal of organic pollutants from industrial effluents by wet oxidation. In addition application of oscillatory motion in electrochemical processing has been of particular interest due to its ability to enhance mass transfer rate, current density and system energy utilization. Recently, it was shown that more than 20-fold increase in the mass transfer rate could be achieved by vibrating vertical electrodes along their length [32]. Among its applications in that field are electrochemical processing, electroplating, metal recovery from bio-leaching solutions, and more recently manufacture of Printed Wiring Board [33–38]. In all of the above mentioned applications, generating of an oscillatory

field at the solid–liquid interface is achieved by vibrating either the solid surface or the fluid surrounding it. Although both approaches achieve the same objective, the former is more energy efficient since the energy dissipation there is mainly focused in the boundary layer adjacent to the solid–liquid interface rather than in the bulk of the fluid medium. When the power needed to vibrate the electrode was taken into consideration, Al Taweel *et al.* [38] found that both amplitude and frequency have almost equal effect on the enhancement obtained per unit power consumed.

From the above it is clear that pulsation or vibration is a good tool for enhancing the rate of hexavalent reduction using scrap iron shreds. In addition scrap iron shreds will improve the economy of the process.

EXPERIMENTAL

Fig. 1 shows the experimental setup used in the present study. It consisted of the vibrating system and the reactor. The vibrating system consisted of a reciprocating perforated plastic disc with different diameters ranging from 6 to 12 cm, with constant perforations fixed at 0.25 cm in diameter and arranged in lines with constant spacing of 1 cm. The perforated disc was placed in a Plexiglas column of 15 cm diameter and 30 cm height. The disc was held inside the column by insulated stainless steel stem of 3 mm diameter which penetrated the disc at its centre by means of epoxy coated steel nuts. The upper end of the stem was connected to the vibrator through a Teflon sleeve. Vertical oscillation was induced to the perforated disc by means of a mechanical vibrator connected to the upper end of the stem. The mechanical vibrator consisted of a disc rotated by means of an electrical motor. The rotating motion of the disc was transferred into a reciprocating motion by means of a crank shaft connected to the disc at a distance from its centre. The frequency of vibration was measured by means of a portable digital tachometer and changed by means of a set of pulleys and gear box connected to the electrical motor. The amplitude was adjusted by adjusting the distance between the rotating disc centre and the point of its connection with the crank shaft. The rate of hexavalent chromium reduction on scrap iron shaving surface was followed by measuring the change in concentration of hexavalent chromium ions solution with time. Before each run, scrap iron shavings were prepared with different mesh ranged from 10 to 50 and soaked in 0.1 N HCl for about 2 minutes to remove any rust or coats, then washed with distilled water, dried and placed in

the column, two litres of freshly prepared acidified potassium dichromate solution were placed in the column that have iron shavings. In the mean time the solution was subjected to oscillation at the required vibration intensity. Samples of the solution (5 ml) were withdrawn at regular time intervals ranged from 1.5 to 3 min at high and low vibration intensities respectively. These samples were titrated against standard 0.1 N ferrous ammonium sulphate using diphenylamine barium salt as indicator [39]. Different initial concentrations of potassium dichromate solution were used in the present study namely, 0.025, 0.05, 0.075 and 0.1 M, all solutions contained 0.5 M H₂SO₄, and prepared using A.R. chemicals and distilled water. Experiments were carried out at room temperature which ranged from 21–22°C, while the pH of the solutions was adjusted at 2.5 in all experiments using a portable digital pH meter and 0.1 N NaOH solutions. The solution viscosity and solution density used in data correlation were measured by an Ostwald viscometer and density bottle respectively. While diffusivity at different temperatures were calculated using Stokes-Einstein equation ($D\mu/T = \text{constant}$), and the literature [40, 41].

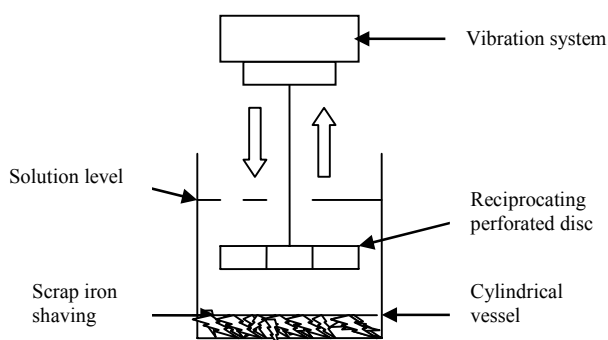


Fig. 1. Experimental setup.

RESULTS AND DISCUSSION

For the simple batch reactor used in the present work the mass transfer coefficient (K) can be calculated using the equation [42]

$$V_s \cdot \lg((C_0 - C_e)/(C - C_e)) = K.A.t \quad (4)$$

Where V_s is the solution volume; C_0 , C_e and C are initial, equilibrium and concentration at any time t of dichromate solution, respectively; A is the active area of the scrap iron shreds; t is the time of reaction. The above equation is the integrated form of the material balance equation of the batch reactor, namely

$$-V_s \cdot d(C - C_e)/dt = K.A.(C - C_e) \quad (5)$$

As the area of iron shavings is not defined and can not be easily determined so the volumetric mass transfer coefficient ($K' = KA$) will be used for data analysis. K' was obtained under different conditions by plotting $\ln((C_0 - C_e)/(C - C_e))$ vs. t as shown in Fig. 2 and then calculating the volumetric mass transfer coefficient from the slope of the resulting plot.

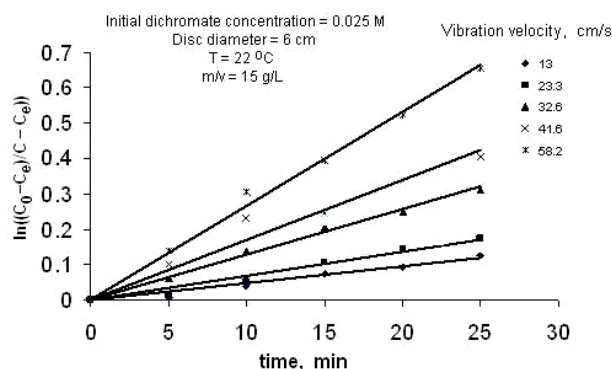


Fig. 2. $\ln((C_0 - C_e)/(C - C_e))$ vs time at different vibration velocity.

Effect of amplitude and frequency of oscillation (vibration velocity)

Figures 2, 3 and 4 show the effect of amplitude (A_m), frequency (f) and vibration velocity V_1 ($V_1 = 4A_m \cdot f$) on the rate of reduction reaction and rate of mass transfer. The volumetric mass transfer coefficient increased by increasing both amplitude and frequency or vibration intensity. The increase in the reduction rate may be attributed to the fact that increasing vibration intensity will increase turbulences especially those of the small scale high frequency eddies, these eddies will reduce the thickness of the diffusion layer and hence increase the rate of mass transfer ($K = D/\delta$) where D is the ions diffusivity and δ is the diffusion layer thickness. In addition increasing vibration velocity increases fluid circulations inside the column which fluidizes iron shreds and increases the contact area between the two phases and hence increases the rate of mass transfer.

Figure 4, shows that the volumetric mass transfer coefficient can be related to the vibration intensity by the relation that: $K' = aV_1 + b$. The value of a can be approximated to the value 0.033 with an average deviation of about 2%, while that of b its value ranges from 0.0658 to 0.6897 at amplitudes of 1cm and 4 cm respectively, which indicates that the volumetric mass transfer coefficient has been increased by a factor of 10.48 by increasing the amplitude from 1cm to 4cm.

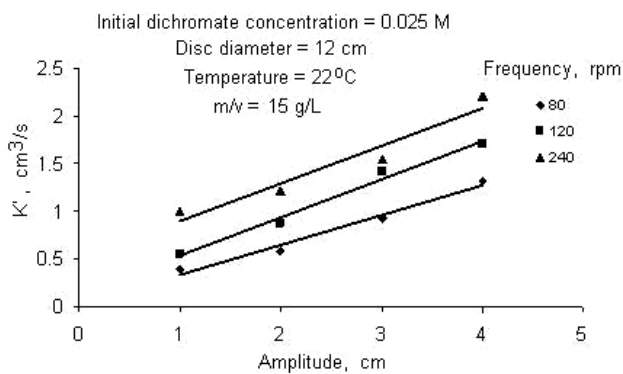


Fig. 3. Volumetric mass transfer coefficient vs amplitude at different frequencies.

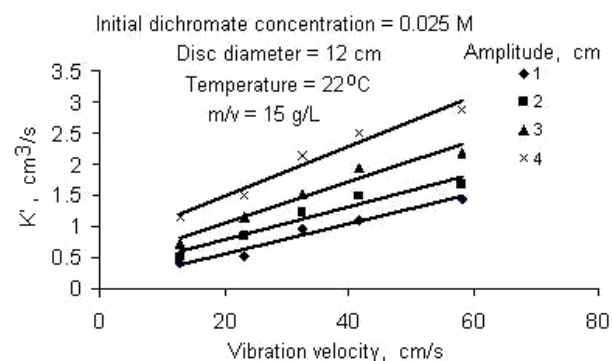


Fig. 4. Volumetric mass transfer coefficient vs vibration velocity at different amplitudes.

Effect of initial dichromate concentration

Figure 5 shows that, the volumetric mass transfer coefficient decreased by increasing the initial concentration of dichromate solution [Cr(VI) concentration]. This can be attributed to the passivation of iron surface and reduction in iron corrosion that stops the main reactions of the reduction process (reactions 1 and 2) [43]. In addition, the diffusivity of dichromate ions decreases with increasing its concentration thus decreasing the rate of reduction reaction ($K = D/\delta$). From figure 5, it is obvious that the % increase in the rate of reduction for higher vibration velocity (58.2 cm/s) is approximately 8 times the rate at the lower velocity (13 cm/s) both at the same amplitude, which confirm the enhancement effect of pulsation for improving the rate of reduction reaction to a good extent.

Effect of phase ratio (solid/liquid)

Figure 6, shows that the volumetric mass transfer coefficient increased by increasing phase ratio, which can be ascribed to the increased surface area available for the reduction reaction. In addition, passivation of iron surface decreases by increasing surface area of iron, thus the rate of reduction reaction increase.

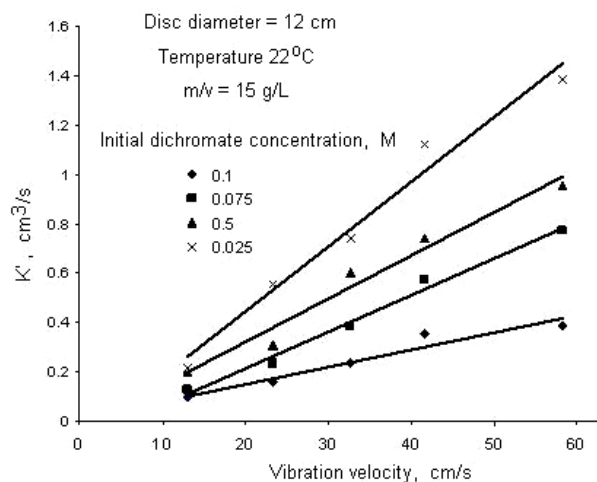


Fig. 5. Volumetric mass transfer coefficient vs vibration velocity at different initial dichromate concentrations.

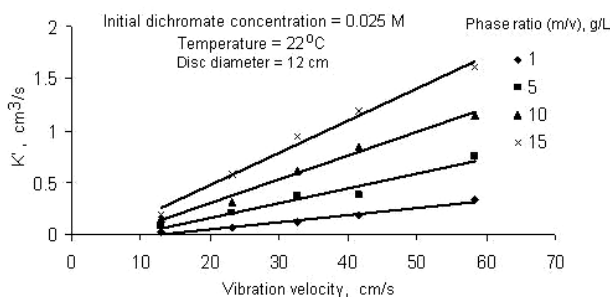


Fig. 6. Volumetric mass transfer coefficient vs vibration velocity at different phase ratio.

Effect of perforated disc diameter

Figure 7, shows that the volumetric mass transfer coefficient increased by increasing disc diameter, which can be attributed to the fact that increasing disc diameter will reduce the annular free area (axial flow area) between the disc and the column wall. Reducing flow area will certainly increase the axial flow velocity in the annular space and increase the jetting effect of solution flow through the disc perforations and hence increase eddies and turbulences inside the column that increases the rate of mass transfer and reduction rate of Cr (VI) ions.

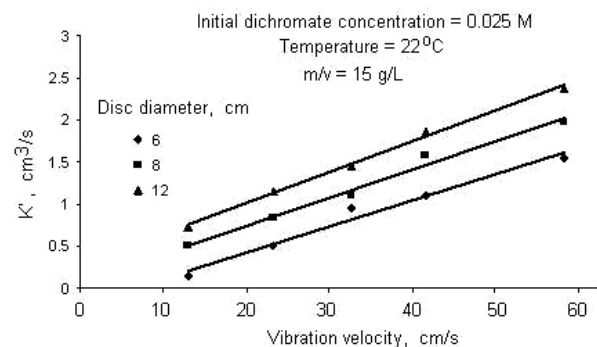


Fig. 7. Volumetric mass transfer coefficient vs vibration velocity at different disc diameter.

Overall correlation using dimensional analysis

For the purpose of design consideration dimensional analysis was used for correlating the main variables affecting the reduction operation. It was found that the data fits the general mass transfer equation that

$$Sh = a Re_v^\alpha \cdot Sc^{0.33} \quad (6)$$

The exponent of Sc was proved by other investigators to be 0.33 [44], Where a and α are constants. As mentioned before the true area of mass transfer is not easy to be determined so the modified Sherwood number (Sh_m) will be used instead of Sh, where $Sh_m = 4 K' / \pi d D$, where d is the column diameter and D is the ions diffusivity. The exponent of vibrational Reynolds (constants α) was obtained by plotting $\log Sh_m$ vs. $\log Re_v$ for different Sc as shown in Figure 8 and it was found to be about 1.12.

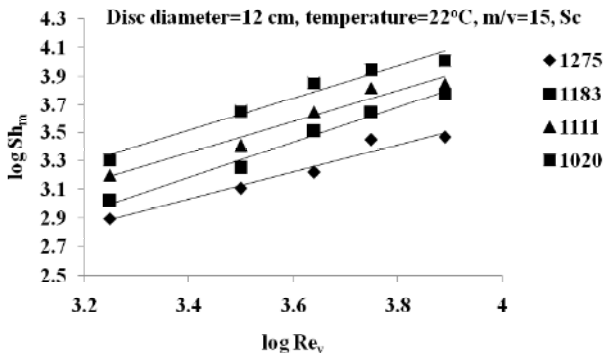
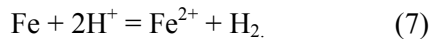


Fig. 8. $\log Sh_m$ vs. $\log Re_v$ at different Sc.

The higher value of exponent α (1.12) confirms that the reaction is diffusion controlled one. In addition, this higher value compared to the theoretical value 0.5–0.57 [44] may be attributed to the enhancing effects of H_2 evolution, which occurs simultaneously with chro-mate reduction at the shreds surface (observed visually) as a result of the reaction:



The rising H_2 bubbles collide with the surface of iron shreds and disturb the diffusion layer with a consequent increase in the mass transfer coefficient K ($K = D/\delta$).

As shown in Figure (9), Sh_m was drawn versus $Re_v^{1.12} \cdot Sc^{0.33}$, for finding out the value of constant a. The overall correlation was found to fit the equation that:

$$Sh_m = 0.032 Re_v^{1.12} \cdot Sc^{0.33} \quad (8)$$

This equation is valid in the range $1275 > Sc > 1020$ and $7900 > Re_v > 1764$.

The deviation of data was found to be high as the value of R^2 was found to be about 0.75 this higher deviation of data may be ascribed to the complex nature of the mass transfer mechanism over the iron shreds surface as a result of simultaneous H_2 evolution with direct chromate reduction on the iron surface [24]. In the design consideration of pulsating or reciprocating system using iron shreds for the reduction of hexavalent chromium, experimental investigations, with the given correlation will be more reliable with the aid of the obtained results for each variable studied.

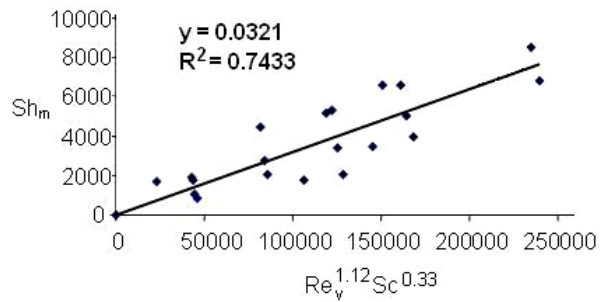


Fig. 9. Overall correlation for hexavalent chromium reduction by scrap iron shreds using vibrating module.

CONCLUSION

The reduction kinetics of hexavalent chromium to trivalent chromium using a fixed bed of scrap iron shreds subjected to pulsation using reciprocating perforated disc was investigated under different conditions of amplitude and frequency (vibration intensity) of vibration, initial concentration of a synthetic solution of acidified potassium dichromate, phase ratio(solid/liquid), and disc diameter. It was found that the mass transfer coefficient and the rate of reduction reaction increased by increasing frequency and amplitude of vibration (vibration intensity), disc diameter and phase ratio (solid/liquid) and decreasing by increasing the initial concentration of the acidified potassium dichromate solution. The results show that the volumetric mass transfer coefficient has increased by a factor ranging from 5 to 10 depending on vibration intensity. For the rational design and operation of batch reactor using scrap iron shreds subjected to reciprocation and used for the reduction of hexavalent chromium from waste solutions the following mass transfer correlation was obtained $Sh_m = 0.032 Re_v^{1.12} \cdot Sc^{0.33}$.

This equation is valid in the range $1275 > Sc > 1020$ and $7900 > Re_v > 1764$. The deviation of data was found to be high as the value of R^2 was found to be about 0.75 this higher deviation of data may be ascribed to the complex nature of the mass transfer mechanism over the iron shreds surface as a

result of simultaneous H₂ evolution with direct chromate reduction on the iron surface.

This system is suitable for treating higher discharge rates of industrial wastewater polluted with the toxic hexavalent chromium ions with lower cost.

List of symbols and nomenclatures

- A* active area of iron shreds (cm²);
A_m the amplitude of oscillation (cm);
C₀, C_e, and C are initial, equilibrium and concentration at any time of dichromate solution (M);
d disc diameter (cm)
D diffusivity of dichromate ions (cm²/s);
F frequency of oscillation (s⁻¹);
K mass transfer coefficient (cm/s);
K' volumetric mass transfer coefficient (cm³/s);
t time (s);
V_s solution volume (cm³);
Sc Schmidt number (μ/ρD);
Sh Sherwood number (Kd/D);
Sh_m modified Sherwood number (4K^{1/3}/πDd);
Re_v vibrational Reynolds number (ρV_I d/ μ);
μ solution viscosity (g/cm.s);
ρ solution density (g/cm³);
δ diffusion layer thickness (cm).

REFERENCES

- J. Kotas, Z. Stasicka, *Environ. Pollut.*, **107**, 263 (2000).
- D. E. Kimbrough, Y. Cohen, A. M. Winer, L. Greelman, C. Mabuni, *Crit. Rev. Environ. Sci. Technol.*, **29**, 1 (1999).
- A. R. Bowers, C. P. Huang, *Prog. Water Technol.*, **12**, 629 (1980).
- N. K. Hamadi, X. D. Chen, M. M. Farid, M. G. Q. Lu, *Chem. Eng. J.*, **84**, 95 (2001).
- K. Fetyanose, P. Fachantidis, *Toxicol. Environ. Chem.*, **64**, 197 (1997).
- A. Radwan, A. El-Kayar, H. A. Farag, G. H. Sedahmed, *J. Appl. Electrochem.*, **22**, 116 (1992).
- D. Golub and, Y. Oren, *J. Appl. Electrochem.*, **19**, 311 (1989).
- M. Erdem, H. S. Altundoğan, A. Ozer, F. Tümen, *Environ Technol.*, **22**, 22 (2001).
- C. Kim, Q. Zhou, B. Deng, E. C. Thornton, H. Xu, *Environ. Sci. Technol.*, **35**, 2219 (2001).
- K. Muthukumar, N. Balasubramanian, T. V. Ramakrishna, *Met. Finish.*, **93**, 11 (1995).
- J. Kim, P. K. Jung, H. S. Moon, C. M. Chon, *Environ. Geol.*, **42**, 642 (2002).
- M. Mullet, S. Boursiquot, J. J. Ehrhardt, *Colloids Surf. A: Physicochem. Eng. Aspects*, **244**, 77 (2004).
- F. Sevim, D. Demir, *Chem. Eng. J.*, **143**, 161 (2008).
- D. W. Blowes, C. J. Ptacek, S. G. Benner, C. W. T. McRae, T. A. Bennett, R. W. Puls, *J. Contam. Hydrol.*, **45**, 123 (2000).
- B. Gu, L. Liang, M. J. Dickey, X. Yin, S. Dai, *Environ. Sci. Technol.*, **32**, (1998) 3366–3373.
- K. J. Cantrell, D. I. Kaplan, T. W. Wietsma, *J. Hazard. Mater.*, **42**, (1995) 201–212.
- D. W. Blowes, C. J. Ptacek, J. L. Jambor, *Environ. Sci. Technol.*, **31**, 3348 (1997).
- R. W. Puls, C. J. Paul, R. M. Powell, *Appl. Geochem.*, **14**, 989 (1999).
- M. Gheju, A. Iovi, *J. Hazard. Mater.*, **B135**, 66 (2006).
- J. P. Gould, *Water Res.*, **16**, 871 (1982).
- A. R. Bowers, C. A. Ortez, R. J. Cardozo, *Pollut. Cont. Met. Finish.*, **37**, 67 (1986).
- M. S. E. Abdo, G. H. Sedahmed, *Energy Convers. Mgmt.*, **39**, 943 (1998).
- M. Hou, H. Wan, T. Liu, Y. Fan, X. Liu, X. Wang, *Appl. Catalysis B: Environmental*, **84**, 170 (2008).
- A. H. El-Shazly, A. A. Mubarak, A. H. Konsowa, *Desalination*, **185**, 307 (2005).
- R. S. Alasser, H. M. Badr, H. A. Mavromatis, *Int. J. Heat Mass Trans.*, **42**, 1289 (1999).
- P. Gao, W. Han Ching, M. Herrmann, C. Kwong, P. L. Yue, *Chem. Eng. Sci.*, **58**, 1013 (2003).
- A. M. Thomas, R. Narayanan, *Int. J. Heat Mass Trans.*, **45**, 4057 (2002).
- F. M. Mahfouz, H. M. Badr, *Int. J. Heat Mass Trans.*, **38**, 477 (2002).
- T. Nishimura, N. Oka, Y. Yoshinak, K. Kunitsugu, *J. Heat Mass Trans.*, **43**, 2365 (2000).
- F. J. Poulin, G. R. Flierl, J. Pedlosky, *J. Fluid Mech.*, **481**, 329 (2003).
- M. M. Zaki, I. Nirdosh, G. H. Sedahmed, *Chem. Eng. J.*, **126**, 67 (2007).
- H. G. Gomaa, A. M. Al-Taweel, J. Landau, *Chem. Eng. J.*, **97**, 141 (2004).
- P. Venkateswarlu, N. Jaya Raj, D. Subba Rao, T. Subbaiah, *Chem. Eng. Process.*, **41**, 349 (2002).
- N. G. Carpenter, E. P. L. Roberts, *Trans. Inst. Chem. Eng.*, **77A**, 212 (1999).
- G. H. Sedahmed, M. Z. El-Abd, A. A. Zatout, Y. A. El-Taweel, M. M. Zaki, *J. Electrochem. Soc.*, **141**, 437 (1994).
- U. Landau, US Patent 6, 2621,433, July 2001.
- R. Omasa, US Patent 6, 2621,435, July 2001.
- A. M. Al Taweel, M. I. Ismail, *J. Appl. Electrochem.*, **6**, 559 (1976).
- A. L. Vogel, A Text-Book of Quantitative Inorganic Analysis, 3rd edition, Longman, London, 1961.
- R. H. Perry, Chemical Engineering Handbook, 8th edition, McGraw-Hill, New-York, 2007.
- L. E. Eary, D. Rai, *Environ. Sci. Technol.*, **22**, 972 (1988).
- O. Levenspiel, Chemical Reaction Engineering, 3rd edition, John Wiley & Sons, New York, 2006.
- N. Melitas, O. Chufe-Moscoco, J. Farrell, *Environ. Sci. Technol.*, **35**, 3948 (2001).
- J. Welty, C. E. Wicks, G. L. Rorrer, R. E. Wilson, Fundamentals of Momentum, Heat and Mass Transfer, 5th edition, John Wiley & Sons, Inc., USA, 2008.

ПОДОБРЯВАНЕ НА ДЕЙСТВИЕТО НА РЕАКТОР С ПЕРИОДИЧНО ДЕЙСТВИЕ
ЗА РЕДУКЦИЯ НА ШЕСТВАЛЕНТЕН ХРОМ ЧРЕЗ ЖЕЛЕЗЕН СКРАП
С ИЗПОЛЗВАНЕ НА ВЪЗВРАТНО-ПОСТЪПАТЕЛЕН ПЕРФОРИРАН ДИСК

А. Х. Елшазли

Департамен по инженерна химия, Университет на Александрия, Египет

Постъпила на 15 юни 2009 г.; Преработена на 22 октомври 2009 г.

(Резюме)

Целта на настоящата работа е подобряване на действието на реактор с периодично действие за редукция на шествалентни хромни йони до тривалентни йони чрез късове от железен скрап с използване на възвратно-постъпателен перфориран диск. Изследвани са много променливи за ефекта върху скоростта на реакцията на редукция като: честота и амплитуда на осцилациите, начална концентрация, на шествалентните хромни йони, фазово съотношение на масата на късовете от железен скрап и обема на разтвора на шествалентните хромни йони (m/v) и диаметъра на диска. Резултатите показват, че скоростта на редукция на шествалентните хромни йони расте с увеличаване на честотата и амплитудата на осцилациите (скоростта на вибриране), увеличаване на фазовото съотношение, и увеличаване на диаметъра на диска. От друга страна, скоростта на редукция намалява с увеличаване на началната концентрация на шествалентни хромни йони. Намерено е, че скоростта на масопренасяне при вибрации на диска се увеличава 5–10 пъти в сравнение с редукция с без осцилации на диска. В допълнение, изследването на процеса на масопренасяне показва, че данните съответстват на безизмерно уравнение $Sh_m = 0.032 Re_v^{1.12} Sc^{0.33}$. Показано е значението на посоченото уравнение за проектирането и действието на реактор с висока производителност.

Evaluation of the antiradical and antioxidant properties of extracts from Indian red chili and black pepper by *in vitro* models

A. G. Gopala Krishna¹, B. R. Lokesh¹, D. Sugasini¹, V. D. Kancheva^{2*}

¹ Department of Lipid Science and Traditional Foods, Central Food Technological Research Institute, Mysore 570020, India

² Laboratory of Lipid Chemistry, Institute of Organic Chemistry with Centre of Phytochemistry, Bulgarian Academy of Sciences, Acad. G. Bonchev St., Block 9, Sofia 1113, Bulgaria

Received July 31, 2009

Oxygen free radicals and lipid peroxides play an important role in increasing the risk factors for many chronic diseases and are also responsible for the deterioration of food products. The objective of this investigation was to evaluate the potentials of some extracts from chili and pepper to scavenge free radicals *in vitro* model systems such as: 1,1-diphenyl-2-picryl-hydrazyl (DPPH), N,N-dimethyl-*p*-phenylenediamine dihydrochloride (DMPD), 2,2-azino-bis-3-ethyl benzthiazoline-6-sulphonic acid (ABTS), ferric cyanide reducing antioxidant power (FRAP), cuprum total antioxidant capacity (CUPRAC) assays and to exhibit antioxidant activities on the lipid peroxidation in rat liver homogenate. Alcohol extracts and oleoresins of chili and pepper showed significant radical scavenging activities and antioxidant potential in all the systems tested. These results can be exploited in preserving processed foods and at the same time get the benefits of medicinal properties of these spices.

Key words: Chili, pepper, oleoresin, radical scavengers, antioxidants, *in vitro* model systems

INTRODUCTION

Antioxidants can protect the human body from damages caused by free radicals mediated lipid peroxidation and deleterious effects of reactive oxygen species. They retard the progress of many chronic diseases [1]. Antioxidant compounds can scavenge free radicals and increase shelf life of food products by retarding the process of lipid peroxidation, which is one of the major reasons for deterioration of food products [2]. Normally synthetic antioxidants such as butylated hydroxyanisole (BHA) or butylated hydroxytoluene (BHT) are used for preservation of processed foods. But indiscriminate use of these synthetic antioxidants can lead to tumor formation and liver damage as has been shown in experimental animals. Hence, a need for identifying alternative and safe source of antioxidants for use in food products has been advocated and the search for natural antioxidants especially of plant origin has notably increased in recent years [3].

Spices are dietary constituents used to enhance the flavor and taste of food. Many of them have been identified to possess potential chemo preventive action. Chili is one of the important spices used in varieties of Indian dishes for imparting color, flavor and pungency to the food. The traditional use of whole ground chilies in food and beverage indus-

tries is now very limited. Now a days, the use of value added chili products such as oleoresin, essential oil, capsaicin, capsanthin have gained importance in the global market as compared to use of whole or ground chili. The export of these products is increasing considerably every year from India.

Chilies contain Vitamin A, Vitamin C and capsaicin which are good antioxidants and antiinflammatory agents, which can also boost immune system. Antioxidants present in the chili are good free radical scavengers [4]. Chilies also act as detoxifier by removing the waste products from our body and increase the blood supply to the tissues. Chilies stimulate the release of endorphins that are natural pain killers. It has been noted that the Vitamin C, β -carotene and folic acid found in chili reduces the risk of colon cancer [5]. Vitamin A present in chili reduces the inflammation of lungs and emphysema resulting from cigarette smoking. Chilies enhance blood flow to the site of infection which helps in fighting infection.

Pepper is an important spice appreciated for both its aroma and pungency. It is valued for its distinct biting quality which is attributed to piperine and its isomers. Black pepper is used not only in diets as an adjunct but also for medicinal purposes and as a preservative. The pepper extract was also shown to enhance the bioavailability of a number of therapeutic drugs as well as phytochemicals [6].

* To whom all correspondence should be sent:
E-mail: vedeka@abv.bg

It is reported that black pepper has digestive stimulating activity. It improves appetite, cures cold, cough, diseases of the throat, intermittent fever, colic dysentery, worms and piles. As with many spices, it also possesses a broad spectrum of antimicrobial activity, analgesic, antipyretic and anti-inflammatory actions. It enhances the secretion of saliva and the activity of salivary amylase. The digestive stimulant action of spices is probably mediated through stimulating the liver to produce and secrete bile acids, which play a very important role in fat digestion and absorption [6, 7].

The pepper oleoresin containing the essential oil contributes to aroma. The oleoresins have many advantages such as convenience of handling and are free from microbial contamination. It also provides convenience for the preparation of processed foods. Unlike the essential oils, oleoresin of spices contains many natural antioxidants which make them more stable.

Chipault *et al.* [8] made a systematic study on antioxidant activity of some common spices and herbs. Since then a large number of studies examined the effect of plant extracts on lipid oxidative stability in order to find new sources of natural antioxidants [9]. India is one of the largest producers of spices in the world. Though they are mainly utilized for food, herbal medicine and flavorings, chili and pepper extracts can also be used as a food preservative (especially for preventing rancidity development in oils) [10]. With this background, the extracts of chili, pepper were studied for their antiradical and antioxidant activities and the results are reported in this paper.

MATERIALS AND METHODS

Chemicals

Tertiary butylated hydroxyquinone (TBHQ), butylated hydroxytoluene (BHT), butylated hydroxyanisole (BHA), gallic acid, N,N-dimethyl-*p*-phenylenediamine dihydrochloride (DMPD), 2,2-azino-bis-3-ethyl benzthiazoline-6 sulphonic acid (ABTS), 1,1-diphenyl-2-picryl hydrazyl radical (DPPH), neocuproine, cupric chloride and adenosine diphosphate (ADP) were obtained from Sigma (Moline, USA). Ascorbic acid, AlCl₃, ferrous sulphate (Fe₂SO₄), trichloroacetic acid, ammonium acetate was purchased from Sisco Research Laboratories, Mumbai, India. All other chemicals used were of analytical grade.

Plant materials and extraction procedures

Chili (Byadagi variety) and pepper (local variety) were procured from the local market of Mysore city. The cleaned spices were dried at 40°C in a labo-

ratory oven and then ground into a fine powder. The powder was extracted by using methanol as extracting solvent. Eight extractions with 3 volumes of the solvent for 4 h duration were carried out with either methanol or ethanol at room temperature (25°C). The extracts were pooled, desolventized and then dried in a dessicator overnight. Oleoresins of chili and pepper were prepared by methylene chloride extraction [11]. These extracts were used for antiradical and antioxidant assays. 10 mg of extracts were dissolved in 10 mL of methanol. Various concentrations of these extracts were used for evaluating antioxidant potentials by DPPH assay, DMPD assay, ABTS assay, reducing power assay, CUPRAC assay and by inhibition of ascorbic acid induced lipid peroxidation in rat liver homogenates.

Radical scavenging activity

Measurement of the radical scavenging activity by 1,1-diphenyl-2-picryl-hydrazyl (DPPH) test. The DPPH radical scavenging activity was measured as described by Gulcin [12]. Briefly, 0.1 mM solution of DPPH radical was prepared in methanol. 0.5 mL of this solution was added to different concentrations of chili extracts or chili oleoresin or pepper extracts or pepper oleoresin in methanol as prepared above at different concentrations (100–2000 µg/mL). Final volume of reaction mixture was made up to 2 mL in methanol. These were mixed thoroughly and incubated in dark for 30 min. The absorbance was measured at 517 nm against appropriate blank samples:

$$\text{DPPH remaining} = (1 - \text{Abs}_0/\text{Abs}_t) \times 100, \quad (\%)$$

where Abs_0 is the absorbance of the control and Abs_t is the absorbance in the presence of test compounds.

*Measurement of radical scavenging activity by N,N-dimethyl-*p*-phenylenediamine dihydrochloride (DMPD) method.* DMPD radical scavenging activity of chili and pepper extracts and their oleoresins was performed according to Fogliano *et al.* [13]. Standard DMPD (100 mM) was prepared by dissolving 209 mg of DMPD in 10 ml of deionized water. 1 ml of this solution was added to 100 ml of 0.1 M acetate buffer (pH 5.25), the coloured radical cation (DMPD^{•+}) was obtained by adding 0.2 mL of ferric chloride (0.2%) and absorbance at 505 nm was measured. Freshly prepared solutions were used for each experiment. Different concentrations of antioxidants (100–2500 µg/mL) were added to test tubes and the total volume was made up to 0.5 ml with distilled water. One ml of DMPD^{•+} solution was directly added to the reaction mixture. Ten minutes later, the absorbance was measured at 505

nm. The scavenging activity was calculated using the following equation:

$$\text{DMPD remaining} = (1 - Abs_0/Abs_t) \times 100, \quad (\%)$$

where Abs_0 is the absorbance of initial concentration of the DMPD^{•+} and Abs_t is the absorbance of DMPD^{•+} in presence of test materials.

2,2-Azino-bis-3-ethyl benzthiazoline-6-sulphonic acid (ABTS) radical cation decolourization assay. ABTS forms a relatively stable free radical, which decolorizes in its non radical form. The ABTS^{•+} radical remaining was determined according to the method of Ree *et al.* (31). The ABTS^{•+} was produced by reacting 2 mM ABTS in H₂O with 2.45 mM potassium persulphate (K₂S₂O₈), kept in the dark at room temperature for 4 hr. The ABTS^{•+} was diluted with ethanol to give an absorbance of 0.750 ± 0.025 at 734 nm. 1 ml of ABTS^{•+} solution was added to 10 μ l of chili and pepper extracts in ethanol at different concentrations (40–600 μ g/mL). The absorbance was recorded after 30 min and the percentage of radical remaining was calculated. The extent of decolourization is calculated as percentage reduction of absorbance:

$$\text{ABTS remaining} = (1 - Abs_0/Abs_t) \times 100, \quad (\%)$$

where Abs_0 is the absorbance of a control without any radical scavenger and Abs_t is the absorbance of the ABTS^{•+} remaining in the presence of the anti-radical scavenger.

Estimation of antioxidant activity

Ferric cyanide (Fe³⁺) reducing antioxidant power assay. The reductive potential of extracts was determined according to the method of Benzie and Strain [14]. Different concentrations of extracts (100–2100 μ g/mL) in 1 mL of distilled water was mixed with 2.5 mL of 0.2 M sodium phosphate buffer, pH 6.6 and potassium ferricyanide [K₃Fe(CN)₆] (2.5 mL, 1%). The mixture was incubated at 50°C for 20 min. Then the reaction was terminated by adding 2.5 mL of trichloroacetic acid (10%). The upper layer of solution (2.5 mL) was mixed with distilled water (2.5 mL) and FeCl₃ (0.5 mL, 0.1%) and the absorbance was measured at 700 nm in a spectrophotometer against a blank sample. Reductive potential was measured with increase in absorbance when extract was added.

Lipid peroxidation by TBARS assay. Liver homogenates in 150 mmol/L KCl, 25 mmol/L, Tris HCl buffer pH 7.5, 2 mmol/L ADP, 10 μ mol/L Fe₂SO₄ were incubated at 37°C for 5min. The final volume of the reaction mixture was made up to 1 mL with Tris HCl buffer. The reaction was initiated by

adding 25 μ L of ascorbic acid (100 mM). The tubes were incubated for 30 min at 37°C and the reactions were terminated by adding 2 mL of thiobarbituric acid. The tubes were heated in boiling water bath for 60 min. The malondialdehyde (MDA) formed was measured at 535 nm and quantitated using an extinction coefficient of $1.56 \times 10^{-5} \text{ M}^{-1} \cdot \text{cm}^{-1}$. The inhibition of lipid peroxidation in the presence of extracts was calculated according to Miller and Aust [15].

CUPRAC total antioxidant capacity assay. 1 ml of CuCl₂ ($1.0 \times 10^{-2} \text{ M}$), 1 mL of neocuproine alcohol solution ($7.5 \times 10^{-3} \text{ M}$) and 1 mL of ammonium acetate buffer solution (0.1 M, pH = 7) was added and mixed thoroughly followed by addition of extract at concentrations ranging from 100 μ g to 1000 μ g. To this deionized water was added to give a total volume of 4.1 mL and mixed well. After 30 min, the absorbance was read at 450 nm against a reagent blank. The antioxidant activity is expressed as mmoles of Trolox equivalent/mg of extract [16].

RESULTS

Effect of radical scavengers from chili and pepper extracts in model systems

DPPH radical scavenging activity. DPPH is usually used to evaluate the free radical scavenging activity of antioxidants. It is a stable free radical and accepts an electron or hydrogen radical to become a stable diamagnetic molecule. Figure 1 illustrates a decrease in the concentration of DPPH radical (column 1) due to the scavenging ability of chili and pepper extracts. This is compared with the effectiveness of synthetic antioxidants such as TBHQ and BHT to scavenge the radical. The free radical scavenging effect of extracts and standards are in the order of TBHQ > BHT > Chili oleoresin > Pepper oleoresin > Chili extracts > Pepper extracts. The effective concentration required to scavenge 50% radical (EC₅₀) were 6.8, 40, 800, 550, 900 and 750 μ g for TBHQ, BHT, extracts of chili, chili oleoresins, pepper extracts and pepper oleoresins, respectively (Table 1). These studies indicated that oleoresins showed better radical scavenging activity compared to methanol extracts of spices.

DMPD radical scavenging activity. Spice extracts showed DMPD^{•+} radical scavenging activity in a concentration dependent manner (Figure 1, column 2). However, BHT and TBHQ showed better radical scavenging activity. EC₅₀ value for chili extracts, pepper extracts, chili oleoresin and pepper oleoresin were 750, 500, 900 and 730 μ g respectively (Table 2). The EC₅₀ values with TBHQ and BHT were 8 μ g and 35 μ g respectively. These trends are similar to that observed with DPPH system.

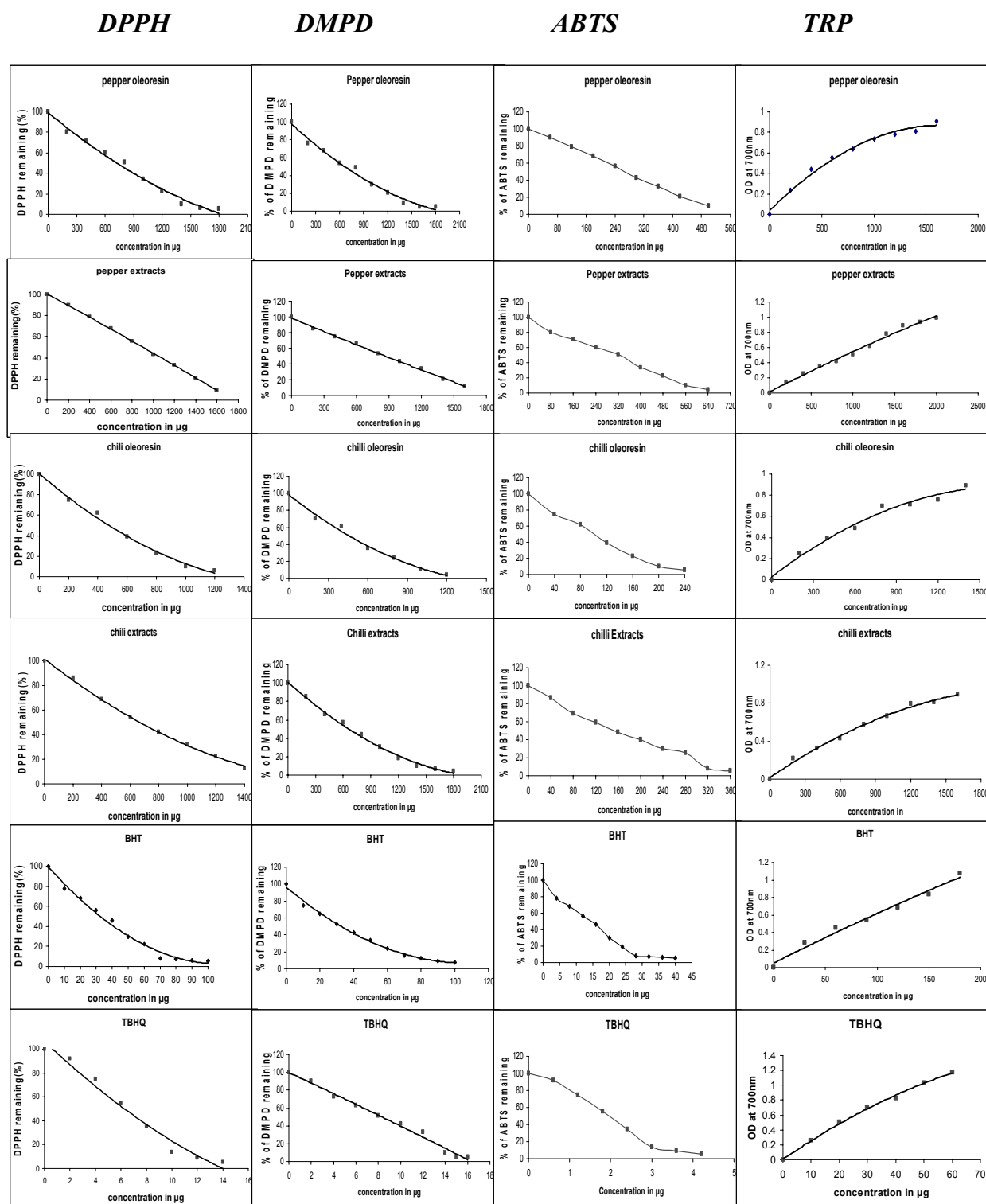


Fig. 1. Radical scavenging activity of spice extracts, BHT and TBHQ measured with DPPH, DMPD, ABTS and TRP (FRAP) assay as indicated in the methods.

ABTS radical cation decolourization assay. The extracts of chili and pepper and oleoresins of chili and pepper exhibited effective cation radical scavenging activity [17]. The EC₅₀ value for radical scavenging activity in the system were 2, 15, 210, 130, 330 and 270 µg for TBHQ, BHT, methanol extracts of chili, chili oleoresin, methanol extracts of pepper and pepper oleoresin respectively (see Figure 1, column 3 and Table 3). These studies indicated that oleoresins showed better radical scavenging activity compared to methanol extracts of spices.

Table 1. Antiradical activity of spice extracts in DPPH assay system.

Additions	EC ₅₀ (µg)
TBHQ	6.8 ± 0.4
BHT	40 ± 2
Chili extracts	800 ± 6
Chili oleoresin	550 ± 4
Pepper extracts	900 ± 5
Pepper oleoresin	750 ± 3

Values are mean ± SD, n = 4; DPPH – Diphenyl picryl hydrazyl; BHT – Butylated hydroxy toluene; TBHQ – Tertiary butylated hydroxy quinone.

Table 2. Antiradical activity of spice extracts in DMPD assay system.

Additions	EC ₅₀ (µg)
TBHQ	8.0 ± 0.2
BHT	35.0 ± 1.3
Chili extracts	750 ± 4
Chili oleoresin	500 ± 5
Pepper extracts	900 ± 4
Pepper oleoresin	730 ± 6

Values are mean ± SD, n = 4.

Table 3. Antiradical activity of spice extracts in ABTS assay system.

Additions	EC ₅₀ (µg)
TBHQ	2.0 ± 0.4
BHT	15.0 ± 0.2
Chili extracts	210 ± 2
Chili oleoresin	130 ± 1
Pepper extracts	330 ± 4
Pepper oleoresin	270 ± 5

Values are mean ± SD, n = 4.

Antioxidant activity

Reducing power assay using the potassium ferric cyanide reduction method. Figure 1 (column 4) shows the reducing power of the spice extracts and standards (TBHQ and BHT) in potassium ferric cyanide reduction method. The reducing power of extracts and standards increased with growing concentration of samples. Reducing power of extracts and standards were of the order: TBHQ > BHT > Chili oleoresin > Chili extracts > Pepper oleoresin > Pepper extracts when reducing power at equal concentrations of extracts were compared.

Inhibition of liver lipid peroxidation by spice extracts. Addition of TBHQ and BHT inhibited lipid peroxidation in rat liver homogenates (Table 4). The inhibition with TBHQ and BHT was 75 and 94% at 100 µg. With chili extracts, chili oleoresin, pepper extracts and pepper oleoresin the inhibition observed at 0.1% was 36, 41, 39 and 44%, respectively. At 1%, the maximum inhibition observed was 46, 55, 42 and 58%, respectively (Figure 2 and Table 4).

Table 4. Inhibition of the lipid peroxidation by spice extracts.

Additions	Concentration (µg)	Inhibition (%)
Chili extracts	100	36
	1000	46
Chili oleoresin	100	41
	1000	55
Pepper extracts	100	39
	1000	42
Pepper oleoresin	100	44
	1000	58
BHT	0.13	75
TBHQ	0.012	94

Control value in the absence of inhibitors: 19.41 ± 2.43 nmoles MDA/mg protein.

Total antioxidant capacity by CUPRAC method. The CUPRAC antioxidant capacities of extracts were measured as Trolox equivalents. Trolox equivalent capacity obtained of chili extracts, chili oleoresin, pepper extracts and pepper oleoresin were 160, 213, 110 and 181 µg, respectively (Table 5).

Table 5. Total antioxidant activity of spice extracts by CUPRAC assay system.

Additions	µg of Trolox equivalents/mg of extract
Chili extracts	160 ± 2
Chili oleoresin	213 ± 2
Pepper extracts	120 ± 1
Pepper oleoresin	181 ± 2

Values are mean ± SD, n = 4.

DISCUSSION

The objective of the investigation was to evaluate the potentials of extracts from chili and pepper to scavenge free radicals and exhibit antioxidant activities which can be exploited in preserving processed foods or to prevent the rancidity of oils and at the same time get the benefits of medicinal properties of these spices. These spices are routinely used in Asian diets as food adjuncts. The medicinal values of these spices are known for many decades from traditional knowledge and by its use in Ayurvedic system of medicine [18]. Many studies in the recent past have also shown the action of these spices and their active principles in beneficially influencing physiological processes as well as controlling disease process.

One of the most thoroughly studied active components of chilis is capsaicin, which is the pungent component of chili. Capsaicin and dihydrocapsaicin inhibit iron mediated lipid peroxidation. It also inhibited copper induced oxidation of low density lipoprotein [19]. This effect is perceived to be mediated by its ability to form complexes with reduced metals and act as hydrogen donors [20].

Capsaicin reduced the generation of reactive oxygen species in activated macrophages and exhibited antiinflammatory effects [21]. It also augmented antioxidant systems by enhancing the activities of enzyme such as superoxide dismutase, catalase and glutathione peroxidase. Capsaicin was found to inhibit the growth of *Helicobacter Pylori*. It inhibited the release of gastrin by stimulating somatostatin. Dairam *et al.* [20] have examined the antioxidant, metal chelating properties and inhibitory effect on oxidative stress by capsaicin in rat brain homogenates. The neuroprotective effects of capsaicin through antioxidant and iron-binding properties of capsaicin was reported in this study. Thus, chilies and its bioactive components have beneficial effect in nullifying the potential damage caused by reactive oxygen species.

Pepper extracts contain piperine and other bioactive compounds [6]. Piperine has been demonstrated to give protection against oxidative damage by quenching free radicals, reactive oxygen species and inhibiting lipid peroxidation [22]. Reddy and Lokesh [23] have reported that piperine had inhibitory effects on ascorbate Fe^{2+} induced lipid peroxidation in rat liver microsomes at concentrations of 600 μ M and above.

Piperine is shown to provide protection to human low density lipoprotein from copper induced lipid peroxidation [24]. The aqueous extract of black pepper as well as piperine have been examined for their effect on human 5-lipoxygenase, the key enzymes involved in biosynthesis of leukotrienes [25]. The formation of 5-hydroxyeicosatetraenoic acid was significantly inhibited in a concentration dependent manner with IC_{50} values of 0.13 mg for aqueous extracts of pepper and 60 μ M for piperine. Thus, piperine in black pepper might exhibit antioxidant activity by modulating 5-lipoxygenase pathway.

Selvendiran and Senthilnathan [26] have investigated the effect of piperine on mitochondrial antioxidant system and lipid peroxidation in benzo-(α)pyrene induced lung carcinogenesis. Oral supplementation of piperine (50 mg/kg body weight) effectively suppressed lung carcinogenesis and decreased extent of mitochondrial lipid peroxidation with concomitant increase in the activities of enzymatic and

non enzymatic antioxidant levels. This suggests that piperine may exhibit its chemo preventive effect by modulating lipid peroxidation and augmenting antioxidant defense system.

Vijayakumar *et al.* [27] have examined the effect of supplementing black pepper or piperine on tissue lipid peroxidation, enzymatic and non-enzymatic antioxidants in rats fed a high fat diet. They observed that black pepper extract and piperine can reduce high fat diet induced oxidative stress. Significantly elevated levels of thiobarbituric acid reactive substances, conjugated dienes and lowered activities of superoxide dismutase, catalase, glutathione peroxidase, glutathione-*s*-transferase, reduced glutathione was observed in the liver, heart, kidney, intestine and aorta of rats fed high fat diet. Supplementation of diet with black pepper or piperine lowered lipid peroxidation and elevated antioxidant enzyme levels to that observed with control rats.

The effect of alcohol extract of piper longum and piperine was studied for immunomodulatory and antitumour activity [28]. The administration of extract (10 mg/animal) or piperine (1.14 mg/animal) inhibited solid tumor development in mice injected with Daltons lymphoma ascites cells. Pepper extracts also increased the survival of mice bearing Ehrlich ascites tumor cells [29].

Because of such varied effects of black pepper and its extracts, it has been used in Indian Ayurvedic system of medicine, folklore medicine of Latin America and West Indies its treatment of asthma, bronchitis, fever, arthritis and gastrointestinal disorders.

The spices and their active principles were found to be safe for consumption even at high doses. Black pepper, its oleoresin or its active principle piperine, fed to rats at doses 5–20 times normal intake levels in humans did not cause any adverse effect on growth, food efficiency ratio, organ weights, blood cell counts and blood constituents like hemoglobin, total serum proteins, albumin, globulin, glucose, cholesterol, activities of serum amino transferases and phosphatases, fat and nitrogen balance [30].

The antiradical and antioxidants from spices such as chili and pepper thus play a vital role in removing damaging free radicals and there by promote health and reduce risk factors for chronic diseases. Our unpublished results also indicated that there is a strong correlation between antioxidant activity of spice extracts and the total phenol content of these extracts. We have thus demonstrated the efficacy of spice extracts as radical scavengers in a number of in vitro models. Spice extracts being nontoxic and by its ability to stabilize the oils can be a useful alternative to synthetic antioxidant in oil and food

preservation, which is the objective of our next paper.

CONCLUSIONS

Comparable analysis based on the different *in vitro* assay systems: DPPH• and DMPD•+ radical scavenging assays, CUPRAC and ABTS decolourization assays, ferric reducing power assay demonstrated that alcohol extracts and oleoresins of chili and pepper have significant radical scavenging activities and antioxidant potential in all the systems tested. Their effects were compared with the reference antioxidants such as TBHQ, BHA and BHT. These studies indicated that chili and pepper extracts can be used for the medicinal properties as well as for food preservations by virtue of their ability to remove dangerous oxygen free radicals.

Acknowledgement: Partial financial support for this study was from the Department of Science and Technology, New Delhi, India (Grant Int/Bulgaria/B-16/2006) and of National Science Fund of Ministry of Education and Science of Bulgaria, Bilateral project with India (Grant BIn4/04) are gratefully acknowledged. The authors also thank Dr. V. Prakash, Director, Central Food Technological Research Institute, Mysore, India and Prof. Tchorbanov, DSc., Director, Institute of Organic Chemistry with Centre of Phytochemistry, Bulgarian Academy of Sciences, Sofia, Bulgaria for keen interest and encouragement for this work.

REFERENCES

1. B. Halliwell, *Ann. Rev. Nutr.*, **16**, 33 (1997).
2. G. O. Adegoke, M. Vijayakumar, A. G. Gopala-krishna, M. C. Varadaraj, K. Sambaiah, B. R. Lokesh, *J. Food Sci. Technol.*, **35**, 283 (1998).
3. B. L. Halvorsen, M. C. W. Holte Myhrstad, *J. Nutr.*, **132**, 461 (2002).
4. A. Rosa, M. Deiana, V. Casu, S. Paccagini, G. Appendino, M. Ballero, A. Dessi, *J. Agr. Food Chem.*, **50**, 7396 (2002).
5. Y. J. Surb, R. C. Lee, K. K. Purk, S. T. Mayre, A. Liem, J. A. Miller, *Carcinogenesis*, **16**, 112 (1995).
6. K. Srinivasan, *Crit. Rev. Food Sci. Nutr.*, **47**, 735 (2007).
7. B. G. Bhat, N. Chandrasekara, *Nahrung*, **31**, 913 (1987).
8. J. R. Chipault, G. R. Mizuno, J. M. Hawkins, W. O. Lundberg, *Food Technol.*, **10**, 209 (1956).
9. H. L. Madsen, G. Bertelsen, *Trends Food Sci. Technol.*, **6**, 271 (1995).
10. N. V. Yanishlieva, E. M. Marinova, *Eur. J. Lipid. Sci. Technol.*, **103**, 752 (2001).
11. K. V. Raghavendra, N. Mahendranath Rao, A. G. Gopala Krishna, *Beverage and Food World*, **29**, 25 (2002).
12. I. Gulcin, *Life Sci.*, **78**, 803 (2006).
13. V. Fogliano, V. Verde, G. Randazzo, A. Ritieni, *J. Agric. Food Chem.*, **47**, 1035 (1999).
14. I. F. F. Benzie, J. J. Strain, *Methods Enzymol.*, **299**, 15 (1999).
15. D. M. Miller, S. D. Aust, *Arch. Biochem. Biophys.*, **271**, 113 (1989).
16. B. Bektasoglu, S. E. Celik, M. Ozyurek, K. Guclu, R. Apak, *Biochem. Biophys. Res. Commun.*, **345**, 1194 (2006).
17. R. Chohan, G. F. Wilkins, E. I. Opara, *Plant Foods Hum. Nutr.*, **63**, 47 (2008).
18. K. Srinivasan, *Food Res. Int.*, **38**, 77 (2005).
19. K. Mukrami, M. Ito, H. H. Htay, R. Tsubouchi, M. Yoshino, *Biomed. Res.*, **22**, 15 (2001).
20. A. Dairam, R. Fogel, S. Daya, L. J. Limson, *J. Agric. Food Chem.*, **56**, 3350 (2008).
21. A. Ch. Pulla Reddy, B. R. Lokesh, *Ann. Nutr. Metab.*, **38**, 349 (1994).
22. R. Mittal, R. L. Gupta, *Meth. Find. Exp. Clin. Pharmacol.*, **22**, 271 (2000).
23. A. C. Reddy, B. R. Lokesh, *Mol. Cell. Biochem.*, **111**, 117 (1992).
24. K. A. Naidu, N. B. Thippeswamy, *Mol. Cell. Biochem.*, **229**, 19 (2002).
25. N. S. Prasad, H. Raghavendra, B. R. Lokesh, K. A. Naidu, *Essent. Fatty Acids*, **70**, 521 (2004).
26. K. Selvendiran, P. Senthilnathan, *Phytomedicine*, **11**, 85 (2004).
27. R. S. Vijayakumar, D. Surya, N. Nalini, *Redox Rep.*, **9**, 105 (2004).
28. E. S. Sunila, R. Kuttan, *J. Ethnopharmacol.*, **90**, 339 (2004).
29. M. C. Unnikrishnan, R. Kuttan, *Cancer Lett.*, **51**, 85 (1990).
30. B. G. Bhat, N. Chandrasekara, *Toxicology*, **40**, 83 (1986).
31. R. Ree, N. Pellegrini, A. Proggente, A. Pannala, M. Yang, C. Rice-Evans, *Free Radical Biol. Med.*, **26**, 1231 (1999).

ОЦЕНКА НА АНТИРАДИКАЛОВИТЕ И АНТИОКСИДАНТНИ СВОЙСТВА НА ЕКСТРАКТИ ОТ ИНДИЙСКО ЧЕРВЕНО ЧИЛИ И ЧЕРЕН ПИПЕР ЧРЕЗ „ИН ВИТРО“ МОДЕЛИ

А. Г. Гопала Кришна¹, Б. Р. Локеш¹, Д. Сугасини¹, В. Д. Кънчева^{2*}

¹ Лаборатория по липидна наука и традиционни храни, Централен изследователски институт по хранителни технологии, Майсур 570020, Индия

² Лаборатория по химия на липидите, Институт по органична химия с център по фитохимия, Българска академия на науките, ул. „Акад. Г. Бончев“ бл. 9, София 1113

Постъпила на 31 юли 2009 г.

(Резюме)

Кислород съдържащите свободни радикали и липидните пероксиди играят важна роля в увеличаване на рисковите фактори за много хронични заболявания и са също така отговорни за влошаване на качеството на хранителните продукти. Целта на това проучване бе да оцени потенциала на екстракти от червено чили и черен пипер да улавят свободни радикали в *in vitro* моделни системи като: 1,1-дифенил-2-пикрил-хидразил (DPPH), N,N-диметил-р-фенилендиамин дихидрохлорид (DMPD), 2,2-азино-бис-3-етилбензтиазолин-6-сулфонова киселина (ABTS), ферицианиден антиоксидантен потенциал (FRAP), тотален антиоксидантен капацитет (CUPRAC) методи и да покаже антиоксидантните активности спрямо липидното перокисление. Алкохолните екстракти и олеорезиновите проби на червено чили и черен пипер показаха значителни активности като уловители на свободни радикали и антиоксидантна активност във всички тествани системи. Тези резултати могат да бъдат използвани за предпазване на храни при преработката им и в същото време показват предимствата на лечебните свойства на тези подправки.

Investigation of hydrogen storage properties of magnesium based composites with addition of activated carbon derived from apricot stones

E. Grigorova^{1*}, Ts. Mandzhukova¹, M. Khristov¹, P. Tzvetkov¹, B. Tsyntsarski²

¹ Institute of General and Inorganic Chemistry, Bulgarian Academy of Sciences,
Acad. G. Bonchev St., Block 11, 1113 Sofia, Bulgaria

² Institute of Organic Chemistry with Centre of Phytochemistry, Bulgarian Academy of Sciences,
Acad. G. Bonchev St., Block 9, 1113 Sofia, Bulgaria

Received October 8, 2009

Hydrogen absorption/desorption characteristics of the 95% Mg-5% activated carbon derived from apricot stones (ACA), 90% Mg-10% ACA and 85%-15% ACA, prepared by ball milling under argon, are studied. Hydriding process is proceeded at $T = 573$ K and 473 K and $P = 1$ MPa and dehydriding at $T = 623$ K and $P = 0.15$ MPa. The highest hydrogen absorption capacity of 6.13% is reached by the 95% Mg-5% ACA at 573 K and 1 MPa. The 90% Mg-10% ACA and 85% Mg-15% ACA reached 5.36% and 5.21% hydrogen absorption capacity, respectively. The absorption curves at $T = 573$ K and $P = 1$ MPa for the composites with 10 and 15% ACA are very similar. The threefold increase of the quantity of the activated carbon in magnesium does not affect substantially the desorption kinetics of the composites.

Key words: hydrogen storage; magnesium-based composites; ball milling; hydriding-dehydriding kinetics.

INTRODUCTION

Magnesium and magnesium-based compounds are promising candidate materials for hydrogen storage. Unfortunately magnesium requires preliminary activation, it is hard to attend its high theoretical hydrogen storage capacity (7.6%) and in addition it posses slow hydrogen sorption kinetics. A lot of investigations were performed in order to improve the hydriding-dehydriding kinetics of magnesium by preparing composites on its base applying the method of high-energy ball milling and containing different additives. Various substances have been used as additives to magnesium composites obtained by ball milling. For example, some transition metals [1–4], intermetallic compounds [5–9], oxides [10–14] and some carbon containing compounds as graphite [15–24], carbon black [15, 20], carbon nanotubes [15, 19, 20] and SiC [25]. Depending of the nature of the additive, which has been added to magnesium, their catalytic effect on hydriding and dehydriding processes may differ. In some cases, as in addition of carbon containing compounds to magnesium, the role is complex and not very well elucidated. Some authors consider that graphite protects magnesium from oxidation and acts as a process control agent during ball milling, due to its lubricant properties and the reason of improvement in hydrogen sorption kinetics of

magnesium is the prevention of particles and crystallites growth.

From our previous study the composite Mg-Mg₂Ni-graphite reached high absorption capacity and showed very good kinetic characteristics at low temperatures [22]. The obtained results indicated that the presence of carbon-containing additive leads to improvement of hydrogen storage properties of magnesium. The aim of the present paper is to investigate the effect of activated carbon derived from apricot stones on the hydrogen sorption properties of magnesium. Moreover the role of the quantity of this additive on hydriding/dehydriding kinetics of magnesium would be also studied.

EXPERIMENTAL

Preparation of activated carbon

Activated carbons were prepared by steam pyrolysis from apricot stones. Raw material was heated up to carbonization temperature of 873 K, in a stainless-steel vertical reactor placed in a tube furnace. After cooling down to ambient temperature, the solid product was activated with water vapour at 973 K for 1 h. More detailed explanation of the preparation procedure of activated carbons can be found in [26]. The activated carbon was characterized by X-ray diffraction analyses with CuK α radiation and an Autosorb-1 instrument (model AS-IT) was used to determine the specific surface area.

* To whom all correspondence should be sent:
E-mail: egeorg@svr.igic.bas.bg

Preparation of composites based on magnesium

Mixtures of powdery Mg – 5, 10 and 15% activated carbon derived from apricot stones were ball milled in planetary monomill Fritsch Pulverisette 6 for 30 min under argon with rotation speed 200 rpm and 1:10 sample to balls weight ratio. All investigated composites were characterized by X-ray diffraction analyses with CuK α radiation and hydrogen absorption and desorption measurements were performed by Sivert's type apparatus. Hydriding was proceeded at 573 K and 473 K and P = 1 MPa and dehydriding at 623 K and P = 0.15 MPa. The crystallite size was calculated according to the Scherrer formula using the Topas V3 programme [27].

RESULTS AND DISCUSSION

X-ray diffraction patterns of activated carbon derived from apricot stones are presented in Fig. 1. Some traces of MgO and CaCO₃ are detected. The nitrogen surface area of activated carbon is 960 m²/g and was calculated by using the BET equation.

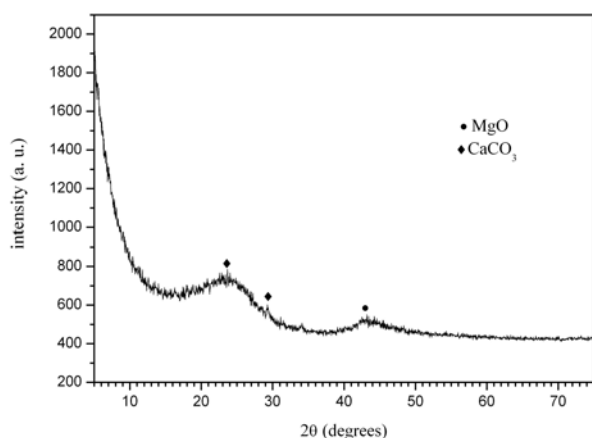


Fig. 1. X-ray diffraction patterns of the activated carbon derived from apricot stones.

X-ray diffraction patterns for the ball milled 30 min under argon composites are presented in Fig. 2. The detected phases are magnesium which is the main one and some small quantity of Mg(OH)₂. There is no substantial difference between the X-ray diffraction patterns of the composites with 5, 10 and 15% activated carbon derived from apricot stones.

The kinetic curves of hydriding for all composites and pure magnesium at temperature 573 K and pressure of 1 MPa are presented in Fig. 3. The addition of activated carbon derived from apricot stones has lead to improvement of hydrogen absorption kinetics and higher absorption capacity after 60 min of hydriding. The composite 95%Mg-5% ACA has reached the highest hydrogen absorption capacity. At the beginning of the process e.g. the

first 5 min all composites have practically the same rate of hydriding reaction. With advancement of the reaction the composite containing the lowest quantity of activated carbon has showed better kinetics and the highest hydrogen absorption capacity than the composites 90%Mg-10% ACA and 85% Mg-15% ACA. The theoretical hydrogen storage capacity of pure magnesium is 7.6%. The use of higher quantity of additives leads to diminution of its theoretical hydrogen storage capacity. For that reason, on the one hand, when additives are used, they reflect favourably on the hydrogen sorption characteristics of magnesium, but on the other hand, the composition has to be chosen carefully.

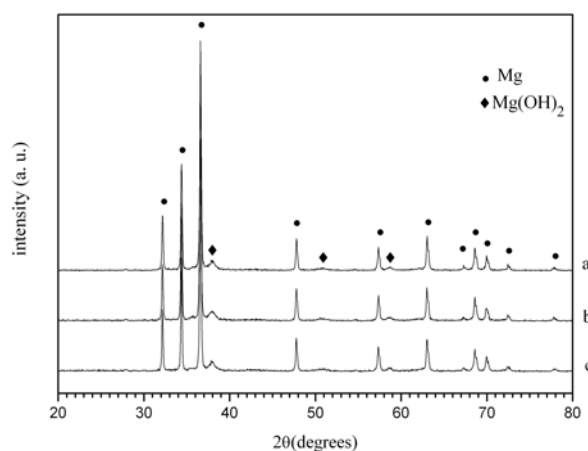


Fig. 2. X-ray diffraction patterns of the composites obtained after ball milling 30 min under argon: a) 95% Mg-5% ACA; b) 90% Mg-10% ACA; c) 85% Mg-15% ACA.

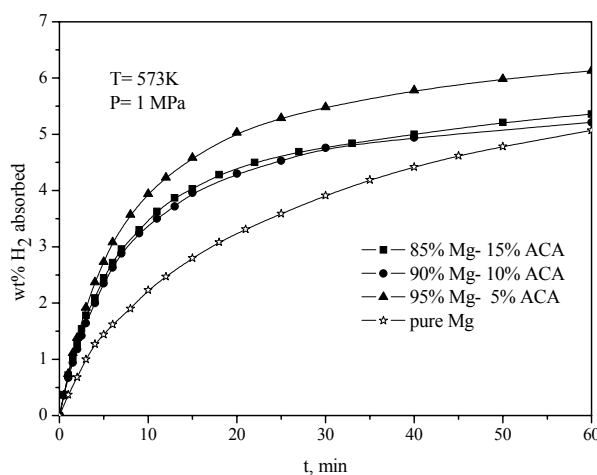


Fig. 3. Kinetic curves of hydriding of the composites 95% Mg-5% ACA, 90% Mg-10% ACA, 85% Mg-15% ACA and pure magnesium.

At 473K and 1 MPa all composites under consideration after 60 min of hydriding reached hydrogen absorption capacity about 1%.

The kinetic curves of dehydriding for all compo-

sites and pure magnesium at 623 K and 0.15 MPa are presented in Fig. 4, here the rate of the hydrogen desorption reaction is very similar for all composites. The quantity of activated carbon does not affect hydrogen desorption kinetics. Pure magnesium has showed slower desorption kinetics, but finally it reached 6.5% desorption capacity. The difference in the desorption capacity is associated with different amount of magnesium in the composites.

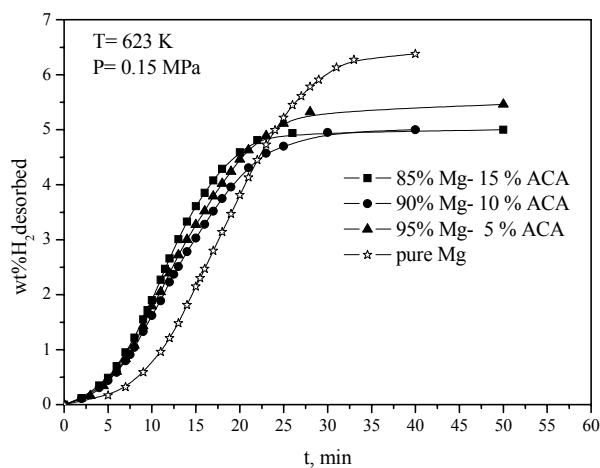


Fig. 4. Kinetic curves of dehydriding of the composites 95% Mg-5% ACA, 90% Mg-10% ACA, 85% Mg-15% ACA and pure magnesium.

The positive effect of carbon addition to magnesium based materials on the hydrogen sorption characteristics is not only associated with augmentation of specific surface area during ball milling, but also with the antisticking effect of carbon and its ability to prevent the restoration of the oxide layer on the surface. In this way carbon eliminates the unfavourable effect of this layer on the dissociative chemisorption of hydrogen. The large amount of carbon containing additive could block the hydrogen diffusion paths and to overtake its positive effect as antistacking agent. Obviously, 15% of activated carbon, derived from apricot stones, is not enough quantity to observe this blocking effect.

The average crystallites size is presented on Table 1. After ball milling of the composites some small diminution of crystallites size by increasing the quantity of activated carbon is observed. The facilitation of the hydrogen diffusion in materials with smaller crystallites should be associated with an increase in absorption capacity. In this connection, due to the fact that the crystallite size of the composites under consideration shows no substantial difference, their hydrogen absorption capacities values should also be similar. The maximum hydrogen absorption capacity for the sample with 5% activated carbon is almost 1% higher than this reached by the other two composites. In the litera-

ture it is usually assumed that the hydrogen sorption characteristics of magnesium based systems strongly affect by crystallites size [3]. From our results it is obviously that even 5% of activated carbon derived from apricot stones has positive effect on the hydrogen absorption/desorption properties of magnesium. Further increase of the quantity of activated carbon e.g. 10% and 15% leads to diminution of the hydrogen absorption rate and capacity. Addition of this type of activated carbon makes also the activation of the composites easier, as could be seen at Table 2. The composite with 15% of activated carbon reached almost 1.49% H_2 at first cycle after 60 min of hydriding and pure magnesium only 0.26% H_2 .

Table 1. Average crystallite size values (in nm) of the composites after ball milling and hydrided at 573 K and 1 MPa.

composite	ball milled	hydrided
95% Mg-5% ACA	80	131
90% Mg-10% ACA	70	122
85% Mg-15% ACA	73	130

Table 2. Hydrogen absorption capacity of the composites after 60 min of hydriding at I cycle at $T = 623$ K and $P = 1$ MPa.

composite	absorption capacity, % H_2
pure Mg	0.26
95% Mg-5% ACA	0.86
90% Mg-10% ACA	0.99
85% Mg-15% ACA	1.48

CONCLUSIONS

The results obtained on the absorption-desorption characteristics of the composites: 95% Mg-5% activated carbon derived from apricot stones (ACA), 90% Mg-10% ACA and 85% Mg-15% ACA demonstrate the positive effect of the additive on the hydrogen absorption properties of magnesium. The investigated composites possess easier activation, increased absorption capacity at temperature 573 K and improved hydriding-dehydriding kinetics, compared to pure magnesium. Due to the fact that the duration of mechanical activation doesn't lead to significant change in the crystallites size, the dehydriding kinetics shows no substantial change. Contrariwise, the hydriding kinetics shows some difference. The best hydrogen absorption kinetics and the highest hydrogen absorption capacity is reached by the composite 95% Mg-5% activated carbon derived from apricot stones.

Acknowledgements: The financial support of Bulgarian Ministry of Science and Education, the National Fund of Scientific Investigations of

Bulgaria under contract YS No 02-220/2008 is highly appreciated.

REFERENCES

- I. G. Konstanchuk, E. Yu. Ivanov, M. Pezat, B. Darriet, V. V. Boldyrev, P. Hagenmuller, *J. Less-Common Met.* **131**, 181, (1987).
- J.-L. Bobet, E. Akiba, B. Darriet, *Int. J. Hydrogen Energy*, **26**, 493, (2001).
- A. Zaluska, L. Zaluski, J. O. Strom-Olsen, *Appl. Phys. A, Mater. Sci. Proc.*, **72**,157, (2001).
- L. E. A. Berlouis, E. Cabrera, E. Hall-Barientos, P. J. Hall, S. B. Dodd, S. Morris, M. A. Imam, *J. Mater. Res.*, **16**, 45, (2001.)
- G. Liang, J. Huot, S. Boily, A. Van Neste, R. Schulz, *J. Alloys Comp.*, **297**, 261, (2000).
- M. Zhu, Y. Gao, X. Z. Che, Y. Q. Yang, C. Y. Chung, *J. Alloys Comp.*, **330–332**, 708, (2002)
- M. Khrussanova, J.-L. Bobet, M. Terzieva, B. Chevalier, D. Radev, P. Peshev, B. Darriet, *J. Alloys Comp.*, **307**, 283 (2000).
- P. Wang, H. F. Zhang, B. Z. Ding, Z. Q. Hu, *Acta Mater.*, **49**, 921, (2001).
- R. Vijay, R. Sundaresan, M. P. Maiya, S. Srinivasa Murthy, *Int. J. Hydrogen Energy*, **32**, 2390, (2007).
- M. Khrussanova, M. Terzieva, P. Peshev, I. Konstanchuk, E. Yu. Ivanov, *Z. Phys. Chem. (N.F.)*, **164**, 1261, (1989).
- W. Oelerich, T. Klassen, R. Bormann, *J. Alloys Comp.*, **315**, 237, (2001).
- J.-L. Bobet , B. Chevalier , M. Y. Song, B. Darriet, *J. Alloys Comp.*, **356–357**, 570, (2003).
- K. S. Jung, E. Y. Lee, K. S. Lee, *J. Alloys Comp.*, **421**, 179, (2006).
- F. Tonus, V. Fuster, G. Urretavizcaya, F. J. Castro, J.-L. Bobet, *Int. J. Hydrogen Energy*, **34**, 3404, (2009).
- C. Z. Wu, P. Wang, X. Yao, C. Liu, D. M. Chen, G. Q. Lu, H. M. Cheng, *J. Alloys Compd.*, **414**, 259, (2006).
- S. Bouaricha, J.-P. Dodelet, D. Guay, J. Huot, R. Schulz, *J. Mater. Res.*, **16**, 2893, (2001).
- C. X. Shang, Z. X. Guo, *J. Power Sources*, **129**, 73, (2004).
- M. Güvendiren, E. Baybörü, T. Öztürk, *Int. J. Hydrogen Energy*, **29**, 491, (2004).
- M. A. Lillo-Ródenas, Z. X. Guo, K. F. Aguey-Zinsou, D. Cazorla-Amorós, *Carbon*, **46**,126, (2008).
- Z. G. Huang, Z. P. Guo, A. Calka, D. Wexler, H. K. Liu, *Mater. Lett.*, **61**,3163, (2007).
- H. Imamura, Y. Takesue, T. Akimoto, S. Tabata, *J. Alloys Compd.*, **293–295**, 564, (1999).
- J.-L. Bobet, E. Grigorova, M. Khrussanova, M. Khristov, P. Stefanov, P. Peshev, D. Radev, *J. Alloys Compd.* **366**, 298, (2004).
- S. Dal Toè, S. Lo Russo, A. Maddalena, G. Principi, A. Saber, S. Sartori, T. Spataru, *Mater. Sci. Eng. B*, **108**, 24, (2004).
- H. Imamura, I. Kitazawa, Y. Tanabe, Y. Sakata, *Int. J. Hydrogen Energy*, **32**, 2408, (2007).
- A. Ranjbara, Z. P. Guoa, X. B. Yu, D. Wexler, A. Calka, C. J. Kim, H. K. Liu, *Mater. Chem. Phys.*, **114**, 168, (2009).
- K. Gergova, N. Petrov, S. Eser, *Carbon*, **32**, 693, (1994).
- Topas V3, General profile and structure analysis software for powder diffraction data, Bruker AXS, Karlsruhe, Germany, 2006.

ИЗСЛЕДВАНЕ НА СОРБЦИОННИТЕ ХАРАКТЕРИСТИКИ ПО ОТНОШЕНИЕ НА ВОДОРОДА НА КОМПОЗИТИ НА БАЗАТА НА МАГНЕЗИЙ С ДОБАВКА ОТ АКТИВЕН ВЪГЛЕН ПОЛУЧЕН ОТ КАЙСИЕВИ КОСТИЛКИ

Е. Григорова^{1*}, Цв. Манджукова¹, М. Христов¹, П. Цветков¹, Б. Цинцарски²

¹ *Институт по обща и неорганична химия, Българска академия на науките,
ул. „Акад. Г. Бончев“, блок 11, София 1113*

² *Институт по органична химия с Център по фитохимия, Българска академия на науките,
ул. „Акад. Г. Бончев“, блок 9, София 1113*

Постъпила на 8 октомври 2009 г.

(Резюме)

Изследвани са абсорбционно-десорбционните характеристики по отношение на водород на композити със състав 95% Mg-5% активен въглен получен от кайсиеви костилки (АСА), 90% Mg-10% АСА и 85%-15% АСА, механоактивирани в инертна среда. Процесът на хидриране протича при $T = 573$ К и $P = 1$ МРа, а на дехидриране при $T = 623$ К и $P = 0.15$ МРа. Композитът 95% Mg-5% АСА достига най-висок абсорбционен капацитет от 6.13% при 573 К и 1 МРа. Композитите 90% Mg-10% АСА и 85%-15% АСА достигат абсорбционен капацитет 5.36% и 5.21% съответно. Ходът на абсорбционните криви при $T = 573$ К и $P = 1$ МРа за композитите съдържащи 10 и 15% АСА е доста сходен. Трикратното увеличаване на количеството на добавката от активен въглен към магнезия не се отразява на кинетиката на десорбция на изследваните композити.

CONTENTS

<i>Y. Dimitrova</i> , Hydrogen-bonded systems of water with dimethyl and diethyl sulfoxides. Theoretical study of structures, stability and vibrational spectra	3
<i>K. B. Umesha, K. M. L. Rai</i> , Synthesis and antimicrobial activity of pyrazole derivatives via 1,3-dipolar cycloaddition of nitrile imines with ethyl acetoacetate	11
<i>N. Petrov, T. Budinova, B. Tsyntsarski, B. Petrova, D. Teodosiev, N. Boncheva</i> , Synthesis of nanoporous carbon from plant wastes and coal treatment products	16
<i>N. I. Abdel-Sayed</i> , Novel synthesis of new symmetrical bis-heterocyclic compounds: Synthesis of bis-thiazolo, bis-pyrazolo-, bis-benzotriazolo-, bis-indolo- and bis-pyrazolyl thiazolo-2,6-diaminopyridine derivatives	20
<i>P. M. Ramdas Bhandarkar, K. N. Mohana</i> , Oxidative cleavage of salbutamol with <i>N</i> -bromosuccinimide in acid and alkaline media: A kinetic and mechanistic study	27
<i>M. T. Akbari, A. Esmaeili, A. H. Zarea, N. Saad, F. Bagheri</i> , Chemical composition and antibacterial activity of essential oil from leaves, stems and flowers of <i>Prangos ferulacea</i> (L.) Lindl. grown in Iran	36
<i>N. Naik, H. Vijay Kumar, H. Swetha</i> , Synthesis and evaluation of novel carbazole derivatives as free radical scavengers	40
<i>M. Krysteva, I. Lalov, V. Beschkov</i> , Acceleration and increase of hydrogen production by simultaneous fermentation of <i>Clostridium butyricum</i> and <i>Rhodobacter sphaeroides</i> on wine-vinasse substrate	46
<i>S. Darakchiev, R. Darakchiev</i> , Gas flow maldistribution in ceramic honeycomb packing	51
<i>A. H. Elshazly</i> , Batch reactor performance improvement for hexavalent chromium reduction by scrap iron using reciprocating perforated disc	55
<i>A. G. Gopala Krishna, B. R. Lokesh, D. Sugasini, V. D. Kancheva</i> , Evaluation of the antiradical and antioxidant properties of extracts from Indian red chili and black pepper by <i>in vitro</i> models ...	62
<i>E. Grigorova, Ts. Mandzhukova, M. Khristov, P. Tzvetkov, B. Tsyntsarski</i> , Investigation of hydrogen storage properties of magnesium based composites with addition of activated carbon derived from apricot stones	70

СЪДЪРЖАНИЕ

<i>Й. Димитрова</i> , Водородно-свързани системи на вода с диметил- и диетилсулфоксиди. Теоретично изследване на структури, стабилност и вибрационни спектри	10
<i>К. Б. Умеша, К. М. Л. Рай</i> , Синтез и антимикробна активност на пиразолови производни получени чрез 1,3-диполлярно циклоприсъединяване на нитрилимини и етилацетоацетат	15
<i>Н. Петров, Т. Будинова, Б. Цинцарски, Б. Петрова, Д. Теодосиев, Н. Бончева</i> , Синтез на напорорест въглен от продукти на преработка на растителни отпадъци и въглища	19
<i>Н. И. Абдел-Сайед</i> , Нови синтети на нови симетрични бис-хетероциклени съединения: синтез на бис-тиазол-, бис-пиразол-, бис-бензотриазол-, бис-индол- и бис-пиразолилтиазол-2,6-диаминпиридинови производни	26
<i>П. М. Рамдас Бхандаркар, К. Н. Мохана</i> , Изследване на кинетиката и механизма на окислително разпадане на салбутамол с <i>N</i> -бромсукцинамид в кисела и алкална среда.....	35
<i>М. Т. Акбари, А. Есмаейли, А. Х. Зареа, Н. Саад, Ф. Багери</i> , Химически състав и антибактериална активност на етерични масла от листа, стъбла и цветовете от <i>Prangos ferulacea</i> (L.) Lindl. растящи в Иран	39
<i>Н. Наик, Х. Виджай Кумар, Х. Суита</i> , Синтез и преценка на нови карбазолови производни като антиоксиданти	45
<i>М. Кръстева, И. Лалов, В. Бешков</i> , Ускоряване и повишаване на продукцията на водород с едновременна ферментацията на <i>Clostridium butyricum</i> и <i>Rhodobacter sphaeroides</i> върху субстрат от винена винаса	50
<i>С. Даракчиев, Р. Даракчиев</i> , Неравномерност на газовото течение в блоков керамичен пълнеж „пчелна пита“	54
<i>А. Х. Елиазли</i> , Подобряване на действието на реактор с периодично действие за редукция на шествалентен хром чрез железен скрап с използване на възвратно-постъпателен перфориран диск	61
<i>А. Г. Гопала Кришна, Б. Р. Локеш, Д. Сугасини, В. Д. Кънчева</i> , Оценка на антирадикаловите и антиоксидантни свойства на екстракти от индийско червено чили и черен пипер чрез „in vitro“ модели	69
<i>Е. Григорова, Цв. Манджукова, М. Христов, П. Цветков, Б. Цинцарски</i> , Изследване на сорбционните характеристики по отношение на водорода на композити на базата на магнезий с добавка от активен въглен получен от кайсиеви костилки	74

BULGARIAN CHEMICAL COMMUNICATIONS

Instructions about Preparation of Manuscripts

General remarks: Manuscripts are submitted in English by e-mail or by mail (in duplicate). The text must be typed double-spaced, on A4 format paper using Times New Roman font size 12, normal character spacing. The manuscript should not exceed 15 pages (about 3500 words), including photographs, tables, drawings, formulae, etc. Authors are requested to use margins of 3 cm on all sides. For mail submission hard copies, made by a clearly legible duplication process, are requested. Manuscripts should be subdivided into labelled sections, e.g. **Introduction, Experimental, Results and Discussion, etc.**

The title page comprises headline, author's names and affiliations, abstract and key words.

Attention is drawn to the following:

a) **The title** of the manuscript should reflect concisely the purpose and findings of the work. Abbreviations, symbols, chemical formulas, references and footnotes should be avoided. If indispensable, abbreviations and formulas should be given in parentheses immediately after the respective full form.

b) **The author's** first and middle name initials, and family name in full should be given, followed by the address (or addresses) of the contributing laboratory (laboratories). **The affiliation** of the author(s) should be listed in detail (no abbreviations!). The author to whom correspondence and/or inquiries should be sent should be indicated by asterisk (*).

The abstract should be self-explanatory and intelligible without any references to the text and containing not more than 250 words. It should be followed by key words (not more than six).

References should be numbered sequentially in the order, in which they are cited in the text. The numbers in the text should be enclosed in brackets [2], [5, 6], [9–12], etc., set on the text line. References, typed with double spacing, are to be listed in numerical order on a separate sheet. All references are to be given in Latin letters. The names of the authors are given without inversion. Titles of journals must be abbreviated according to Chemical Abstracts and given in italics, the volume is typed in bold, the initial page is given and the year in parentheses. Attention is drawn to the following conventions:

a) The names of all authors of a certain publications should be given. The use of “*et al.*” in

the list of references is not acceptable.

b) Only the initials of the first and middle names should be given.

In the manuscripts, the reference to author(s) of cited works should be made without giving initials, e.g. “Bush and Smith [7] pioneered...”. If the reference carries the names of three or more authors it should be quoted as “Bush *et al.* [7]”, if Bush is the first author, or as “Bush and co-workers [7]”, if Bush is the senior author.

Footnotes should be reduced to a minimum. Each footnote should be typed double-spaced at the bottom of the page, on which its subject is first mentioned.

Tables are numbered with Arabic numerals on the left-hand top. Each table should be referred to in the text. Column headings should be as short as possible but they must define units unambiguously. The units are to be separated from the preceding symbols by a comma or brackets.

Note: The following format should be used when figures, equations, *etc.* are referred to the text (followed by the respective numbers): Fig., Eqns., Table, Scheme.

Schemes and figures. Each manuscript (hard copy) should contain or be accompanied by the respective illustrative material as well as by the respective figure captions in a separate file (sheet). As far as presentation of units is concerned, SI units are to be used. However, some non-SI units are also acceptable, such as °C, ml, l, etc.

The author(s) name(s), the title of the manuscript, the number of drawings, photographs, diagrams, etc., should be written in black pencil on the back of the illustrative material (hard copies) in accordance with the list enclosed. Avoid using more than 6 (12 for reviews, respectively) figures in the manuscript. Since most of the illustrative materials are to be presented as 8-cm wide pictures, attention should be paid that all axis titles, numerals, legend(s) and texts are legible.

The authors are asked to submit **the final text** (after the manuscript has been accepted for publication) in electronic form either by e-mail or mail on a 3.5” diskette (CD) using a PC Word-processor. The main text, list of references, tables and figure captions should be saved in separate files (as *.rtf or *.doc) with clearly identifiable file names. It is essential that the name and version of the word-processing program and the format of the

text files is clearly indicated. It is recommended that the pictures are presented in *.tif, *.jpg, *.cdr or *.bmp format, the equations are written using "Equation Editor" and chemical reaction schemes are written using ISIS Draw or ChemDraw

programme. The authors are asked to submit the final text with a list of three potential reviewers. The Editorial Board of the journal is not obliged to accept these proposals.

EXAMPLES FOR PRESENTATION OF REFERENCES

REFERENCES

1. D. S. Newsome, *Catal. Rev.–Sci. Eng.*, **21**, 275 (1980).
2. C.-H. Lin, C.-Y. Hsu, *J. Chem. Soc. Chem. Commun.*, 1479 (1992).
3. R. G. Parr, W. Yang, *Density Functional Theory of Atoms and Molecules*, Oxford Univ. Press, New York, 1989.
4. V. Ponec, G. C. Bond, *Catalysis by Metals and Alloys* (Stud. Surf. Sci. Catal., vol. 95), Elsevier, Amsterdam, 1995.
5. G. Kadinov, S. Todorova, A. Palazov, in: *New Frontiers in Catalysis* (Proc. 10th Int. Congr. Catal., Budapest, 1992), L. Guzzi, F. Solymosi, P. Tetenyi (eds.), Akademiai Kiado, Budapest, 1993, Part C, p. 2817.
6. G. L. C. Maire, F. Garin, in: *Catalysis. Science and Technology*, J. R. Anderson, M. Boudart (eds), vol. 6, Springer-Verlag, Berlin, 1984, p. 161.
7. D. Pocknell, *GB Patent 2 207 355* (1949).
8. G. Angelov, PhD Thesis, UCTM, Sofia, 2001.
9. JCPDS International Center for Diffraction Data, *Power Diffraction File*, Swarthmore, PA, 1991.
10. *CA* **127**, 184 762q (1998).
11. P. Hou, H. Wise, *J. Catal.*, in press.
12. M. Sinev, private communication.
13. <http://www.chemweb.com/alchem/articles/1051611477211.html>.